

Freiberg Online Geoscience

FOG is an electronic journal registered under ISSN 1434-7512



2016, VOL 47



Raghid N. R. Sabri

Geochemical and isotope investigations of carbonate sinter – 2000 years of water supply management in Palestine

.

127 pages, 106 figures, 20 tables, 127 references

# Table of Contents

Table of Contents	I
<i>Acknowledgment</i>	IV
<i>Abstract</i>	VI
<i>List of Figures</i>	VIII
<i>List of Tables</i>	XIV
<i>List of Abbreviations</i>	XV
<i>Terms and definitions</i>	XVII
<b>1. Introduction</b>	<b>1</b>
<b>1.1 Structure of the thesis</b>	<b>1</b>
<b>1.2 General information, background</b>	<b>2</b>
1.2.1 Spiritual value of water in Palestine	2
1.2.2 Water resources and management condition in Palestine	3
1.2.3 Water crisis in Palestine	4
<b>1.3 Motivation</b>	<b>5</b>
<b>1.4 Hypothesis</b>	<b>6</b>
<b>1.5 Location of study area</b>	<b>6</b>
1.5.1 Description of geology and hydrogeology of the study area	8
1.5.2 Climate	13
<b>2. Literature review</b>	<b>18</b>
<b>2.1 Research history of aqueducts</b>	<b>18</b>
<b>2.2 Aqueducts in Palestine</b>	<b>18</b>
2.2.1 Agricultural aqueducts (related to watermills) in Palestine	20
<b>2.3 Utilization of springs in Palestine</b>	<b>21</b>
2.3.1 Ancient water system in Nablus–Sebestia	22
<b>2.4 Carbonate sinter accumulation in aqueducts and artificial water network</b>	<b>24</b>
2.4.1 Research history of secondary carbonate sinter	26
2.4.2 Growth mechanism of secondary carbonate	29
2.4.3 Carbonate sinter analysis	30

<b>3. Methodology</b>	<b>33</b>
3.1 Literature review	33
3.2 Fieldwork	34
3.3 Sampling and analysis	37
3.3.1 Water samples:	37
3.3.2 Carbonate samples	38
3.3.3 U–Th series dating	41
3.4 Software used	43
3.5 Challenges	43
<b>4. Results and discussion (Nablus area)</b>	<b>45</b>
4.1 Ancient water system description	45
4.2 Water sample results and discussion	54
4.2.1 Stable isotope	59
4.2.2 Strontium isotope analysis ( $^{87}\text{Sr}/^{86}\text{Sr}$ )	60
4.2.3 Saturation index	62
4.2.4 Discussion	63
4.3 Carbonate analysis (host rock)	64
4.4 Aqueduct building material	65
4.5 Secondary carbonate analysis	66
4.5.1 Ras Al Ein location (S-2)	66
4.5.2 Ijnisiya location (S-9)	72
4.5.3 Harun Location (S-8)	79
4.5.4 Water tunnel Location (A-1)	86
4.5.5 Water aqueduct Location (A-4)	99
4.6 Discussion	101
4.6.1 Is urbanization a source of groundwater quality degradation?	101
4.6.3 Paleoclimate calculations	105
<b>5. Results and discussion (Al Malih area)</b>	<b>107</b>
5.1 Water system description	107
5.2 Geochemical results (water)	108
5.3 Geochemical results (Carbonate)	111

5.3 Sustainability of watermills	113
<b>6. Conclusions and recommendation</b>	<b>115</b>
6.1 Conclusions	115
6.2 Recommendations	116
6.2.1 Recommendation for further research	116
6.2.2 Recommendation for policy makers	116
<b>References</b>	<b>118</b>

## **Acknowledgment**

I would like to use this opportunity to express my gratitude and thank the following people who made this work possible:

Prof. Broder Merkel for giving me the opportunity to do my research in the Hydrogeology Department, for his continuous supervision, guidance, kindness, and valuable discussion. Mostly, I would like to thank him for the overall positive intellectual atmosphere he created.

My former colleagues from the Department of Hydrogeology; Dr. Sosina Shimeles Haile, Dr. Mohammed Khattab, Mrs. Karina Schlothmann, PD Dr. Volkmar Dunger, Dr. Nicolai Alexeji Kummer, Dipl.-Ing. Hajo Peter, Dr. Rudy Abo, Shimelis Berhanu (M.Sc.), Nadja Schmidt (M.Sc.), Dr. Ramadan Abdel Aziz, Dr. Lotfallah Karimzadeh, Dr. Nair Sreejesh, Dr. Eyad Abushandi, Iwona Wolszyn (M.Sc.), Dr. Samer Bachmaf, Anne Kaulisky (M.Sc.), Dipl.-nat. Bianca Störr, Dr. Hussein Jassas, Dr. Omed Mustafa, Dr. Shwan Ismael, Dr. Mustafa Almkhtar, Wael Kanoua (M.Sc.), Alireza Arab (M.Sc.), Mandy Hoyer (M.Sc.), Mrs. Gisela Schmiedgen and Mr. Tino Beier for their support and friendship

Prof. Marion Tichomirowa for her help regarding Sr isotope analysis and guidance in geochemical analysis. Dipl-Ing Klaus Bombach, Mrs. Angelika Braun and Jennifer Schlicke for their support in Isotope laboratories.

Dr. Norman Pohl from the Institute for Industrial Archaeology, History of Science and Technology (IWTG) for his valuable discussions.

Prof. Marion Tichomirowa and Prof. Jörg Matschullat for providing working space for me.

PD Dr. Edwige Pons-Branchu, Prof. Eric Douville, Mrs. Lorna Foliot and the entire LCSE (Le Laboratoire des Sciences du Climat et de l'Environnement) team for facilitating U/Th analysis at their facility, for their support, discussion and helping me with dating and rare earth elements analysis.

Dr. Michael Magnus, Mrs. G. Mendel and G. Geyer from the Geology Institute TU Bergakademie Freiberg for preparing the thin sections in very high quality. Anja Obst for her guidance in SEM–EDS measurements.

Mrs. Anne de Grosbois with her help in the language correction and her English lessons and Mr. Achim Schröder with his help in German language correction.

The German Academic Exchange Service (DAAD) for the grant and giving me the opportunity to come to Germany and work towards my doctoral degree.

The Centre of Advanced Study and Research (GraFA) and the International Centre (IUZ) at the TU Bergakademie Freiberg for facilitating my work.

M.Sc. Safa Ministry of Agriculture Palestine, M.Sc. Ibrahim Shalsh, Isam Maqbol and M.Sc. Rashid Sabri for providing me with rainfall, runoff and snow samples.

Mr. Isam Maqbol, M.Sc. Rashid Sabri and Mr. Seif Shenawi and all the working for their support during the field sampling.

Eng. Gilbert Wiplinger from the Austrian Archaeological Institute for organizing the International Congress on the History of Water Management and Hydraulic Engineering in the Mediterranean Region.

My family, for their support, encouragement, and good example to be an independent scientist.

My dear Kamal, for his companionship, unlimited support and for his patience during difficult times. Matin, for his presence that has significantly enhanced the outcome of this work.

## Abstract

Over thousands of years, the eastern part of the Mediterranean has developed ways to supply and manage its water resources. The most important evidence of this is the water networks that are distributed in the area. Case studies involving a literature review, fieldwork, sample collection and analysis were conducted that focused on two areas in the West Bank: Nablus city and the northern part of Jordan Valley. These locations were chosen because Nablus city and its vicinity have many of Roman tunnels and aqueducts while the Jordan Valley has many watermills.

This study aims to examine the changes in water quality over time in various ways; in an attempt to explain environmental degradation, to understand archeological aspects relating to the water management system, and to piece together what sustained the past environmental development.

Throughout centuries carbonate deposits have accumulated along the sidewalls of the water system, containing and archiving geochemical and hydraulic information. These carbonate deposits were sampled from the walls of tunnels together with water samples from the tunnel and surrounding springs in the area. In addition, carbonate sinter has accumulated at the outlet of the watermill on the water shaft. This sinter was also sampled along with water samples from the springs and the water in the Wadi in the area. Water and carbonate samples were analyzed. Water analysis included major cations and anions, trace elements, rare earth elements,  $^{18}\text{O}/^{16}\text{O}$  isotope ratio, and  $^{87}\text{Sr}/^{86}\text{Sr}$  isotope ratio. Results indicate the presence of different underground water bodies and Sr resources.

Furthermore, thin sections were made from the carbonate samples for SEM–EDX analyses and microscopic investigations. The microscope analysis showed that the distribution of minerals precipitated differs within one sample. Likewise, SEM–EDX results show a variation in element distribution along the growth axis.

After finishing the analysis of water samples and thin sections, the layers of the carbonate samples were acidified and trace elements and rare earth elements were measured by means of ICP–MS. Then selected layers were prepared for isotope analyses ( $^{18}\text{O}$ ,  $^{13}\text{C}$ , and  $^{87}\text{Sr}/^{86}\text{Sr}$ ) and subsequently measured. The carbonate samples were dated using the U–Th method.

Rare earth elements and trace elements measurements provide clear evidence that urbanization has an adverse effect on groundwater quality. Different groundwater bodies were identified by means of geochemical analysis. In the same way, the water sources used to feed the ancient water system were also identified. Through petrological and geochemical analysis, the sustainability of the watermill concept could be demonstrated.

This study recommends a more controlled regulation of urbanization expansion. It will only be possible to continue living in this region with sufficient amounts of groundwater and innovative techniques for water supply and management that are environmentally sustainable, as it used to be centuries ago.

## List of Figures

Figure 1: Map shows the study area in the West Bank (upper left) and its location in the Middle East _____	7
Figure 2: Buildings at Al Malih, left: Al Malih watermill and aqueduct, right: Al Malih hotel_8	
Figure 3: Stratigraphic table for the study area comparing eastern and northern zones _____	10
Figure 4: Geological map of the study area _____	11
Figure 5: The average discharge of the springs in Nablus area from 1965–2000_____	12
Figure 6: The average discharge of the springs in Al Malih area from 1965–2000 _____	12
Figure 7: Wadi Al Malih surface water (modified after Palestinian Water Authority 2008; QGIS 2016)_____	13
Figure 8: Wadi Qilt bridge aqueduct from Herod era (Photo taken by Raghid Sabri 2008)___	19
Figure 9: Nablus aqueduct from Islamic era (Pointed Arches) (Photo taken by Raghid Sabri 2011) _____	20
Figure 10: Rainfall drain at Hisham Palace that was utilized until the 1400 A.D. (Whitcomb 1988) _____	20
Figure 11: Aqueduct connected to the watermill in Wadi Tufah area in Nablus (Photo taken by Raghid Sabri 2011) _____	21
Figure 12: Speleothem under the western side of the dam to support the great pool (Conder and Kitchener 1884) _____	25
Figure 13: $^{238}\text{U}$ decay through $^{230}\text{Th}$ , with half-life (modified after Edwards 1988; Fairchild and Baker 2012) _____	30
Figure 14: Topographic map of the study area in Palestine shows the sampling locations of springs (S) and aqueducts (A) _____	35
Figure 15: Clean oven for drying water samples at the Isotope Geochemistry and Geochronology Laboratory at the Mineralogy Department of the Technical University Bergakademie Freiberg, Germany _____	38
Figure 16: Sampling methods using: left a core drill and right a chisel _____	39
Figure 17: Drill bit of 0.5 mm _____	40
Figure 18: Sampling Ras al Ein Sample for U–Th series analysis _____	42
Figure 19: The Ras al Ein spring S-2 (Photo taken by Raghid Sabri 2011) _____	45
Figure 20: Qaryon spring house S-3 (Photo taken by Raghid Sabri 2011)_____	46
Figure 21: Tunnel to Al Subyan spring S-5 (Photo taken by Raghid Sabri 2011) _____	47
Figure 22: One tunnel at Harun spring S-8 (Photo taken by Raghid Sabri 2011)_____	48
Figure 23: Harun Spring at the connection of the two tunnels S-8 (Photo taken by Raghid Sabri 2011) _____	49

Figure 24: Carbonate sinter accumulated at the entrance of Harun spring tunnel S-8 (Photo taken by Raghid Sabri 2011)	50
Figure 25: Ijnisinya spring S-9 (Photo taken by Raghid Sabri 2011)	50
Figure 26: Different carbonate shapes at Ijnisinya spring walls (S-10) left: drapery cave minerals, top right: popcorn cave minerals, lower right: down flowstone (Photos taken by Seif Shenawi 2011)	51
Figure 27: Section of the tunnel from Dafna spring to the extraction well, corner left shows the view to the drop shaft looking upwards (Photo taken by Raghid Sabri 2011)	52
Figure 28: Right: Wadi Tufah aqueduct (A-4), left: part of Masudiah aqueduct (A-3), where no trace of carbonate was found (Photos taken by Raghid Sabri 2011)	53
Figure 29: Aqueduct Beit Iba A-5 (Photo taken by Raghid Sabri 2011)	53
Figure 30: Left: Part of Wadi Tufah Aqueduct shows the soda straw sampled; right: thin section of sample from Al-Bezrah aqueduct shows the dimension of the sinter	53
Figure 31: Piper diagram shows springs distributions (water sampling conducted August 2011)	54
Figure 32: Piper diagram shows distribution of springs, an average during 1954–2009	55
Figure 33: Normalized values to (A-1) trace element concentration in water samples	55
Figure 34: Total dissolve solids (TDS) trends with elevation (Nablus group springs)	56
Figure 35: Total dissolve solids (TDS) trends with elevation (Sebestia group springs)	56
Figure 36: Spider patterns of groundwater are similar to patterns between the two groups, above: Nablus group, below: Sebestia group	57
Figure 37: REE patterns show two different spring groups	58
Figure 38: Ce anomaly values for springs show positive anomalies for water samples (A-1, S-4, S-6, S-7, S-8) and negative anomaly for water samples (S-1, A-2, S-2, S-3, S-5, S-9, S-10, S-11) depending on oxidation condition along the pathway of the groundwater	59
Figure 39: Distributions of the stable isotopes $\delta^{18}\text{O}$ and $\delta^2\text{H}$ in different water bodies in the study area	60
Figure 40: Sr isotope ratios $^{87}\text{Sr}/^{86}\text{Sr}$ vs. mean reciprocal Sr concentrations (mg/l) for the springs shows two Sr sources in the aquifer (Error of 0.00005 is derived by replicate analysis of standard)	61
Figure 41: Box-and-whisker plot of the Sr ratio values of the two water groups show a significant difference between the two groups	61
Figure 42: Sr isotope ratios $^{87}\text{Sr}/^{86}\text{Sr}$ vs. mean reciprocal Sr concentrations (mg/l) for springs and rainfall samples show a wide variation in the isotopic Sr value for rainfall (Error of 0.00005 derived by replicate analysis of standard)	62

Figure 43: Different thin sections show carbonate rocks in the study area, upper left: calcite micrite mudstone at S-8, lower left: intrasparite rock including foraminiferal wackestone at S-10, upper right: calcite micrite mudstone at S-2, lower right: limestone (oomicrite) at S-3	64
Figure 44: REE normalized values patterns normalized to NASC <sup>1</sup> (Gromet et al. 1984) show different Ce and Gd anomalies in host rocks	65
Figure 45: Different thin sections of the building material and plaster applied on the aqueducts and theater	66
Figure 46: Sample S-2, left: cross section of the sample shows laminations, brown, light brown dark brown, right: sample before cutting	67
Figure 47: Sample S-2 thin section shows main crystals type code and their features:	67
Figure 48: Sr isotope ratio <sup>87</sup> Sr/ <sup>86</sup> Sr vs. mean reciprocal Sr concentrations (mg/l) shows no significant difference between the three laminations at S-2 and a significant difference between the laminations and the host rock	68
Figure 49: Top: Mg, Fe, Sr peaks along the growth axis of the sinter (k.a. before 2011) show an increase in Sr concentrations towards the recent growth, bottom: crystal variation along the growth axis of the sinter: 9 (microsparite), 11 (mosaic calcite) and 1 (columnar). Fe concentrations are high at crystal types 11, 9	70
Figure 50: Total REY concentration for sample S-2 verses age (before 2011 A.D.) shows a decreasing trend	71
Figure 51: REE values patterns normalized to NASC for selected lamination and the host rock show similarity between the lamination and the host rock except for the last lamina 3.8 k.a. due to a change of the oxidizing conditions, <sup>1</sup> (Gromet et al. 1984)	71
Figure 52: Samples S-9 (a): left: polished cross section shows different lamination colors (white, gray and brown), right: sample before cutting	72
Figure 53: Sample S-9 thin section shows main crystals type code and their features crystal type code are based on Frisia (2015) classification shown in section (2.4.3)	73
Figure 54: Sample S-9(b) a block of overlapping calcite tubes	74
Figure 55: SEM image S-9(b), left: view to the tube opening, right tube structure	74
Figure 56: Sr isotope ratio <sup>87</sup> Sr/ <sup>86</sup> Sr vs. mean reciprocal Sr concentrations (mg/l) shows no significant difference between the three laminations of S-9(a) and the water sample but different Sr value for sample S-9(b)	75
Figure 57: Top: Mg, Fe, Sr and Al peaks along the growth axis of the sinter from 287–1979 A.D.	77
Figure 58: Total REY concentration for sample S-9 (a) along the growth axis of the sinter from 290–1779 A.D., shows robust increase after 1929 A.D. Question sign (?) indicates that the age was not determined	78

Figure 59: Mn vs. Nd show a linear relation in the first growth 290–335 A.D. and second growth, and a nonlinear relation for the third growth 1929–1979 A.D. _____	78
Figure 60: Selected REE values patterns normalized to NASC, <sup>1</sup> (Gromet et al. 1984) with corresponding age. From 1929 to 1979 A.D show a change in the oxidation condition in 1979 A.D. _____	79
Figure 61: Left: polished cross section shows different lamination colors (gray, black, white and brown), right: sample before cutting _____	79
Figure 62: Sample S-8 thin section shows main crystals type code and their features _____	80
Figure 63: Strontium isotope ratio <sup>87</sup> Sr/ <sup>86</sup> Sr vs. their reciprocal Sr concentrations show no significant different between sample S-8, S-9 and the origin water (Error of 0.00005 is derived by replicate analysis of standard) _____	81
Figure 64: Variations of Sr isotopic ratios ( <sup>87</sup> Sr/ <sup>86</sup> Sr) and $\delta^{234}\text{U}$ in carbonate sinter samples provide a means to identify two different groups _____	81
Figure 65: Al, Pb and Fe variation within the growth of the S-8 sinter from 880–1054 A.D. _____	83
Figure 66: Sr and Mg variation within the growth of S-8 sinter from 880–1054 A.D. _____	84
Figure 67: Mg concentration vs. Sr concentration show two different trends depending on Mg concentration in the S-8 sinter _____	84
Figure 68: Total REY concentrations along the growth axis of the sinter from 880–1054 A.D. for sinter S-8, show an increase of REY in the first 20 years, then a decrease _____	85
Figure 69: Mn vs. Nd in sample S-8, show a linear relationship, which suggests that the input of the both elements is from the same source _____	85
Figure 70: Selected REE values patterns normalized to NASC in sample S-8 <sup>1</sup> (Gromet et al. 1984) and corresponding age A.D. show similar patterns along the growth axis of the sinter _____	86
Figure 71: Sample A-1(a) cross section shows the lamination and outer side of the sample _____	87
Figure 72: Sample A-1(b) cross section and the sample before cutting _____	87
Figure 73: Sample A-1(c) cross section and the sample before cutting _____	87
Figure 74: Sample A-1(d) cross section and the sample before cutting _____	87
Figure 75: Sample A-1(b) thin section shows the main crystal type codes and their features _____	88
Figure 76: Sample A-1(c) thin section shows main crystals type codes and their features _____	89
Figure 77: Sr isotope ratio <sup>87</sup> Sr/ <sup>86</sup> Sr vs. mean reciprocal Sr concentrations for samples in tunnel _____	90
Figure 78: Variations of Sr isotopic ratios ( <sup>87</sup> Sr/ <sup>86</sup> Sr) and $\delta^{234}\text{U}$ in carbonate sinter samples provide a means to identify three different groups _____	90
Figure 79: Stable isotope variation, $\delta^{18}\text{O}$ ‰ VPDB verses $\delta^{13}\text{C}$ ‰ VPDB for the tunnel samples _____	93
Figure 80: S/Ca ratio for sample A-1 (c) show an increase of the ratio after 1959 with seasonal frequency due to the increase of S emissions in water with the use of diesel heating _____	94

Figure 81: Mg, Sr and Fe concentrations along the growth axis (A.D. calendar year) sample A-1 (c)	94
Figure 82: Mg concentrations verses Sr concentration in the sinter A-1 (c), shows no correlation	95
Figure 83: As concentration along the growth axis (calendar year) of sample A-1 (c), shows an increase after 1991	95
Figure 84: As concentration along the growth axis (calendar year) of sample A-1 (b), shows an increase after 1920	96
Figure 85: REY concentration along the growth axis (calendar year) in sample A-1 (c), show an increase after 1991	96
Figure 86: REY concentration along the growth axis (calendar year) in sample A-1 (b), show an increase after 1991	97
Figure 87: Mn verses REY concentration in samples A-1 (c) and (b), show a correlation between Mn and REY in sample A-1 (b) $R^2$ 0.86 and an elevated Mn concentration in sample A-1 (c) with no correlation with REY $R^2$ 0.17	97
Figure 88: REE patterns for selected years normalized to NASC, <sup>1</sup> (Gromet et al. 1984) in sample A-1 (c), show a change in the patterns in Gd and Ce, a Gd positive anomaly due to high salinity and a Ce positive anomaly due to reducing conditions	98
Figure 89: Ce anomaly values along the growth axis (A.D. calendar years) calculated according to formula 3 on page 57. Sample A-1 (c) shows a frequent change from a positive to negative anomaly that indicates a variation in oxygen level in the water	98
Figure 90: REE patterns normalized to NASC, <sup>1</sup> (Gromet et al. 1984) sample A-1 (b), show a different pattern for the first growth at 1483 A.D. than the rest with a positive Ce anomaly	99
Figure 91: Samples collected from location A-4, top: A-4(b), bottom: A-4(a)	99
Figure 92: Thin section images for sample shows circular lamination calcite with voids not suitable for dating A-4 (a), left: cross section, right: longitudinal section	100
Figure 93: Thin section sample shows circular lamination calcite with voids not suitable for dating A-4(b), Left: tip of the sample, right: along the side of sample	100
Figure 94: Sr isotope ratios <sup>87</sup> Sr/ <sup>86</sup> Sr vs. mean reciprocal Sr concentrations in sample A-4	101
Figure 95: Land-use maps of the study area show an increase in building development.	103
Figure 96: Probable connection between water system (modified after Sabri et al. 2015)	104
Figure 97: Actual connection between the water systems revised according to the geochemical analysis results, (USGS 2011) with sampling locations generated by QGIS	105
Figure 98: Two different groundwater outlets (Photo taken by Raghid Sabri 2011)	107
Figure 99: Arrows represent the water flow through the aqueduct and millhouse at Al Malih	108

Figure 100: Water outlet at the watermill at Al Malih, shows the accumulation of the carbonate (Photo taken by Raghid Sabri 2011)	108
Figure 101: Spider patterns for groundwater bodies Al Malih area show similar patterns within the three water samples: Y, Cs, Ba and HCO <sub>3</sub> concentrations in S-12 and S-14 exceed sea level concentrations	109
Figure 102: Distributions of the stable isotopes $\delta^{18}\text{O}$ and $\delta^2\text{H}$ at Al Malih shows a mixing line between brine water in contact with halite and recent precipitation. EMWL: Eastern Mediterranean Meteoric Water Line ( $\delta^2\text{H}=8 \delta^{18}\text{O}+22$ ; Gat and Carmi 1970; Gat 1983), Brine MWL: Brine Meteoric Water Line ( $\delta^2\text{H}=8 \delta^{18}\text{O}+9$ ; Fontes and Matray 1993)	110
Figure 103: Sr isotope ratios $^{87}\text{Sr}/^{86}\text{Sr}$ vs. mean reciprocal Sr concentrations (mg/l) for the springs	111
Figure 104: Sample A-6, left: cross section of sample, right: thin section shows lamination	112
Figure 105: Sr isotope ratios $^{87}\text{Sr}/^{86}\text{Sr}$ vs. mean reciprocal Sr concentrations (mg/l)	112
Figure 106: REE values patterns normalized to NASC <sup>1</sup> (Gromet et al. 1984) with the age, a positive Ce anomalies appear in all laminae of A-6 except the first lamina from 1740 A.D., meaning oxidizing conditions were present at the beginning	113

## List of Tables

Table 1: Aridity zone according to P/PET index for the study area and its surrounding. __	13
Table 2: Average monthly precipitation:_____	14
Table 3: Ancient climate description of Palestine and surrounding areas and comparison between rainfall amounts calculated from isotopic data for two temperatures. _____	17
Table 4: Summary of the research history of carbonate deposits _____	28
Table 5: Crystal type and the representing code number as suggested by Frisia (2015) __	32
Table 6: Sample type and locations _____	36
Table 7: Saturation indices for springs selected minerals _____	63
Table 8: U–Th data measured for sample S-2 (Ras al Ein) _____	69
Table 9: Measured ages before 2011 for S-2 (Ras al Ein)_____	69
Table 10: U–Th data measured for S-9 (a) (Ijnisinya spring) _____	75
Table 11: Measured ages for S-9 a, <sup>1</sup> (Roy-Barman and Pons-Branchu 2016)_____	76
Table 12: U–Th data measured for samples S-9 and S-8_____	82
Table 13: Measured ages for S-8, _____	82
Table 14: U–Th data measured for A-1(b)_____	91
Table 15: Measured ages for A-1 (b),_____	91
Table 16: U–Th data measured for A-1(c)_____	92
Table 17: Measured ages for A-1 (c),_____	92
Table 18: Calculated rainfall amounts based on $\delta^{18}\text{O}$ values_____	106
Table 19: Selected cation and anion measured in Al Malih area_____	109
Table 20: Selected parameters measured in Al Malih area _____	109

## List of Abbreviations

A.D.	Anno Domini (years of the Gregorian calendar)
ASTER GDEM	Advanced spaceborne thermal emission and reflection radiometer, Global digital elevation map
B.C.	Before Christ
CCD	Charge-coupled devices
cm <sup>2</sup>	Square centimeter
DEM	Digital elevation model
EMWL	Eastern Mediterranean meteoric water line
GMWL	Global meteoric water line
GOCAD	Computer-aided approach to model subsurface geological objects
IC	Ion chromatography
ICP-MS	Inductive coupled plasma mass spectrometry
m a.s.l.	Meters above sea level
m <sup>3</sup>	Cubic meter
MCM	Million cubic meter
NDVI	Normalized difference vegetation index
P <sub>co2</sub>	Water partial pressure
PET	Potential evapotranspiration
PMWL	Paleo-eastern Mediterranean water line
QGIS	Quantum geographic information system
REE	Rare earth elements
REY	Rare earth elements and yttrium
SEM-EDS	Scanning electron microscopy-Energy dispersive X-ray spectroscopy
SI	Saturation index
SRTM	Shuttle radar topography mission
TDS	Total dissolve solids
TIC	Total inorganic carbon
TIMS	Thermal ionization mass spectrometer
UNEP	United Nations Environment Programme
USGS	United States Geological Survey

VPDB	Vienna Pee Dee Belemnite
NASC	North American Shale composite
VASClmO	Variability Analyses of Surface Climate Observations
k.a.	Kilo annum
VSMOW	Vienna Standard mean ocean water
ppm	Part per million
ppb	Part per billion
mg/l	Milligram per liter
km	Kilo meter
cm	Centimeter
UPS	Universal polar stereographic
WGS 84	World Geodetic System

## Terms and definitions

Aqueduct	Water structure with a low slope that is used to transport water from the source to the population
Water tunnel (part of aqueduct)	Underground structure with a low slope that is used to transport water from the source to the population
Agricultural aqueduct	Aqueduct used to transport water for agricultural purposes including providing water to the watermills
Drop shaft (in watermills)	Shaft in an agricultural aqueduct in order to rotate the milling wheel using gravity forces
Well shaft	Access shaft built along a tunnel to permit access to the tunnel
Spring house	Enclosing structure (small building) built around a spring to protect the outlet of the water from pollution
Spring dewatering tunnel	Tunnel that transports the water from the source to the entrance of a spring house.
Wadi	A watercourse that contains water only during storm events in semi-arid and arid regions
Speleothem	Secondary carbonate or secondary deposited cave minerals. Speleothem include: stalactites, stalagmite, flowstone, flowers, popcorn, curtains, straw and much more types (Hill & Forti 1997; Lowe & Waltham 2002; Pedley & Rogerson 2010).
Sinter (carbonate sinter)	Hard mineral deposit precipitated from flowing water (Bögli 1980; Lowe and Waltham 2002).
Travertine	Calcium carbonate deposit at the surface, (biological and evaporation processes are also included with precipitation) (Pentecost 2005). In English literature, travertine means deposit in a thermal spring (Bögli 1980)
Tufa	Spongy carbonate precipitating at ambient temperature (Bögli 1980; Lowe and Waltham 2002; Pentecost 2005; Pedley & Rogerson 2010)

## **1. Introduction**

### **1.1 Structure of the thesis**

This thesis is divided into six chapters. The first chapter introduces the doctoral work, describing background information, as well as the underlying motivation and the hypothesis. Chapter two involves a literature review that examines the current knowledge and significant published investigations of aqueducts, by looking at the history of aqueduct research, and in particular by discussing aqueducts in historical Palestine and carbonate sinter growth in aqueducts. This chapter includes a relevant study on aqueducts and caves in a semi-arid region. Chapter three provides the details on the methodology used here in this work including fieldwork, laboratory work and data interpretation methods. Chapter four and five include results and discussion. First, in general test results of water samples are described, and then specific results are given about each location for the carbonate sample, followed by a discussion as shown below:

- Chap. 4, Nablus area
  - Water system description
  - Geochemical results
  - Discussion
- Chap. 5, Wadi Al-Malih area
  - Water system description
  - Geochemical results
  - Sustainability Watermill

In the conclusions of the final chapter (Chap. 6) the geochemical investigations are evaluated and discussed; recommendations on further research and general recommendation for policy makers are presented.

## **1.2 General information, background**

### **1.2.1 Spiritual value of water in Palestine**

Nowadays in the Fertile Crescent countries of the Middle East springs water, rainfall, and watermills are part of the culture and folklore. Moreover, water plays a very spiritual role in various religions. It is used in baptism, in preparing for prayer, cleansing the souls and ablution (Dierx and Garbrecht 2011). According to the bible, water is both a blessing and a curse (Dierx and Garbrecht 2011). In the Quran, water is considered as the source of life and tool for demolition. In the same direction, we could say water is a source of development economically and socially and a source of destruction. All this reflects how spiritually significant and vital water is in these countries and by the way as well in other countries.

Not only Abrahamic religions are replacing a spiritual value of the water, also in Greek mythology explaining natural karst phenomena was all related to goddess act (Kresic 2013). In particular, water has very spiritual value to Palestinians. With the start of religion in Palestine Cannon time (3300 B.C.) the people believed in the storm God 'Ba'al' to provide them with rainfall (López-Ruiz 2014). Until now, the term *Ba'al agriculture* in Arabic literature refers to rain-fed agriculture.

During the Islamic period in Palestine (starting around 900 A.D.), hydrotherapy was used for treating some medical conditions such as scabies, wound infections and fistula. With the presence of hot- and cold-water springs in the area, the sick person could take alternating hot/cold baths until cured (Al-Maqdisī 1906).

Moving to the last century, people still believed in the spirituality of water in particular springs. "Springs" represent a meeting point for lovers, brooks convey messages to the lost partner, and important events take place near water sources. Tales have been told about evil people trying to destroy a water source and how good spirits could protect the spring (Amsha 2009). There were tales as well of some springs that were haunted by evil powers (Canaan 1922). Springs also reflect Palestinian society's perception of men and woman, as Palestinian refer to springs that have continuous flow as "male springs" (Amsha 2009).

Spiritual values were also reflected in management practices during the Ottoman period. Since the establishment of the Nablus municipality in 1868 *springs were protected by law*. Spring houses and covered canal were built to safeguard them from pollution (Nablus Municipality). Later on, during the British mandate era, residents were concerned about the cleanliness of the spring area, about water leakage, and springs protection (Nablus Municipality 1925). Moreover, the municipality assigned inspectors to control the quality of spring areas (Nablus Municipality 1945).

Without doubt, water should be treated with respect and in a wise manner—for spiritual reasons, its sustainable utilization, its importance to biodiversity, and for the basis of governing and studying it.

### **1.2.2 Water resources and management condition in Palestine**

Despite the nonexistence of major rivers or surface water in Palestine, there has been an early development of agriculture. It is notable that the oldest evidence of agricultural practices was found to be implemented by the Natufian culture in the village of Shoqba, Palestine (Bar-Yosef 1998), which dates back to 11000 B.C. As this was one of the first communities to start agriculture on a small scale, water was the basis of development.

The rain-fed irrigation started with the beginning of agriculture. Fig and olive trees have been always considered as rain-fed plantations. In 1045, Naser el Khosraw wrote in his book *Safarnama* that rain-fed crops of olive, figs and grapes were planted in the vicinity of Jerusalem and Hebron. Olive oil was exported from Jerusalem to all over the world (Thackston 1986).

Currently, groundwater (springs, pumping wells) is the main supply for agricultural, domestic and industrial use as reported in *Status Report of Water Resources in the occupied State of Palestine–2012* (Palestinian Water Authority 2013). In 2013, it was estimated that 96.4% of the household were connected to the water network (PCBS 2015c). Yet, rain-fed irrigation is still a primary contributor for field crops and horticulture products (Haensel and Zurba 2015).

Water harvesting, water storage by cistern and mostly the transport of spring water via aqueducts were techniques used since Hellenistic times (Patrich and Amit 2002) until the introduction of modern water networks in the last century.

Specifically, aqueducts, they contain chemical, hydraulic information and management skills information. The chemical signature of the water is presented in the carbonate deposit of any old water structure (Underhill 1969; Carlut et al., 2009; Bobée et al. 2011; Sürmelihindi et al. 2013a; Sürmelihindi et al. 2013b; Pons-Branchu et al. 2014; Pons-Branchu et al. 2015). Moreover, carbonate deposits can also serve as chronological indicators and archives (Porath 2002). There are limited publications that deal with the analysis of carbonate as a chemical archive of the water quality, especially in the study area.

### **1.2.3 Water crisis in Palestine**

The fact that Palestinians neither have control of their water resources (Amnesty International 2009; Temper 2009; Hareuveni 2011), nor have sufficient management practices, the area faces a water supply crisis especially in the summer. The supply water deficit in 2014 was estimated at 37.8 million m<sup>3</sup> in the West Bank (PCBS 2015b). Currently, the area suffers from disputes over water supplies not only between itself and Israel but also at local levels.

Moreover, it is increasingly difficult to cope with droughts and floods that the area is facing. While the quantity and duration of rain did not change since the 1950s (Haensel and Zurba 2015), the problem of flooding can be only attributed to land use change and poor run-off drainage. For example, Jirzim mountain was once described in 1881 as a ‘Green Mountain’ (Conder and Kitchener 1882a) and as a green very intensively planted area around 900 A.D. to 1300 A.D. (Al-Maqdisī 1906; Ibn-Batuta 1964). It is now a fully developed urban area—a ‘concrete mountain’—as a result of the built-up area increasing tremendously after the Oslo agreements in 1994. The poorly designed system to collect run-off is not coping with the quantity of rain, which inevitably will cause floods. In some cases, flooding occurs due to the drainage being blocked by disposed waste.

In order to think out of the box, old water management practices were examined. While there is usually no accumulation of carbonate found in the ancient cisterns because harvested rainwater has a low saturation index (SI) with respect to carbonate minerals, there is accumulation in aqueducts and springs, which is the main topic here. The carbonate sinter sitting in the old aqueducts and springs has a story to tell. This thesis will explore that story in order to lay out the problems and analyze them.

### **1.3 Motivation**

Based on the background information it is possible to conclude that Palestine has abundant aqueducts, water conducts, and other historical water management tools. Nevertheless, the area suffers from acute water shortage and poor water management.

So the main objective of this thesis is to try to identify the mismanagement and try to examine these problems through e.g. geochemical analysis of carbonate sinter that has accumulated in layers in old water conducts. This thesis will also try to explain the growth mechanism of the secondary growth rate in this specific region. The reason behind element and isotope fractionation in the carbonate sinter is also a goal of this thesis.

Although a few studies have been conducted about this subject in the Mediterranean region, this is the first one in Palestine. This thesis will include underground tunnels that have carbonate sinter and aqueducts that have travertine. It is possible to compare these and determine best methods for managing the water supply, which will give this study an additional advantage.

One important objective of this study is trying to answer archeological questions through geochemical investigations (geo-archeology). Archeologist and humanities try to describe the picture (in this case the critical water situation) without going into explanations (Issar and Zohar 2004); this includes field studies, archeological excavations, and historical documents. Even more, it is not possible to have a complete picture due to political and logistic difficulties. While geo-archeology can give a comprehensive description of the area it also gives explanations of the history and the incitement factor of cultural change (Issar and Zohar 2004; Ruddiman 2013).

This study has three main objectives:

1. To examine the variation of the water quality over the last 2000 years in order to outline and explain the reasons for environmental degradation (i.e. anthropogenic input or climate change) in the study area.
2. To answer unsolved archeological questions in order to understand the water management system in Palestine.

3. To reconstruct or reinvent innovations for water and energy supplies and for management that are environmentally sustainable.

## **1.4 Hypothesis**

This research work focuses on Roman and Ottoman aqueducts in two areas of Palestine and in particular investigates the carbonate deposits and water sampled from the tunnels, springs, and watermills that form this water supply system. Through geochemical analysis, it examines and attempts to resolve the following questions:

1. Is urbanization a source of groundwater quality degradation?
2. Have water management practices been sustainable in the area?
3. Is it possible to answer archeological questions in this area through geochemical analysis?

## **1.5 Location of study area**

Basically there are two study areas located in Palestine: the first one is Nablus city and its surrounding area that represents the urban water network and the second is Al-Malih area, which is a remote nomad community in the northern part of the Jordan valley that represents the rural water utilization. Both study areas have climate and geological settings that are distinct from one another and will be described in the following section (Figure 1).

Nablus Governorate: Nablus city is the second largest city in the West Bank with 146493 people (PCBS 2015a). It is an ancient Palestinian city, with the oldest location (Tell Balata) belonging to the Bronze age (Campbell et al. 2002) and continued until the second century B.C. (Isaac 1998). The earliest beginnings of the current Nablus city history began the Iron Age, with settlement starting in the Hellenistic era 331 B.C. and developing into a city in 27 A.D. (Fanni 1999).

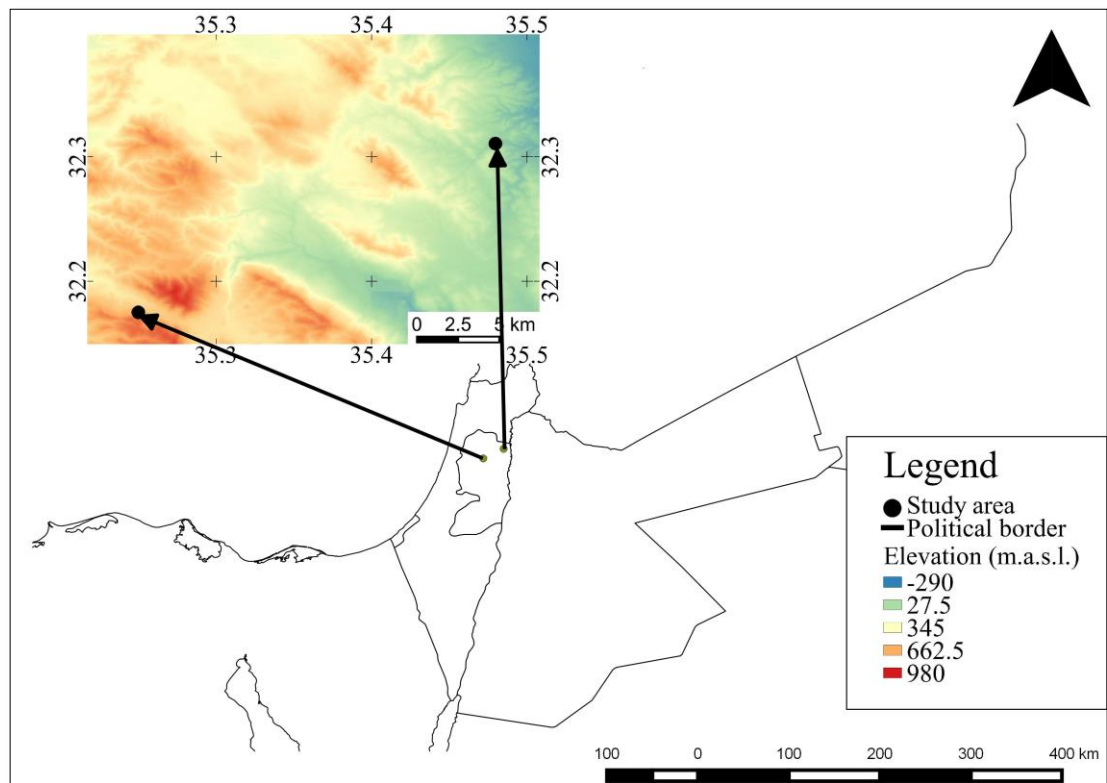


**Figure 1:** Map shows the study area in the West Bank (*upper left*) and its location in the Middle East (modified QGIS 2016; database for map generation: ASTER GDEM 2 satellite data from USGS Earth Explorer recorded in October 2011, <http://earthexplorer.usgs.gov> accessed on 20.07.2015).

In the same governorate, two ancient Palestinian villages are located to the north-western of Nablus, Sebastia (3036 inhabitants) and Ijnisinya (587 inhabitants) (PCBS 2015a). Sebastia was constructed by Herod in 27 B.C. Both villages were connected with roads (Chancey and Porter 2001).

Al Malih Locality is a very small remote area (370 inhabitants) (PCBS 2008). The location has limited buildings units (57 units) (PCBS 2008). Most of the buildings are simple and consist of cloth or plastic covers (Daraghma 2010). Yet, there are two stone buildings at this location that date back to at least the Ottoman period (Conder and Kitchener 1880; 1882a): the hotel and the watermill (Figure 2). The hotel is a two-story building; the first story belongs probably to the Ottoman period but the second story has steel I-beam structure which was introduced as construction technology during the British mandate period.



**Figure 2:** Buildings at Al Malih, *left:* Al Malih watermill and aqueduct, *right:* Al Malih hotel (Photo taken by Raghid Sabri, 2011)

### **1.5.1 Description of geology and hydrogeology of the study area**

The study area is part of the African–Arabian plate located in the north western margins of the Arabian Nubian continental craton (Flexer and Yellin-Dror 2009). Unlike the rest of the Arabian Peninsula, this part is characterized with a highly diversified morphology (Bender 1974). The western part of the study area, which represents the urban area, is on the border of the Dead Sea rift system. The eastern part of the study area which presents the rural area is part of the Jordan Valley–Dead Sea rift system (Flexer et al. 2009). The two areas differ distinguishably with respect to the stratigraphical level (Figure 3).

The outcrops of rocks in Nablus area are mainly Cretaceous carbonate sediments (Figure 4), whereas, the oldest rock outcropping in Al Malih area belong to the Jurassic period .

In the Nablus area Bethlehem and Jerusalem formations form the major aquifer with a thickness of 200–500 m. Mainly limestone and marl horizons contain well developed secondary porosity and permeability. The karstification process is still in development in this area, but the mature karst was developed during Pleistocene (Rofe and Raferty Consulting Engineers 1965). In Al Malih area, Lower Malih karstic and Ramali formations show high aquifer potential happening in a faulted area (Rofe and Raferty Consulting Engineers 1965).

Accordingly the groundwater movement in the area is divided at Faria anticline which is one of the dominating structures as a no flow boundary (Rofe and Raferty

Consulting Engineers 1965; Anker et al. 2009). The eastern and northern groundwater zones are considered in the study area.

Springs in the study area are divided into three groups; Nablus springs, Sebestia springs and Al Malih springs. Nablus and Sebestia springs groups are located to the west of Faria anticline and Al Malih group is located to the east of it.

Nablus springs originate from the base of Eocene, (at the boundary between Eocene and Senonian) (Rofe and Raferty Consulting Engineers 1965; Alawi et al. 2015). Sebestia (Sabastiya) springs group originate at the contact between limestone (Eocene) and chalk (lower Eocene) (Rofe and Raferty Consulting Engineers 1965). Both Nablus and Sebestia springs group are calcium carbonate type with calcium is the predominate cation.

Al Malih springs group: includes both thermal and minerals springs. The thermal springs group originate from Malih and Ramali formation (limestone and sandstone) with very high salinity and water temperatures of around 37°C (Rofe and Raferty Consulting Engineers 1965; Bender 1974; Möller et al. 2009a). Sodium is the dominate cation (20 times more Na than in the bicarbonate springs) and chloride is the predominate anion and this indicates possible water contact with halites evaporites. Halites are present in lower Beit Kahl formation (Raab, M et al. 1997).

The mineral springs, have less sodium but 3 times higher than in the calcium carbonate springs. The water originate from Ramali formation and has contact with igneous rock and limestone (Rofe and Raferty Consulting Engineers 1965).

The discharge trend of Nablus and Sebestia springs group differs from that of the Al Malih group. In Nablus and Sebestia the water discharge decreases in summer due to the absence of rainfall. The maximum spring discharge occurs four month after the maximum rainfall amount (Figure 5). Yet the Hammam Al Malih spring, respond differently to rainfall (Figure 6).

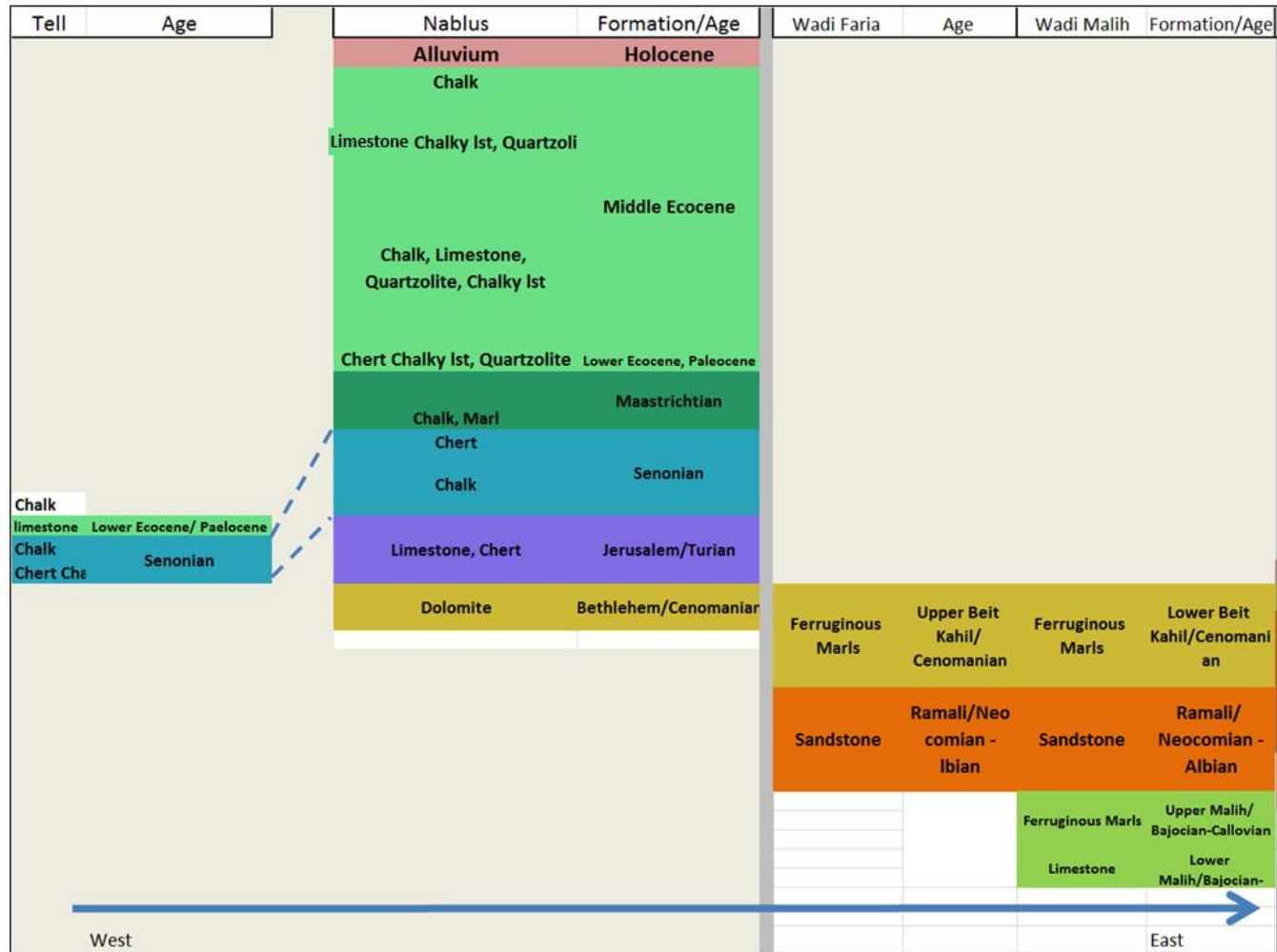


**Figure 3:** Stratigraphic table for the study area comparing eastern and northern zones (modified after Rofe and Raferty Consulting Engineers 1965; Cook 2011)

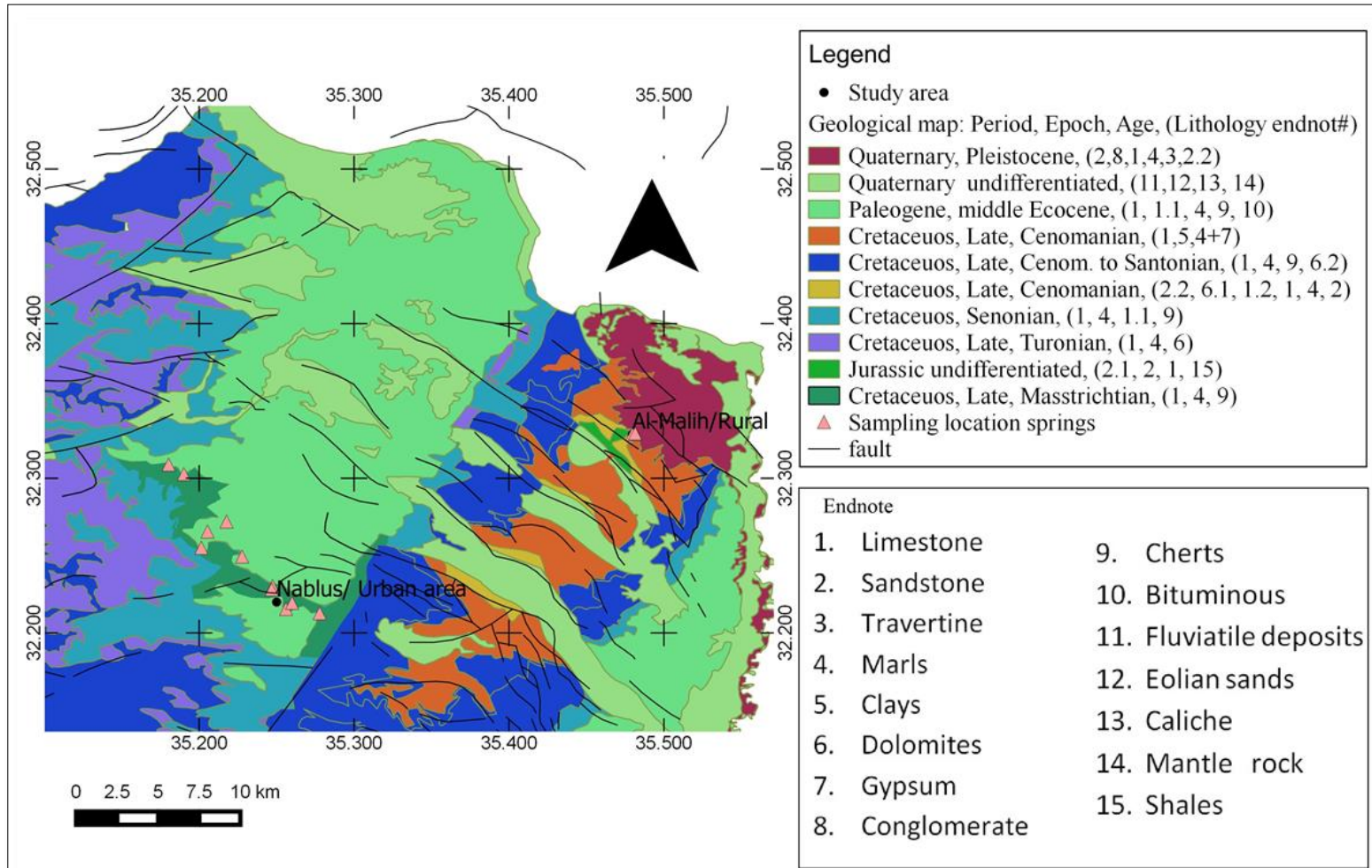


**Figure 4:** Geological map of the study area (modified using QGIS 2016 after Bender 1974; Palestinian Water Authority 2008; Cook 2011)

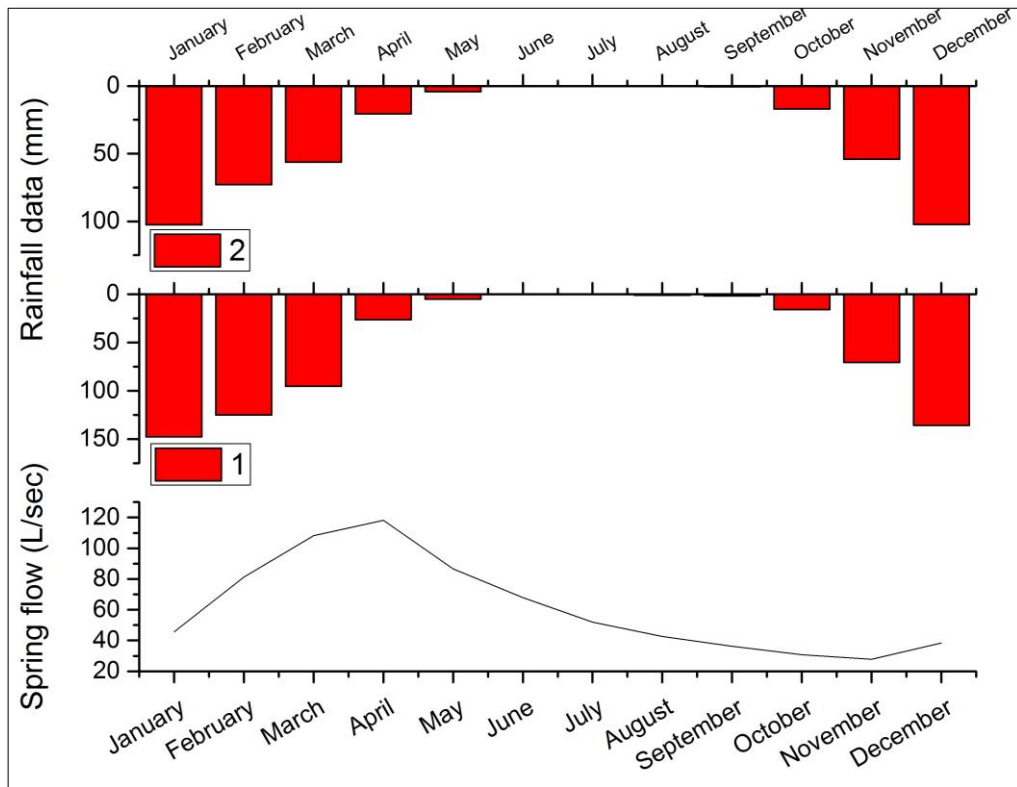


**Figure 5:** The average discharge of the springs in Nablus area from 1965–2000  
 Discharge data from (Palestinian Water Authority 2011a) <sup>1</sup>Rainfall data (AlKhalili 2000) and <sup>2</sup>Rainfall data VASClimO data grid 36707 (Beck et al. 2004)

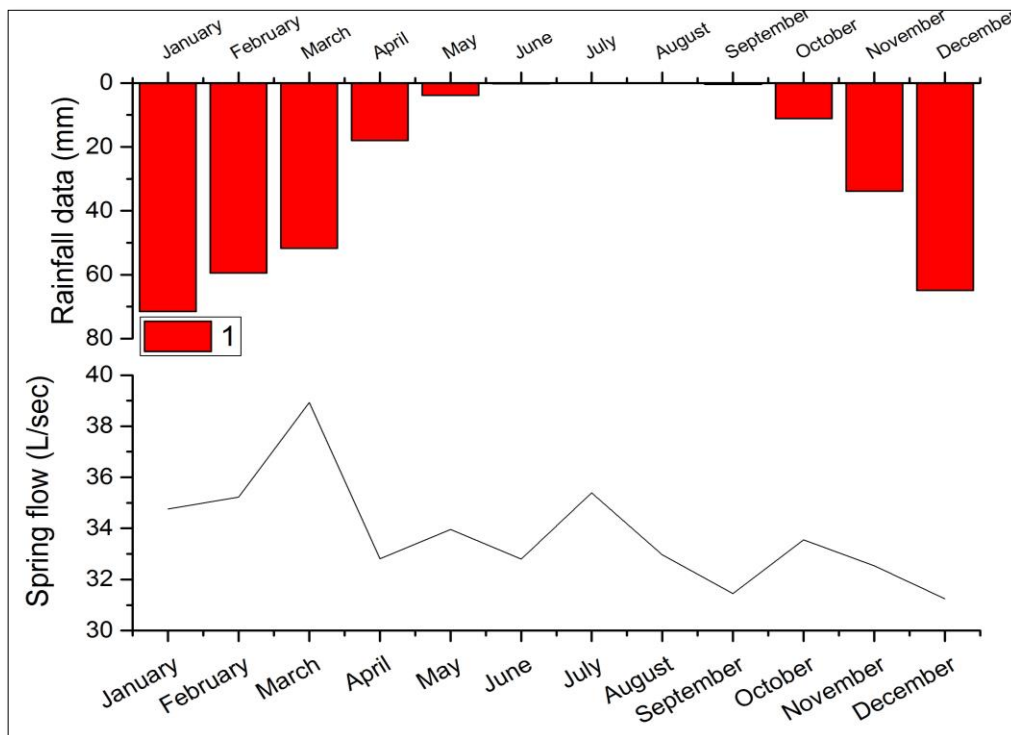


**Figure 6:** The average discharge of the springs in Al Malih area from 1965–2000  
 (Data from Palestinian Water Authority 2011a). <sup>1</sup>Rainfall data VASClimO data grid 36708 (Beck et al. 2004)

**Surface water**

As previously mentioned, surface water is not a reliable water resource in Palestine. In the study area, Wadi Malih contains the only catchment with a permanent small river. This size of catchment is 120 km<sup>2</sup> as shown in Figure 7, starting with an elevation around 500 m a.s.l. and ending –200 m a.s.l. m downstream. For the period 1962–1963, its estimated base flow was 1879300 m<sup>3</sup> (Rofe and Raferty Consulting Engineers 1965).

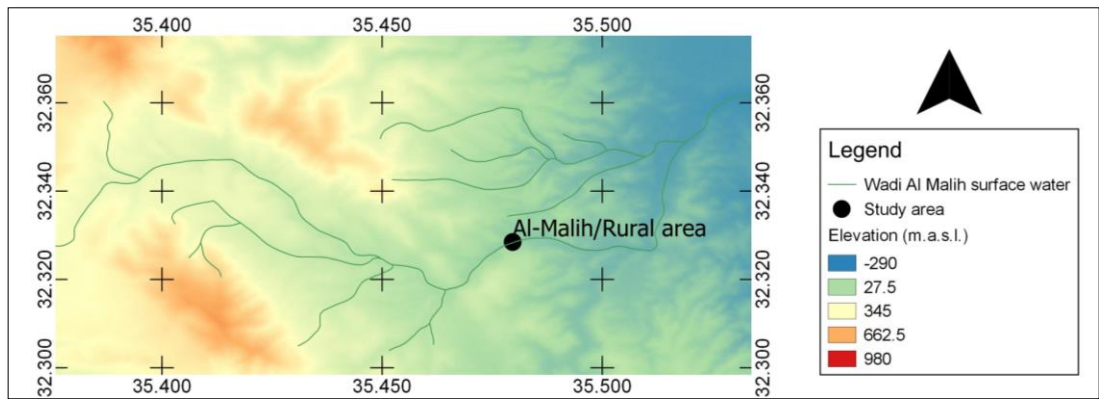


**Figure 7:** Wadi Al Malih surface water (modified after Palestinian Water Authority 2008; QGIS 2016)

**1.5.2 Climate**

The climate of the study area ranges from arid to dry sub humid and aridity increases moving towards the south-east. Dry rainfall years shift the scale towards aridity (Table 1). The aridity index is measured using P (precipitation) and PET (potential evapotranspiration) based on UNEP classification (UNEP 1992).

**Table 1:** Aridity zone according to P/PET index for the study area and its surrounding. (Temperature and potential evapotranspiration data are taken from: <sup>1</sup>Rofe and Raferty Consulting Engineers 1965; <sup>2</sup>PCBS 2009) \*dry year

Locations		Monitoring Periods			
		1952–1962 <sup>1</sup>	1962–1963 <sup>1*</sup>	1972–1997 <sup>2</sup>	1997–2008 <sup>2</sup>
Jenin		0.3	0.3	n/a	0.1
Tulkarem	Al Malih	0.4	0.2	n/a	0.5
	Nablus	0.4	0.2	0.3	0.3
	Jericho	n/a	n/a	0.1	0.1

Aridity Scale	Dry sub humid	0.5	Semi-arid	0.2	0.4	0.5	Arid	0.05	0.1	0.2
---------------	---------------	-----	-----------	-----	-----	-----	------	------	-----	-----

Between 1972–2008 the mean air temperature ranged from 17.6°C to 19.0°C in the Nablus area, mean maximum air temperature ranged from 21°C to 23°C and minimum mean air temperature ranged between 13.3°C and 14.8°C (PCBS 2009). There are no current readings at Al Malih, yet in 1962–1963, its mean air temperature was 28.1°C (Rofe and Raferty Consulting Engineers 1965).

The average rainfall in Nablus is 660 mm, in Al Malih (Tubas station) 431 mm and in Jerusalem 476.4 mm (Abualhaija et al. 2013). However, the average rainfall in Jerusalem during 1860–1880 was 586 mm (Rice 1886). This means that there is a 100 mm difference in average rainfall in the past 100 years.

The maximum rainfall amount happens between December and January (Table 2). In the past fifty years the wettest coldest winter was 1991/1992 and the driest hottest season was 1989/1990 (Haensel and Zurba 2015). There is a trend of temperature increase and precipitation decrease in the study area and at similar locations in the region (Kafle and Bruins 2009). Furthermore, the length of the rainy season has shortened (Haensel and Zurba 2015).

**Table 2:** Average monthly precipitation:

(Data from: <sup>1</sup>Rofe and Raferty Consulting Engineers 1965; <sup>2</sup>AlKhalili 2000; <sup>3</sup>Beck et al. 2004)

Year Span	1952–1963 <sup>1</sup>	1952–2000 <sup>2</sup>	1952–2000 <sup>3</sup>	1952–1963 <sup>1</sup>	1952–2000 <sup>3</sup>
Location	Nablus			Al Malih	
Unit	mm				
January		147.75	102.10		70.98
February		125.13	72.22		59.69
March		95.14	54.84		51.29
April		26.28	19.78		17.67
May		5.21	4.04		3.94
June		0.15	0.00		0.22
July		0.00	0.00		0.00
August		1.20	0.00		0.00
September		1.65	0.71		0.35
October		16.07	17.31		10.82
November		70.64	55.33		35.71
December		135.86	100.22		62.33
Annual Rainfall	594	625.07	426.55	332.00	313.00

### *Description of ancient climate*

The stable isotope analysis of the secondary carbonate precipitates of Soreq cave revealed that the climate before 6500 years differed completely from the present climate (Bar-Matthews et al. 1998). Within the past 6500 years there have been climate fluctuations; nevertheless, these were not vast fluctuations (Bar-Matthews et al. 1998). While the climate has been challenging for agriculture activity during the past 6500 years, the beginning of agriculture during the Natufian cultural 10000 years ago must have been in better conditions.

Based on historical events, Huntington (1908) stated that the area had once better climatic conditions making living easier in the Byzantine era. Other refused his theory and claimed that according to ancient scripts the climatic conditions have been always challenging and Huntington claims were not correlated with social, economic and cultural reasoning (Olmstead 1912). Many authors agreed with Olmstead (1912) as the understanding of advance research tools was missing and their theories were based on historical events explanations only (Issar and Zohar 2004). Huntington (1908) hypothesis was then proven by Hirschfeld (2004) research that the rainfall amount was higher in the Byzantine era, Hirschfeld (2004) performed paleoclimate construction based on archeological evidence. Furthermore, based on stable isotope data, evidence is given that the abandonments of upper Chalcolithic settlement was due to a warm dry period (Issar 1998). Moreover, the reduction of Al-Naqab desert settlements reached its maximum during the 8<sup>th</sup>/9<sup>th</sup> centuries due to a long drought period (Issar 1998).

On the other hand, from 650 A.D. to 1500 A.D., Arab and Muslims travelers were astonished by the natural fertility of the area (Le Strange 1890). Ibn-Batutua had described the area as having moderate climate not hot and not cold, with a plenty of green planted areas with small water brooks and springs (Ibn-Batuta 1964).

Even during summer around 900 A.D. dew accumulated in Al Aqsa gutters in sufficient quantities is reported (Al-Maqdisi 1906) Yet, the climate was described as hot with no wind in Jericho region, moderate temperature in Jerusalem and to the north (Baalbek in Lebanon) the temperature decreased (Al-Maqdisi 1906).

According to Al-Maqdisi (1906), Palestine had four seasons in the year and the rainy season started at the beginning of December. The water quality was good and in particular in Nablus, yet the water was also described as “rough” (Al-Maqdisi 1906). He also divided the land into four zones: the coastal area in the west, the mountainous planted area (trees, springs and farms, Nablus is included), the valley area planted with palms trees in the east and finally the desert in the south (Al-Maqdisi 1906).

To quantify the above descriptive information about the climate, the following table compares between the travelers and historical description and the responding calculated rainfall quantities for that period obtained from the literature.

Carbon isotope measurements ( $\delta^{13}\text{C}$ ) of Soreq cave samples indicate a variation of vegetation type. Values of  $\delta^{13}\text{C}$  fluctuated over 6500 years, nevertheless, it increases significantly through the past 800 years (Bar-Matthews et al. 1998). As can be seen from Table 3, the vegetation type changed from grapes and figs to wheat and cotton through the past 800 years.

The climate variation is noticeable as shown in Table 3 and it might have affected the agricultural activity, but it cannot be the only reason or the main reason for this. Different populations have lived under a variety of climate conditions in Jericho area for 10000 years; nevertheless, it has been an agricultural city in the driest phase. The ability to reach groundwater was the main factor of continuity (Issar and Zohar 2004; Koutsoyiannis et al. 2008). This same situation can be seen in the Nablus study area, during low precipitation periods (900–1300) the agricultural activities were intensive and formed the main economical drive. So the capability to utilize groundwater made agriculture possible.

On the other hand, climate condition affected historical events such as desert crossing. Excluding other factors, at precipitation rate of 460 mm Alexander the Great was able to cross Sinai desert but Napoleon’s army at precipitation rate of 380 mm could not (Huntington 1911).

**Table 3:** Ancient climate description of Palestine and surrounding areas and comparison between rainfall amounts calculated from isotopic data for two temperatures.

(Rainfall data: <sup>1</sup>Bar-Matthews et al. 1998; and climate descriptions: <sup>2</sup>Huntington 1911; <sup>3</sup>Campbell et al. 2002; <sup>4</sup>Iwais 2008; <sup>5</sup>Al-Maqdisi 1906; <sup>6</sup>Stern 1999, Natsheh et al. 2007, Milwright 2009, Taha 2009; <sup>7</sup>Ibn-Batuta 1964; <sup>8</sup>Rice 1886; <sup>9</sup>Abdel-Raheem 2011)

Year	Climate description	Rainfall (mm) calculated based on two different temperatures during carbonate precipitations	
		18°C <sup>1</sup>	20°C <sup>1</sup>
2294–2270 B.C.	The expansion of Lugalzagesi rule to the Syrian desert would not have happened in a climate similar to the current climate condition <sup>2</sup>	610	560
1500–1200 B.C.	Forests in the area <sup>2</sup> The absence of human settlement in Tel-Balata <sup>3</sup>	500	450
300–400 B.C.	Alexander crossing the Sinai desert <sup>2</sup>	510	460
B.C.–A.D.	Trade roads in the Roman times would be impossible to travel if it was as dry as it is now. Water supply of the city of Petra <sup>2</sup>	500	450
300–400 A.D.	Flourishment of agriculture in the early Byzantine era <sup>4</sup>	530	540
500–700 A.D.	Decline of agriculture in the late Byzantine era <sup>4</sup>	480	483
900 A.D.	Jericho was described as a hot area with no wind. To the north the area was more humid, yet, agricultural activity was intense in the area with fig, grape, and olive tree plantations <sup>5</sup>	505	445
1100 A.D.	The production of sugar flourished <sup>6</sup>	480	430
1300 A.D.	Ibn Batuta described the area as a “planted green area” (grapes, figs, and olive oil) with a moderate climate <sup>7</sup>	490	440
1500 A.D.	Production of sugar continued to flourish <sup>6</sup>	570	480
1779 A.D.	Napoleon’s army nearly unable to cross the Sinai desert <sup>2</sup>	450	380
1860–1880 A.D.	Actual rainfall quantity (586 mm) <sup>8</sup> Expansion of the agricultural activity, planting wheat, cotton and olive trees—although suffered drought years that ruined the production <sup>9</sup>	500	560

## **2. Literature review**

### **2.1 Research history of aqueducts**

Aqueducts have been studied for long time. Sextus Julius Frontinus maybe is the most famous one, writing about aqueducts in his book *The Water Supply of the City of Rome*. Although Frontinus's book did not include siphon (Nikolic 2008), Vitruvius' book *de architectura* included one section on aqueducts (section 8 Pollio 1860) and reported about siphon, which might be the only written record from antiquity that described siphon (Nikolic 2008).

*De architectura* contains information about constructing aqueducts and the instrument used to measure the slope. It also includes a water inspection method and detailed explanations about siphons and ventilation towers (Pollio 1860). Kessener tried to explain the purpose of the Aspendos<sup>1</sup> towers through numerical calculation (Kessener 2000) and hydraulic simulations (Kessener 2016).

Several scientists have tried to solve hydraulic questions through numerical equation and simulations. These studies mainly focus on aqueducts and have included Frontinus' work on the design, dimensions, slope, path and flow (Ortloff and Crouch 1998; Ortloff and Crouch 2001; Ortloff and Kassinos 2003; Ortloff 2005; Nikolic 2008; Long 2008; Temporelli and De Novellis 2010; De Feo et al. 2013).

### **2.2 Aqueducts in Palestine**

In this study aqueducts are divided according to their structural purpose: aqueducts at watermills and aqueducts for water transporting. In Palestine 60 watermills with adjacent aqueduct to operate the mills have been documented (Sabri et al. 2016).

In the book series *The Survey of Western Palestine*, 63 aqueducts or aqueduct systems were documented, of which 12 were used to provide water to watermills (Conder and Kitchener 1882a; 1882b; 1882c). These aqueducts were built between

---

<sup>1</sup> Aspendos towers are part of Aspendos aqueduct built in the 2<sup>nd</sup> Century in Aspendos, 50 km east of Antalya Turkey.

333 B.C. and the last century, mainly in the Roman period (Conder and Kitchener 1880; 1882a; 1882b).

In the book, *Aqueducts in Israel*, 28 water systems from the Hellenistic until the Byzantine period are described (Patrich and Amit 2002). The water systems components are tunnels, bridges (Figure 8), pipes and siphons. Herod Aqueduct shown in Figure 8 was mentioned in the work of Flavius Josephus (Josephus 1889).



**Figure 8:** Wadi Qilt bridge aqueduct from Herod era (Photo taken by Raghid Sabri 2008)

During the Islamic era several developments were made to the water systems in the area. This included additional water systems to newly developed cities and enlargement of the existing system (Petersen 2001) (Figure 9). A city like Jerusalem was supplied by springs through aqueducts in the Roman time (Conder and Kitchener 1882a; 1882b; 1882c; Masterman 1902; Frumkin and Shimron 2006), however, around 1000 A.D. the city was supplied by rainwater harvesting that used a sophisticated clean harvesting system with drains (Figure 10) and conduits so that “no drop of rain” could escape the system (Al-Maqdisi 1906; Thackston 1986).

During the Mamluk era around 1400 A.D., special efforts were made to supply water to Jerusalem through the rehabilitation of old aqueducts in order to convey the water

from Solomon's pool to Jerusalem, in addition to building new rainwater harvesting cisterns (Bakeer 2005).

In the late Ottoman era, water cisterns were abundant in houses and freshwater from springs was available (Sabri 1992). Water was transported using covered canals built in this era (Nablus Municipality).



**Figure 9:** Nablus aqueduct from Islamic era (Pointed Arches) (Photo taken by Raghid Sabri 2011)



**Figure 10:** Rainfall drain at Hisham Palace that was utilized until the 1400 A.D. (Whitcomb 1988) (Photo taken by Nidal Zorba)

### **2.2.1 Agricultural aqueducts (related to watermills) in Palestine**

From the Crusader period (1099–1187 A.D.) until the Mamluk (1291–1516 A.D.), sugar production flourished (Stern 1999; Natsheh et al. 2007; Milwright 2009; Taha 2009). One stage of sugar production involved the grinding of sugar cane with the

use of watermills. Accordingly, aqueducts for providing water to the watermills were built again.

After the Mamluk period, the sugar production ceased but the grinding of wheat using watermills continued until the introduction of electricity. Agriculture expanded during the Ottoman period, with increase of number of watermills and aqueducts (Ibraheem 2011). In some cases, the previous domestic aqueducts were adapted for agricultural use. As shown in (Figure 11), the stone building material that was used had different sizes. Large-sized stones at the base of the aqueduct wall represent the Roman time and the smaller sizes above that represent the Ottoman period.



**Figure 11:** Aqueduct connected to the watermill in Wadi Tufah area in Nablus (Photo taken by Raghid Sabri 2011)

The total number of aqueducts has not been identified yet, since there are continuous discoveries of aqueducts and water channels. Recently, in August 2015 a water channel that transported water to a church was found in Ramallah.

### **2.3 Utilization of springs in Palestine**

There are around 300 major springs in the West Bank, which produce an annual discharge of 54 MCM (million cubic meters) (Palestinian Water Authority 2013). Typically springs in the north-western West Bank are fracture springs and belong to

karst aquifers (Rofe and Raferty Consulting Engineers 1965; Abusaada and Sauter 2012; Alawi et al. 2015).

The utilization of springs for accessing groundwater sources has been a standard practice in Palestine for a long time. Of the documented aqueducts, 40% of the water sources were springs (Conder and Kitchener 1882a; 1882b; 1882c) and the other 60% were a combination of rivers and water harvesting pools. In the Nablus area, 3 springs have been in use since pre-Roman times, 8 since the Roman Empire, 1 since the Crusader period and another 2 since the Mamluk era. In the late Ottoman period, the major source of water besides rainfall was spring water (Sabri 1992).

The utilization of springs has also reached the energy sector. Groundwater springs were used to operate watermills since 2<sup>nd</sup> century A.D. (Oleson 1984; Wikander 1985). More to the point, hot springs had been used for heating houses and public baths (Al-Maqdisi 1906).

### **2.3.1 Ancient water system in Nablus–Sebestia**

As previously mentioned, Palestine suffers from water supply deficit that was estimated to be 36 million m<sup>3</sup> in 2014 (PCBS 2015b). This study area takes into account the ancient complicated water system in Nablus that is still visible but the connections between its parts are incomplete, damaged, or lost.

Many springs in Nablus–Sebestia (Dafna, Ras Al Ein, Qaryon, Harun and Ijnisinya) are still functioning as the main water supply and have been operating since ancient times (Crowfoot et al. 1966; Alawi et al. 2015). To enhance the production of springs, some were rehabilitated recently and the carbonate deposits were removed. Like the springs, the water aqueduct and tunnels remain as part of the heritage system.

Many researchers have investigated these springs in order to clarify the links between the water supply systems (Conder and Kitchener 1882a; Crowfoot et al. 1966 Fanni 1999; Frumkin 2002a; Frumkin and Shimron 2006). A brief description of the studied springs based on literature review follows:

- The Dafna spring house used to have large-sized stones and an aqueduct leading from the spring (Conder and Kitchener 1882a), but the aqueduct no longer exists. The spring was first utilized at the Hellenistic period (Alawi et al. 2015). It is connected to the Jacoup well (Alawi et al. 2015) to the east and is considered to be connected to six successive wells to the west through a tunnel (Fanni 1999; Frumkin 2002a). The tunnel was discovered in the 1970s. This tunnel is considered to have run under the main road during Roman times (*cardo decumanus*) and according to archeological findings is dated to the 2<sup>nd</sup> Century A.D. (Fanni 1999). On the other hand, it may have been possible that this tunnel was utilized for run-off water collection during the Mamluk period (Fanni 1999).
- Ras Al Ein is another major spring, which was dated to the Roman period, it has inspection chamber and tunnel leading to two different water sources (Fanni 1999; Frumkin 2002a).
- Qaryon spring was used to supply the Roman city Neoplis (now Nablus). A tunnel system was discovered to the south of the spring with no possibility to access it (Frumkin 2002a).
- Harun spring, which is located in Sebestia, has an inspection chamber and tunnel system similar to the Ras Al Ein spring (Frumkin 2002a), however, the dewatering tunnel was connected to additional sources (Crowfoot et al. 1966).
- Ijnisinya spring is very similar to Harun spring, however, with a much steeper slope and finer stone work (Crowfoot et al. 1966).
- The aqueduct in Al-Bezrah area (Beit Iba) is considered as part of the Nablus Roman water system going further to Harun spring and collecting water from Kfar Farat and Zawata springs (Frumkin 2002a)

One of the open questions about the ancient water system in Nablus city is whether there was any connection between the water networks in Nablus listed above and those in Sebestia (Frumkin 2002a). From the observations, three questions arise:

1. What was/were the earlier water source(s) for the tunnel in Nablus?
2. Was the tunnel used for collecting runoff surface water?
3. Which additional water source supplied Sebestia in the past (Harun spring)?

## **2.4 Carbonate sinter accumulation in aqueducts and artificial water network**

The dimension of aqueducts, water flow and numerical simulation are not described and discussed in this dissertation; instead, this work focuses on the occurrence of secondary carbonate in aqueducts, tunnels and spring houses is one of the major topics. Nearly all water structures contain secondary carbonate.

The accumulation of carbonate sinter in aqueducts and water structures was mentioned in *The water supply of the Rome* by Sextus Julius Frontinus as part of maintenance requirements (Frontinus 1925). Removing sinter from aqueducts and canals during the Roman times was the most important activity (Isaac 1958). Until now, the formation of scales due to an oversaturation of the water with respect to calcite is still a great problem that requires regular exchange of pipes in the water system.

The following picture (Figure 12) shows the growth of speleothem under the great pool in Jerusalem pool as Charles Warren examined it, as depicted in his book *The survey of western Palestine: Jerusalem*. In addition, Crowfoot et al. (1966) included a description of how thick the carbonate sinter lay inside the walls of the Ijnisinya spring were. It is very likely to have thick carbonate scale around the spring in this area (Underhill 1969).

Research on the sinter accumulation went from being descriptive to more analytical in the last 40 years. The scale growth rate was investigated in the Roman canal in the Jordan Valley (Underhill 1969).

Carbonate sinter from a water tower in the antique city of Ostia (Italy) was analyzed with high resolution laser ablation ICP–MS, the result shows high resolution seasonal trends that could help to explore past water management practices policies (Carlut et. al., 2009). By the use of high resolution particle induced X-ray emission, the carbonate deposits in a Roman aqueduct in Frejus (France) were investigated and their suitability for paleohydrological studies determined (Bobée et al. 2011).

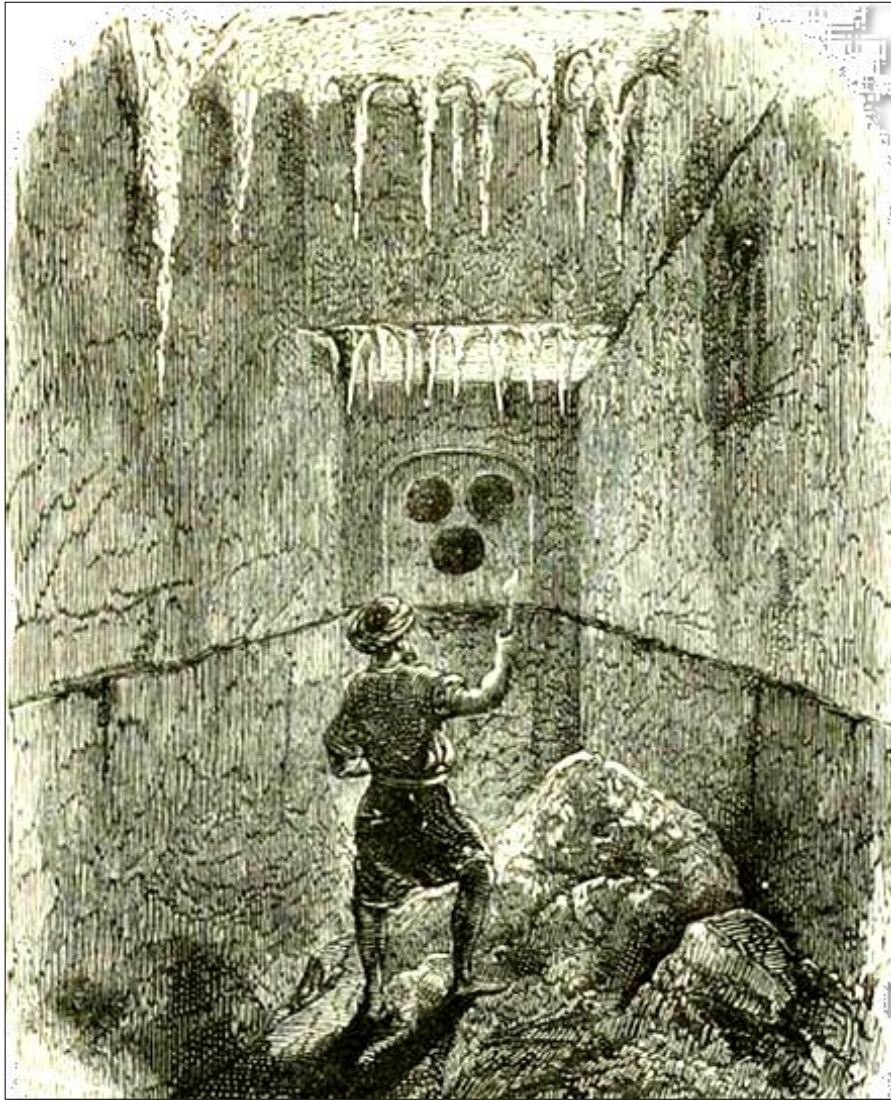


**Figure 12:** Speleothem under the western side of the dam to support the great pool (Conder and Kitchener 1884)

The Roman aqueducts in Patara and Aspendos (Turkey) were also studied. The carbonate deposits were sampled and analyzed optically and revealed the seasonality of the lamination. Stable isotope analyses were used to calculate the operating years of the aqueducts (Sürmelihindi et al. 2013a; 2013b).

The effect of urbanization was studied at the Parisian underground water aqueduct through the analysis of carbonate deposits. These deposits were dated and rare earth element (REE) variations in the deposits were measured. This revealed an increase in the REE concentration in second half of the 20<sup>th</sup> Century due to urbanization (Pons-Branchu et al. 2014). In another study at the Parisian aqueduct, high concentrations of heavy metals were recorded in carbonate deposits due to urban contamination since 1900, however, in the older part of this aqueduct, heavy metals concentrations

were also high due to application of fertilizer in vineyards located above it (Pons-Branchu et al. 2015).

Thus, it is clear to see how attention focused on the problematic build-up of carbonate deposit. The growth of carbonate particularly in Palestine is more likely to happen based on the aquifer type and water quality. Although carbonate represented an obstacle in the former times, carbonate now provides a record of what happened in the past.

In order to understand the entire process, key elements of carbonate growth have to be understood. The following section includes a brief history of speleothem, definitions, growth mechanism and speleothem analysis.

#### **2.4.1 Research history of secondary carbonate sinter**

Even before the process of carbonate sinter growth was understood, sinter was utilized for different purposes. As water was considered as medicine with very high spiritual values, secondary carbonate (especially moonmilk) powders were also used medically (Shaw 1997). From an architectural viewpoint, the ancient Maya employed and modified speleothem as part of their cave art production (Griffith and Jack 2005), although it is not known in which time period this happened. On the other hand, in the Mamluk era, speleothem and other natural shapes were visualized in ornate doors, as part of the Mamluk architecture. Most importantly, travertine was used as building material (Pentecost 2005). Yet, observing the secondary carbonate sinter and using it were insufficient pursuits, and there was an effort to learn more.

Hence, until the basic understanding of the chemical processes behind carbonate deposition became clear in the 19<sup>th</sup> century, there were many theories concerning the growth of speleothem. The oldest carbonate mineral script found on a bronze plate goes back to 823 B.C. In 1676 the growing mechanism of carbonate was studied with the idea that it grew like plants (Shaw 1997).

Table 4 is a brief summary of the milestones in understanding the speleothem phenomenon.

**Table 4:** Summary of the research history of carbonate deposits (modified after: <sup>1</sup>Shaw 1997; <sup>2</sup>Needham 1992; <sup>3</sup>Strabo 1854; <sup>4</sup>Pliny 1885; <sup>5</sup>Frontinus 1925; <sup>6</sup>Pentecost 2005; <sup>7</sup>Al-Maqdisi 1906; <sup>8</sup>Allison 1926; <sup>9</sup>Fairchild and Baker 2012)

<i>Year</i>	<i>Milestone</i>
823 B.C.	Bronze panels describe the trip of Shalmaneser King of Assyria to a cave with stalagmites <sup>1</sup>
400 B.C.	In China, Chi Ni Tzu described cave sediments <sup>2</sup>
100 B.C.	The growth of speleothem had no logical cause <sup>1</sup>
20 B.C.	Secondary carbonate were mentioned in Strabo's geography book 13, as consolidated water <sup>3</sup>
77 A.D.	Elder Pliny mentioned secondary carbonate as consolidated water in his book <i>Natural History</i> <sup>4</sup>
100 A.D.	For maintenance purposes, Sextus Julius Frontinus mentioned the accumulation of calcareous sinter in aqueducts and water structure <sup>5</sup> , but did not include its growth mechanism <sup>6</sup>
300 A.D.	In China, Ko Hung mentioned stalagmites in a cave in the Sho-shih <sup>1</sup>
600 A.D.	During the Tang dynasty epigeal travertine was well documented <sup>6</sup>
750 A.D.	Travertine as term was used in German-speaking area <sup>6</sup>
900 A.D.	Cave near Jerusalem was mentioned in Al-Maqdisi's book of travels <sup>7</sup>
1022 A.D.	Avicenna explained the growth of speleothem as an external petrifying power, deposited by material carried in water <sup>1</sup>
1535 A.D.	Berthold Buchner described the Breitenwinnerhöhle in Germany <sup>1</sup>
1564 A.D.	Palissy explained the growth as a deposit from solution in water <sup>1</sup>
1676 A.D.	Beaumont had several theories about growing speleothem: Vegetative growth, condensation from vapors and petrifying influence of vapor and air <sup>1</sup>
ca. 1700 A.D.	Ray and Woodward explained the growth as deposit from suspension in water <sup>1</sup>
1748 A.D.	Carlo Besuzzi and Josef Nagel made drawings about Macocha Cave <sup>1</sup>
1800 A.D.	Patrin: low form of life <sup>1</sup>
1811 A.D.	Macleay explained the growth as a deposit from solution in water <sup>1</sup>
1812–1881 A.D.	The growth of carbonate: as precipitation from solution in carbonic acid <sup>1</sup>
1926 A.D.	Secondary carbonate dating in Jacob's Cave <sup>8</sup>
1980 A.D.	Dreybrodt attempted the first kinetic model <sup>10</sup>

### 2.4.2 Growth mechanism of secondary carbonate

#### *Dissolution of carbonate (calcite)*

Dissolution of  $\text{CaCO}_3$  means that ions of Ca,  $\text{CO}_3^{2-}$  and  $\text{H}^+$  will leave the ionic lattice through marginal layer by diffusion. The dissolution rate will depend on the crystal type of the carbonate and the  $\text{CO}_2$  partial pressure ( $P_{\text{CO}_2}$ ) in the water (Bögli 1980).

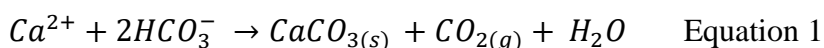
In shallow karst aquifers, percolating water partial pressure  $P_{\text{CO}_2}$  will increase due to soil respiration and organic matter decomposition. This water will dissolve carbonate minerals when it reaches the aquifer. As a consequence, the calcium and hydrogen-carbonate concentration will increase until they reach saturation with respect to calcite (Fairchild and Baker 2012).

But this cannot explain the dissolution happening in deep aquifers. Other conditions that can cause dissolution involve the mixing of two types of water with: different Ca content, different temperatures, different pressure dissolutions (Bögli 1980), different microbial biofilms (Jones 2010), volcanic  $\text{CO}_2$  and sulfuric acid due to oxidation of  $\text{H}_2\text{S}$ .

#### *Precipitation of secondary carbonate*

Any change in temperature,  $P_{\text{CO}_2}$  or in the concentration of any component will make the system to readjust of equilibrium (Bögli 1980). In this way, when the groundwater in a karst aquifer reaches a spring or tunnels, the water comes in contact with ambient air with lower  $P_{\text{CO}_2}$ , thus water will degas  $\text{CO}_2$  and thereby become oversaturated. As a consequence, this lead to carbonate precipitation (Bögli 1980; Fairchild and Baker 2012).

In addition, the  $\text{CO}_2$  in water can be also consumed by assimilating plants. Increasing the water temperature will as well reduce the amount of soluble  $\text{CO}_2$ . Any change in the channel shape will change the water volume and ultimately all of these processes will lead to precipitation (Bögli 1980).



However, several factors will limit the precipitation rates: the diffusion of  $\text{CO}_2$  molecules in the solution, the diffusion of  $\text{Ca}^{2+}$  and  $\text{CO}_3^{2-}$  in the solution, the

production of CO<sub>2</sub>, the deposition of calcite at the solid surface (Fairchild and Baker 2012), the presences of impurities in water and activity ratio (Tai et al. 2012).

### 2.4.3 Carbonate sinter analysis

Different isotopic, elemental and morphological analysis can be carried out on the different carbonate minerals to have different proxies for paleo climate, anthropogenic contamination and archeological connection. Here, a few of these analyses will be explained.

**Strontium isotope ( $^{87}\text{Sr}/^{86}\text{Sr}$ ) analysis:**  $^{87}\text{Sr}$  is radiogenic generated by decay of  $^{87}\text{Rb}$ . During precipitation, there is no strong fractionation of the ratio because of the rather identical chemical properties of both isotopes  $^{87}\text{Sr}$  and  $^{86}\text{Sr}$  (Fairchild and Baker 2012; Slovak and Paytan 2012). Thus, the ratio can be used to identify the water source (Fairchild and Baker 2012) and paleomobility (Slovak and Paytan 2012).

**Uranium isotope ( $^{234}\text{U}/^{238}\text{U}$ ) analysis:**  $^{234}\text{U}$  is generated by the  $\beta$ -decay of  $^{238}\text{U}$  and due to weathering of rocks and water–rock interaction, fractionation of  $^{234}\text{U}$  to  $^{238}\text{U}$  occurs and this give different signature to different water bodies (Zhao et al. 2009). This ratio is used for U–Th dating, and can be also used/correlated with the Strontium isotope ratio to identify the water source (Drexler et al. 2014). As for Sr, there is also only minor fractionation during precipitation (Andersen et al. 2009; Fairchild and Baker 2012).

**U/Th disequilibrium dating (carbonate dating):** Th has a rather low solubility in comparison with U. Therefore, U is likely to be transported and eventually incorporated in carbonate, while this is not the case for Th. The U will start radioactive decay to Th as shown in Figure 13 (Fairchild and Baker 2012). Thus, the built up of Th can be used as indicator for time since precipitation.

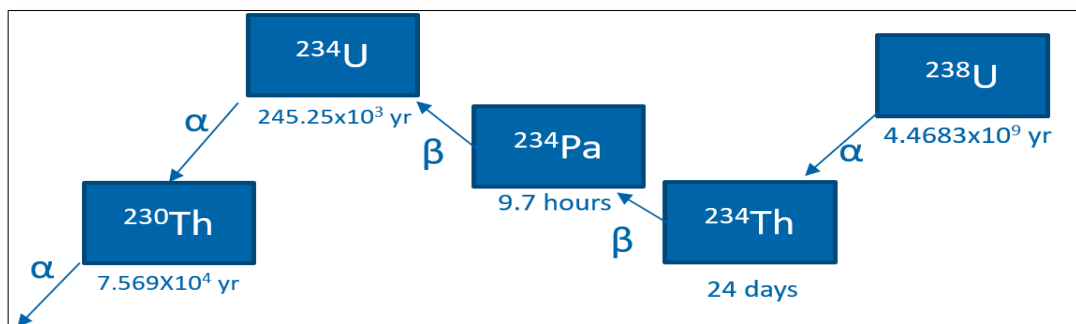


**Figure 13:**  $^{238}\text{U}$  decay through  $^{230}\text{Th}$ , with half-life (modified after Edwards 1988; Fairchild and Baker 2012)

**Stable isotope analysis ( $\delta^{18}\text{O}$ ,  $\delta^{13}\text{C}$ ):**  $\delta^{13}\text{C}$  isotopic signature in the secondary carbonate reflects the geochemical condition during precipitation (Clark and Fritz 1997). Usually the ratio values for carbonate are reported as per mil (‰) relative to Vienna Pee Dee Belemnite (VPDB) standard. However, before using up the total amount of this standard, it was calibrated to NBS19 or NBS18 (Clark and Fritz 1997). The production of  $\delta^{13}\text{C}$  is a result of reactions in soil- $\text{CO}_2$  that is derived from C3 and C4 plants (Bar-Matthews et al. 1998). Therefore, it is possible to use  $\delta^{13}\text{C}$  to identify the origin of the water (Clark and Fritz 1997) and the type of vegetation cover (C3, C4) that the water went through during percolations (Bar-Matthews et al. 1998).

Unlike  $\delta^{13}\text{C}$ , it is not possible to use  $^{18}\text{O}$  as a tracer because in the dissolved phase  $^{18}\text{O}$  exchange with water (Clark and Fritz 1997). However,  $^{18}\text{O}$  in secondary carbonate reflects the composition of water; the fractionation is high and temperature dependent (Fairchild and Baker 2012). Hence, the temperature during the precipitation can be revealed (Clark and Fritz 1997). In Palestine, lower  $^{18}\text{O}$  values mean wetter conditions, and higher  $^{18}\text{O}$  values mean drier conditions (Bar-Matthews et al. 1998). Finally, all these isotopic values can be used as a multi isotope systematic approach, which is a powerful tool to trace the source of the water.

**Element analysis:** any element (mostly metals with valence 2) in the periodic table can incorporate within the calcite crystals due to the bound shape and position between the oxygen atoms and cations (Fairchild and Baker 2012). Trace elements and rare earth elements can reveal seasonality, climate condition and anthropological pollution (Fairchild and Baker 2012; Pons-Branchu et al. 2014; Pons-Branchu et al. 2015). Partitioning of trace element is controlled by the chemical bonding between cation and calcite, the size difference and chemical potential between the  $\text{Ca}^{2+}$  and the substituting ions (Fairchild and Baker 2012). Yet, Mg and Sr behavior is coupled and the partitioning depends highly on the growth rate speed (Fairchild and Baker 2012) On the other hand, rare earth element partitioning does not depend on growth rate (Fairchild and Baker 2012). Close to the study area, the correlation between Mg and Sr is observed in a dry year (Orland et al. 2014).

**Petrological analysis:** Defining the crystals' shapes can reveal the important information about the hydrogeology, the influence of bio-precipitation and the diagenesis identification. Moreover, the crystal type and dimension give information

about the water flow rate (Frisia and Borsato 2010). To include crystal type analysis in the geochemistry data, a coding system is used (Table 5) (Frisia 2015).

**Table 5:** Crystal type and the representing code number as suggested by Frisia (2015)

<i>Crystal type</i>	<i>Code number</i>
Columnar	1
Columnar open	2
Columnar elongated	3
Columnar with lateral overgrowths	4
Columnar fascicular optic	5
Columnar radial fibrous	5.5
Columnar microcrystalline	6
Dendritic	7
Micrite	8
Microsparite	9
Mimetic	10
Mosaic calcite	11
Mosaic calcite with visible aragonite needle relicts	12

Counting the carbonate laminae can be used to date the carbonate sinter if the hydrological conditions are known. This method as well as trace element peak counting has proven to give accurate results (< 3%) (Fairchild and Baker 2012).

### 3. Methodology

#### 3.1 Literature review

University libraries that have old archives and Ottoman records were visited. The Nablus municipality library was also visited; all documents relating to water resources were collected. All the documents in the municipality of Nablus go back to the British mandate period and were scanned for later reference. The Internet Archive database portal, <https://archive.org>, was used to download ancient text.

The Ministry of Agriculture in Palestine provided information on daily rainfall data. The Palestinian Water Authority (PWA) provided the spring discharge data: from 1965 to 2000 monthly data for the discharge from springs were available; from 2000 to 2010 the data provided are averaged monthly flow rates. In addition to the PWA database (Palestinian Water Authority 2011b), the ‘Nablus District Water Resources Survey: Geological and Hydrological Report’ from February 1965 (Rofe and Raftery Consulting Engineers 1965) and the book *Nablus Spring Source of Life Through History* (Alawi et al. 2015) were also used.

Using the USGS Earth Explorer database, ASTER GDEM 2 images were downloaded (USGS 2011) for further processing using GOCAD (a computer-aided approach for modeling of geological objects in the subsurface) and QGIS (Quantum Geographic Information System). Furthermore, images from Landsat 1 (USGS 1973), Landsat 5 (USGS 1987), Landsat 7 (USGS 2009), Landsat 8 (USGS 2015) were also downloaded for landuse analysis.

This was done to clearly delineate the study area, which includes two locations: the Nablus area representing a typical urban area and Al Malih representing a remote rural area. As shown in Chapter 2, aqueducts and spring houses/wells (small buildings constructed over a spring or well) are distributed throughout the entire region. The aqueduct in the city of Nablus was just archeologically excavated in 1970s and no further studies were conducted so far. Al Malih in the Jordan Valley, part of the study area, suffers from negligence.

### **3.2 Fieldwork**

Field trips were made through the study area in summers of 2011 and 2014 in order to observe the condition of the ancient water supply system condition and sample its water and carbonate deposits. Subsequently, water samples, carbonate sinter samples from aqueduct and deposit from springs were taken.

After receiving official approval from the Nablus municipality, water and carbonate samples were taken from five springs in the city of Nablus accompanied by a representative from the municipal water quality department. All springs were visited and both carbonate and water samples were taken from each. This included villages located to the west of Nablus city, where the main sources of water are historical springs. After receiving approval from the Ministry of Tourism and Archeology in Ramallah, field visits were made to the aqueduct and archeological locations, accompanied by the Ministry field engineer.

During the fieldwork, in-situ measurements of the pH-value, temperature, dissolved oxygen, redox potential and electrical conductivity of the spring waters were carried out using WTW® field instruments.

All sampling locations and the number of samples are summarized in Figure 14 and Table 6, in which the entrance points of springs are indicated by the letter *S* and aqueducts are indicated by *A*.

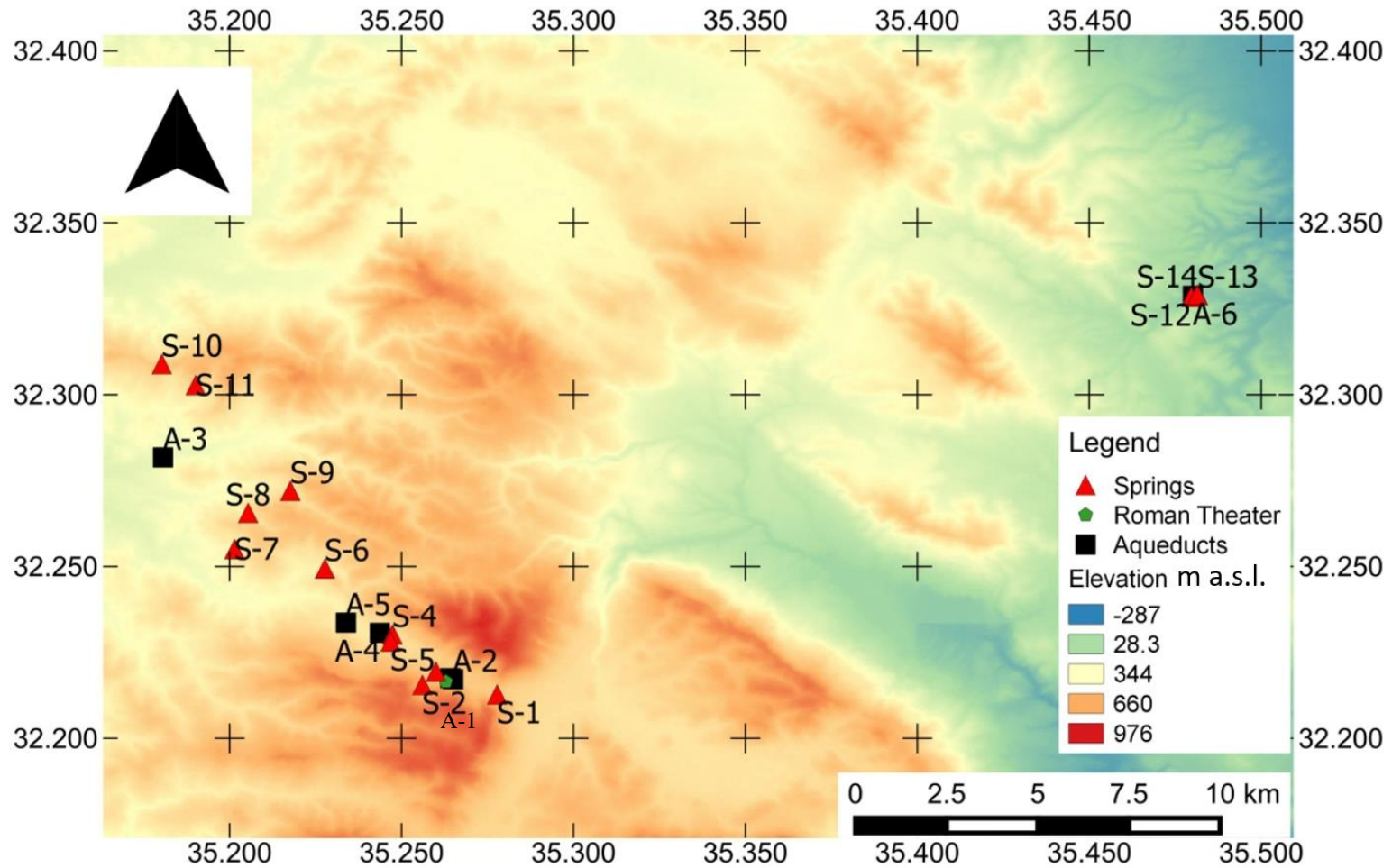


**Figure 14:** Topographic map of the study area in Palestine shows the sampling locations of springs (S) and aqueducts (A) (QGIS 2016, USGS 2011: Data base for map generation: ASTER GDEM 2 satellite data 60x60 recorded in October 2011 from USGS Earth Explorer: <http://earthexplorer.usgs.gov> (accessed on 20.07.2015))

**Table 6:** Sample type and locations

<i>Sample names</i>	<i>Sample #</i>	<i>Coordinates (UPS,WGS 84)</i>		<i>Elevation m.a.s.l</i>	<i>Sample type</i>	
		Easting	Northing		Water	Carbonate sinters
Dafna	S-1	35 16 678	32 12 806	560	×	—
Ras al Ein	S-2	35 15 21.60	32 12 55.86	620	×	×
Qaryon	S-3	351535.7	32 13 8.52	470	×	×
Beit Al-Ma	S-4	35 14 842	32 13 802	458	×	—
Al Subyan	S-5	35 14 811	32 13 685	474	×	—
Zawata	S-6	35 13 657	32 14 944	412	×	—
Kfar Farat	S-7	35 12 081	32 15 293	416	×	—
Harun	S-8	35 12 306	32 15 927	449	×	×
Ijnisinya	S-9	35 13 055	32 16 315	445	×	×
Ein Al Hud	S-10	35 10 845	32 18 323	478	×	—
Qabu	S-11	35 11 406	32 18 176	503	×	—
Hammam Al Malih	S-12	35 28 779	32 19 708	-30	×	—
Tayoon	S-13	35 28 896	32 19 739	-31	×	×
Wadi Al Malih	S-14	35 28 887	32 19 742	-28	×	×
Tunnel	A-1	35 15 847	32 13 057	560	×	×
Well Shaft	A-2				—	×
Masudiah*	A-3	35 10 837	32 16 905	283	—	×
Wadi Tufah*	A-4	35 14 37	32 13 50	450	—	×
Al-Bezrah*	A-5	35 14 03	32 14 02	414	—	×
Theater		35 15 772	32 12 989	563	—	×
Watermill	A-6	35 28 48	32 19 43	-28	—	×

\* Aqueduct

### 3.3 Sampling and analysis

#### 3.3.1 Water samples:

In total 17 water samples were collected from 16 groundwater sources. Nine precipitation samples (rainwater, snow and runoff) were collected for isotope analysis during the period 2011 until 2014. High-density polyethylene bottles with a 30-ml volume were used for isotope analysis samples. For trace analysis, the samples were filtered in the field into these bottles and two drops of 65% ultra-pure HNO<sub>3</sub> were added. For the TIC (total inorganic carbon), cation and anion measurements, 100-ml polyethylene bottles were used for sampling.

Oxygen stable isotopes (<sup>16</sup>O, <sup>18</sup>O) and <sup>2</sup>H were measured by means of an LGR liquid–water isotope analyzer (DLT-100), with a precision of < 0.3‰ for oxygen isotope and 0.6 ‰ for <sup>2</sup>H. An ICP–MS (inductive coupled plasma mass spectrometry, X Series 2, Thermo Scientific) instrument was used for determining the element concentration in the water samples. Internal standards (5 mg/l Ge, 1 mg/l Rh and 1 mg/l Re) were used to compensate matrix effect with reproducibility of 5%. Direct mode or collision mode was used according to the measured element. The precision and reproducibility was about 5%.

In addition, ion chromatography (IC Metrohm 881 compact) was used to analyze cations (Li, Na, NH<sub>4</sub>, K) with Metrohm column C4/100, using 2 mM HNO<sub>3</sub> + 0.7 mM dipicolinic acid eluent. Anions (Cl<sup>-</sup>, Br<sup>-</sup>, NO<sub>2</sub><sup>-</sup>, NO<sub>3</sub><sup>-</sup>, SO<sub>4</sub><sup>2-</sup>) were analyzed with Metrohm A Sub A 15/150 /4.0 and with 3 mM NaHCO<sub>3</sub> and 3.5 mM Na<sub>2</sub>CO<sub>3</sub> as eluent. Total inorganic carbon measurements were analyzed using the LiquiTOC II instrument. The above equipment was available at the Hydrogeology Department of the TU Bergakademie Freiberg.

##### 3.3.1.1 Strontium analysis: <sup>87</sup>Sr/<sup>86</sup>Sr

For <sup>87</sup>Sr/<sup>86</sup>Sr analysis, clean Savillex Teflon<sup>®</sup> vials were used. After the vials were rinsed with distilled water and placed for 10 min in an ultrasonic cleaner, they were soaked first for 1 week with HNO<sub>3</sub>, thereafter 1 week with HF, and finally 1 week with HCl.

Depending on the Sr concentration of the sample, 7 ml of each groundwater sample and 50 ml of each rainfall/runoff/snow sample were evaporated at 80°C (Figure 15). The residue was dissolved in 0.1 ml 3.5 N HNO<sub>3</sub>.



**Figure 15:** Clean oven for drying water samples at the Isotope Geochemistry and Geochronology Laboratory at the Mineralogy Department of the Technical University Bergakademie Freiberg, Germany.

The samples were then passed through resin spec (50–100 µm) preconditioned cation–exchange micro columns (200 µl) and loaded into tungsten filament with 1 N H<sub>3</sub>PO<sub>4</sub> (Pin and Bassin 1992). Finally, the samples were measured with the TIMS (thermal ionization mass spectrometer Finnigan MAT 262). For determining the Sr isotope ratio, NBS 987 standard was used with external reproducibility of ±0.00005. The external reproducibility was used as the instrument error because it was higher than the internal error of the measurements. The entire equipment for Sr–isotope determination was available at the Mineralogy Department of TU Bergakademie Freiberg.

#### 3.3.2 Carbonate samples

Around 20 kg of solid samples were extracted from the depositions in either spring dewatering tunnels (when available) or in aqueduct depositions—in total at 9 locations, represented by 30 samples. Other water samples and core samples were

taken from aqueducts and canals at 5 locations, represented by 33 samples. The samples comprised mainly specimens of carbonate, clay, plaster and building stone.

#### ***Sampling methods***

When possible, an electric drill corer 10 cm in diameter was used to extract samples. A chisel and hammer were used inside the spring in order to not pollute the spring with dust from drilling (Figure 16). For each sample, carbonate was extracted towards the host rock to ensure sample material representative of its complete growth from the beginning of precipitation.



**Figure 16:** Sampling methods using: *left* a core drill and *right* a chisel

#### ***Sample processing and analysis***

According to the type of the analysis, each carbonate sample was processed in different way. Samples were cut in half along the growth axis. Polished thin sections were made using one half of each sample at the Institute of Geology and Paleontology (TU Bergakademie Freiberg). First, the thin sections were examined using polarized optical microscopy with a CCD (charge-coupled devices) camera at different magnifications. These images provide information about the crystal type, growth and lamination thickness; furthermore, the number of laminations were counted. Then the thin sections were examined using a Bruker Nano GmbH, Quantax SEM-EDS (scanning electron microscopy with energy-dispersive X-ray spectroscopy). Each sample was examined along its axis of total growth. Several spots on the same layer were more closely examined to classify types of minerals and

identify impurities in the calcite. The detection limit ranges between 1500–2000 ppm. The result is converted from counts/elements-to-weight concentration. It was possible with SEM–EDS to obtain high-resolution results, but because the detection limit was problematic, it was not possible to quantify REE (rare earth elements).

The other half of each sample was washed with deionized water, and then polished (Dorale et al. 2004; Spötl and Matthey 2006). Thereafter, each laminated layer was extracted using Olympus SZ61 New Wave research MicroMill with the smallest bit diameter of 0.5 mm (Figure 17). After each extraction, the drill bit was cleaned with ethanol 99%. Extraction of the sample is time consuming in comparison to laser ablation, but it has higher precision (Spötl and Matthey 2006; Hoffmann et al. 2009). Moreover, for each layer 3 portions of the same sample were needed for the  $^{18}\text{O}$ ,  $^{13}\text{C}$ , and Sr isotope ratio and element analysis.



**Figure 17:** Drill bit of 0.5 mm

The MicroMill instrument was equipped with a computer, high-resolution microscope and CCD video camera to control the drilling. Using the software (MicroMill software V1.4.1), each drill line was assigned after calibrating the X, Y for the sample. Depending on carbonate sinter type, mostly it was possible to do

continuous drill line, however, sometimes drilling was only possible with spot drilling. The drill depth never exceeded 90  $\mu\text{m}$ .

For the element concentration measurements, 5 mg of each extracted lamination layer was dissolved in 100  $\mu\text{L}$   $\text{HNO}_3$  and subsequently analyzed using ICP–MS (Fairchild and Baker 2012). To avoid the problem of high intensity of the samples, blank samples were placed frequently between the samples. As all the analytes are detectable, no separation of elements was needed. Yet external calibration with three internal standards (5mg/l Ge, 1 mg/l Rh and 1 mg/l Re ) was performed (Agatemor and Beauchemin 2011). Any value below the blank was discarded.

For the Sr isotope ratio analysis, 2 to 5 laminations from each sample were selected. For the sample preparation, the drilled samples were washed with a weak acid to remove the detritus material (Ruppel et al. 1996; Bailey et al. 2000; Li et al. 2011).

Thereafter, 10 mg of the sample was diluted in 1 ml 0.05 M HCl for 2 h without heating and the solutions were centrifuged. The supernatant was discarded. This procedure ensures a 40% mass reduction of the sample. Then, the residue was diluted in 1 ml 0.5 M HCl subsequently analyzed using TIMS (thermal ionization mass spectrometer Finnigan MAT 262). Using the Sr isotope ratio, it is possible to define the source of water and estimate the age of the carbonate if it belongs to marine water.

In the same way, selected layers of each sample were chosen for stable isotope analysis ( $^{18}\text{O}$ ,  $^{13}\text{C}$ ). The analyses were conducted at the GeoZentrum Nordbayern, Erlangen University. At 70°C the carbonate powder reacted with 100% phosphoric acid using a Gasbench II, which was connected to a ThermoFinnigan Five Plus masspectrometer. The analyses were performed using standard that is calibrated to NBS19 with a reproducibility  $\pm 0.06\%$ .

#### **3.3.3 U–Th series dating**

Dating carbonate was done using U–Th series. For the U–Th series, the values of  $^{238}\text{U}$  and  $\left[\frac{^{234}\text{U}}{^{238}\text{U}}\right]$  and  $\left[\frac{^{230}\text{Th}}{^{234}\text{U}}\right]$  are needed. The  $^{230}\text{Th}$  concentration is very low in any

sample, so separation and purification was essential in order to be able to do the measurement (Dorale et al. 2004).

#### *Sample preparation for U–Th series dating*

Five samples were chosen depending on the microstructure of the lamination for U–Th dating. The compaction of the lamination layer is an indicator of a closed system, which means a good candidate sample for U–Th–Pa dating (Dorale et al. 2004; Spötl and Boch 2012) From each sample, two to four laminations were sampled using a micro sawing drill (Figure 18). This is important to reduce the contamination of the sample.

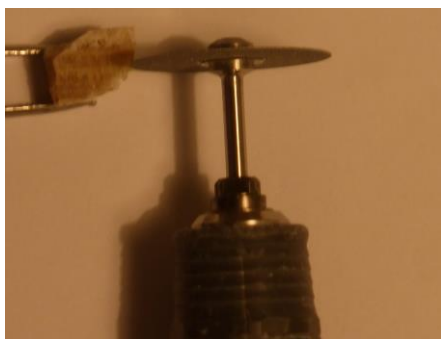


**Figure 18:** Sampling Ras al Ein Sample for U–Th series analysis

A spike ( $^{229}\text{Th}$ – $^{233}\text{U}$ – $^{236}\text{U}$ ) was weighed and added to each sample in a Teflon beaker. To dissolve the sample, 11 N HCl pure was used and drops of water were added to avoid the dust and aggressive reaction. Coprecipitation of U–Th was done using  $\text{Fe}(\text{OH})_3$ , which is added to the solution to have acidic solution. Then  $\text{NH}_4\text{OH}$  is added to form a precipitate. After centrifuging at 3000 revolutions per minute (RPM), the supernatant is discarded. Then the precipitate was dissolved with 500  $\mu\text{l}$  3 N  $\text{HNO}_3$ . At this point, the samples were ready for the separation process.

#### *U–Th separation*

The separation and purification of U–Th was done according to the procedure of Pons-Branchu et. al at the Laboratoire des Sciences du Climat et de l'Environnement (LSCE, France). A 0.5-ml column filled with Teva resin (Eichrom) was used for the separation. At the bottom of the column, a pre-filter resin (Eichrom) was used to remove organic colloids from the solution. The Th fraction was eluted by 2.5 ml 3N HCl and U fraction was eluted by 3.5 ml 1N HCl.

### ***U–Th measurements***

After preparing the U–Th fraction solutions, the concentration of  $^{238}\text{U}$  and  $\left[\frac{^{234}\text{U}}{^{238}\text{U}}\right]$  and  $\left[\frac{^{230}\text{Th}}{^{234}\text{U}}\right]$  were measured using the Thermo Neptune plus MC–ICP–MS instrument at the LSCE. The  $^{230}\text{Th} / ^{234}\text{U}$  values were measured using the ion counting and  $^{238}\text{U}$  and  $^{229}\text{Th}$  were measured using the faraday cup. The standard sample bracketing (spike and HU–1 uraninite standard) method was used to correct the matrix effect of ICP–MS. After measuring the values, the following equation (Dorale et al. 2004) was used to calculate the age.

$$\left[\frac{^{230}\text{Th}}{^{238}\text{U}}\right] = 1 - e^{-\lambda_{230}T} + \left(\frac{\delta^{234}\text{U}_{(m)}}{1000}\right) \left(\frac{\lambda_{230}}{\lambda_{230} - \lambda_{234}}\right) (1 - e^{(\lambda_{234} - \lambda_{230})T})$$

**Equation 2**

The STRUTages numerical calculation program was used to correct for the high initial  $\frac{^{230}\text{Th}}{^{232}\text{Th}}$  and activity ratio in carbonates using a Monte Carlo Method by combining the isochron techniques and stratigraphical constrains (Roy-Barman and Pons-Branchu 2016).

### **3.4 Software used**

PHREEQC was used to calculate the percentage error and saturation index with WATEQ4F database. Furthermore, different statistical analyses were performed using Excel, STATGRAPHICS Centurion XVI version 16.1.11 and OriginPro 2015. The software, GOCAD (a computer-aided approach for modeling of 3D geological objects) was used to build a simplified geological model. QGIS (Quantum Geographic Information System) was used for digital elevation model and land-use processing.

### **3.5 Challenges**

Organizing and obtaining permission from local authorities took quite some time before sampling could begin. Access to some of the springs required permissions from two authorities. There were also numerous technical and official difficulties. For example, it was not possible to carry the sample core all the time within the

spring sample sites, as the physical movement at sites was difficult. Although court records could not be accessed from the Ottoman period, which mention the types of aqueduct in the Palestinian history, several documents written about these court records were available. Only the data record on spring flow and water level from the last 10 years could be obtained from the Palestinian Water Authority.

## 4. Results and discussion (Nablus area)

### 4.1 Ancient water system description

During the field visit, descriptive data on the springs and aqueducts was collected. A brief summary about the locations follows.

S-1: Dafna spring (meaning oleander) is located at 560 m a.s.l. It is a major spring supplying the eastern part of the city and is supervised by the municipality. Its water runs through a water pipe driven by two pumps. Carbonate deposits were not found since these deposits were all destroyed during rehabilitation of the infrastructure of the spring in 2010.

S-2: Ras al Ein (Figure 19), located at 620 m a.s.l. It is located on the Mountain Jirzim and may be accessed via a locked door located on the mountainside at some distance from the street. This door leads down a flight of hundreds of stairs to an underground tunnel, where walking is difficult and crawling is the only way to reach the spring.

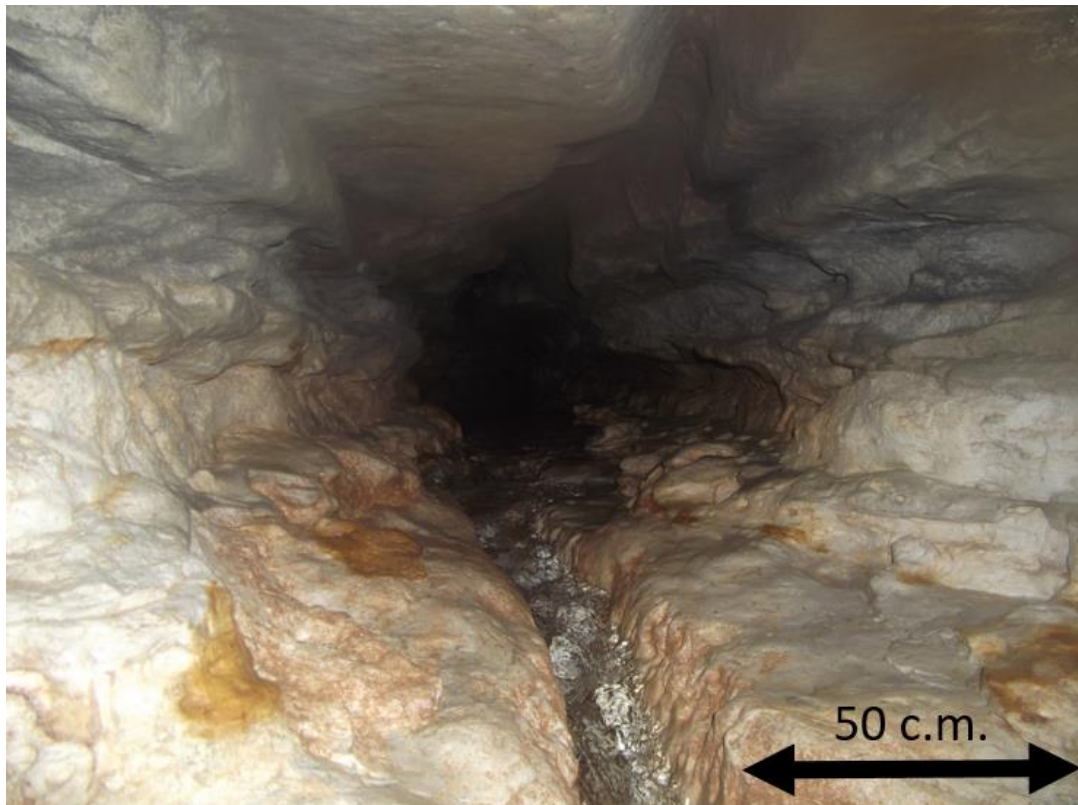


**Figure 19:** The Ras al Ein spring S-2 (Photo taken by Raghid Sabri 2011)

S-3: Qaryon spring is in a huge Roman building (Figure 20) located 470 m a.s.l. Inside the building, a stairs descends underground to a door that enters into a tunnel leading to the spring. The host rock in the tunnels is soft.

S-4: Beit Al-Ma spring is located at 458 m a.s.l. in an underground stone chamber beneath a street, where the water is pumped to supply the west section of the city. Water seeps into the cave, via by a small channel from the northern side. It is possible to reach the cave by stairs, but it was difficult to pass through the channel. Carbonate deposits were not found in this spring.

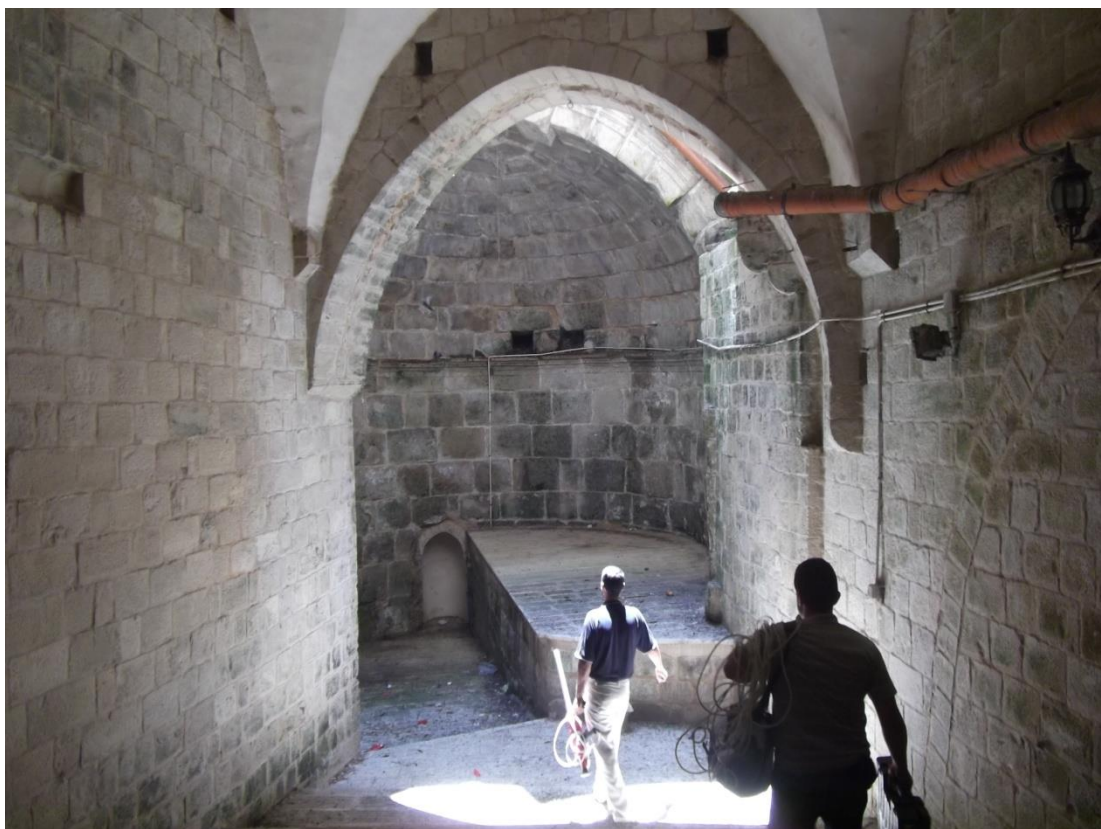


**Figure 20:** Qaryon spring house S-3 (Photo taken by Raghid Sabri 2011)

S-5: Al Subyan spring, located at 474 m a.s.l. is a small spring used by local people. It has a long narrow tunnel under the surface (Figure 21), that leads the water to a 1-m<sup>2</sup> room, with the water depth of circa 50 cm.

S-6: Zawata spring is located in Zawata village at 412 m a.s.l. The spring was rehabilitated recently and only its outlet was accessible. It was not possible to access the tunnel or to investigate the carbonate sinter.

S-7: Kfar Farat spring is located in Naqoura village to the west of Nablus at 416 m a.s.l. This spring is believed to be a source of water for the main aqueduct from Nablus to the village of Sebestia. This spring was rehabilitated and now is covered by a concrete structure with a metal opening on the top. At the northern side inside the concrete structure, there is a tunnel leading to the spring source that was dug into the host rock, which is soft.



**Figure 21:** Tunnel to Al Subyan spring S-5 (Photo taken by Raghid Sabri 2011)

S-8: Harun is the major spring in Sebestia located at 449 m a.s.l. The entrance to the spring is immediately at the spring chamber. A metal ladder is used to enter the spring, which descends to a small room that leads to a tunnel dug out of the stone. The dimensions of this tunnel are: circa 50 m long and 50 cm wide and high. The tunnel is built of large stone blocks and becomes wider as it proceeds to a second room that has cross-shaped roof with very small opening at the top. The entire room and its roof were built of stone blocks. At the opposite side of the chamber, there is another tunnel of a different size (Figure 22) where water enters the room. At the end of the second tunnel, there is a collecting chamber where water seeps in from beneath

it (Figure 23). It has been reported that this room was connected to a tunnel with an unknown source (Crowfoot et al. 1966).



**Figure 22:** One tunnel at Harun spring S-8 (Photo taken by Raghid Sabri 2011)

There are two hypotheses linked to this probable connection. Either it was linked to the Ijnisinya water system or to the water system in Nablus through Naqoura village (Crowfoot et al. 1966; Frumkin and Shimron 2006), which are based on remains of aqueducts found in the surrounding area. The carbonate sinter accumulation is located under a manmade hole that is now closed with debris where currently no water is flowing. The shape of the carbonate sinter appear as if the water was exiting the pipe and by this it is concluded that this chamber was connected to additional source (Figure 24).

S-9: Ijnisinya spring is located in Ijnisinya village (near Sebestia) at 445 m a.s.l. In addition to the public network, the spring is a major water supply for the village. The entrance to the spring is located between houses in the village. A 40-cm<sup>2</sup> metal door on the ground surface provides access to a deep round shaft, which has a diameter of about 2 m and a depth of 5 m. It is only accessible by using a portable ladder (Figure

25). The depth of the water was around 1 m, however, at the time of this visit the spring's supply was insufficient. Above the water level, there are two openings: one is completely blocked with soil and mud, while the other is partially closed with mud. It was possible to enter through the opening and after 400 m, there was a room in to which water seeps.



**Figure 23:** Harun Spring at the connection of the two tunnels S-8 (Photo taken by Raghid Sabri 2011)

It was possible to observe the similarities in the inspection room and tunnels during the field visit between Ijnisinya spring and Harun spring. In general, the carbonate sinter in Ijnisinya is the more diverse than all other springs and aqueduct (Figure 26).

S-10: Ein Al-Hud at 478 m a.s.l. and S-11: Al Qabu at 503 m a.s.l. are two springs located in the town Burqa. These springs, along with the seasonally running Wadi in winter, head towards an aqueduct located downhill at a location called Al-Masudiah.

A-1: The tunnel with its entrance level is located at 560 m a.s.l. It was not possible to explore the total length of it, but based on six shaft wells between Dafna spring and the tunnel entrance, it has been suggested that the water from Dafna spring had been feeding into this tunnel (Figure 27) (Fanni 1999).

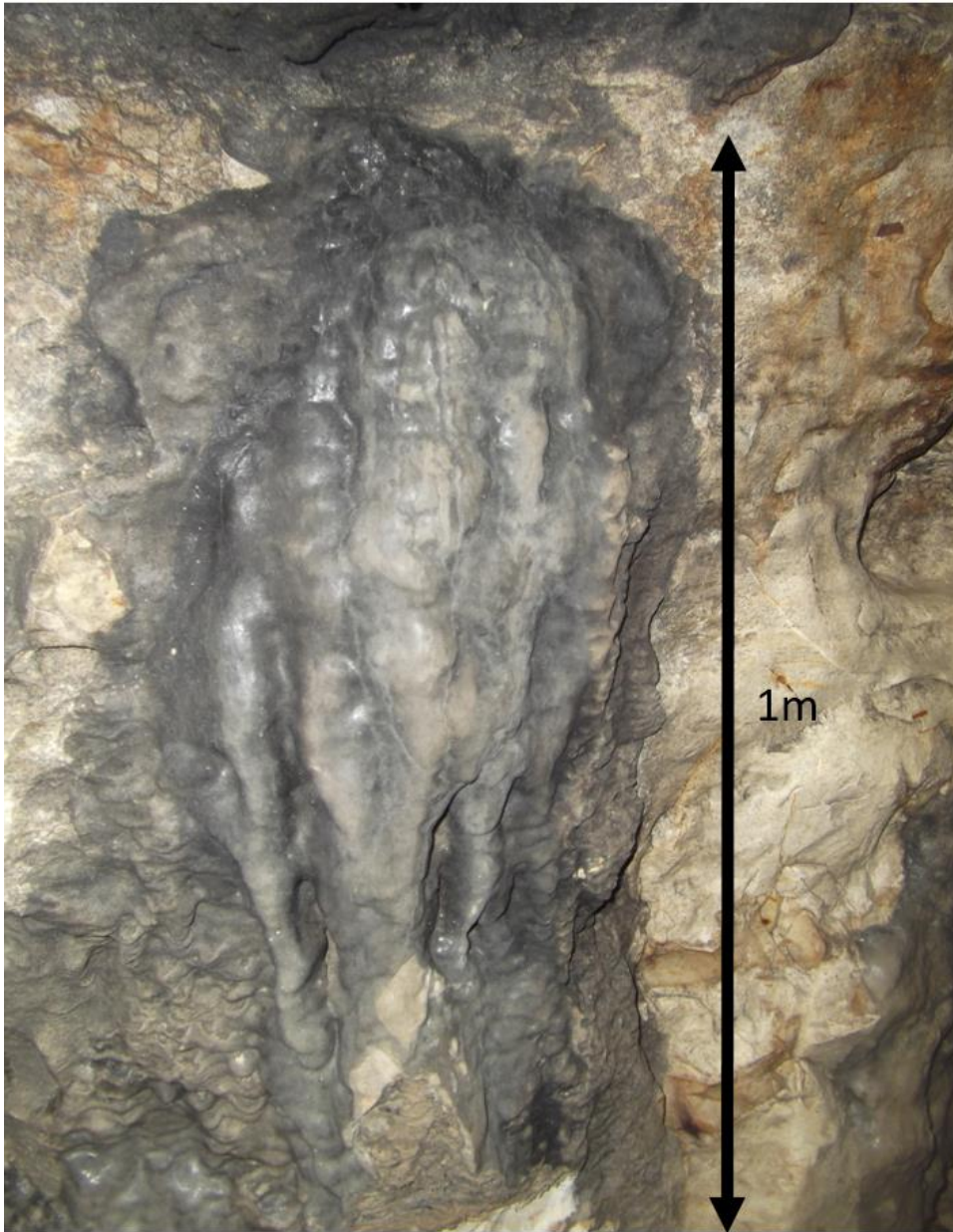


**Figure 24:** Carbonate sinter accumulated at the entrance of Harun spring tunnel S-8 (Photo taken by Raghid Sabri 2011)



**Figure 25:** Ijnisinya spring S-9 (Photo taken by Raghid Sabri 2011)  
*Left:* Access down by a portable ladder (view from below), *right:* the tunnel towards Ijnisinya spring



**Figure 26:** Different carbonate shapes at Ijnisinya spring walls (S-10) *left: drapery cave minerals, top right: popcorn cave minerals, lower right: down flowstone* (Photos taken by Seif Shenawi 2011)

From its upper entrance, 74 steps descend down to the tunnel. Then a slab is reached to enter the tunnel, where the tunnel runs eastward to arrive at one shaft well, Dullab A-2 (Figure 27), which is located 16 m below street level. The tunnel varies in its dimensions. At first, walking is easy at a 2-m height and 0.6-m width and then it becomes more difficult as the height lowers to 1.3 m. Water seeps in through the cracks in the well. This well shaft was known to the local people before the discovery of the tunnel and was considered as the water source.

A-3: The Aqueduct Masudiah (Figure 28), located at 283 m a.s.l., is connected to a watermill. No carbonate deposits were visible.

A-4: The Wadi Tufah Aqueduct (Figure 28), located at 450 m a.s.l., is considered to be an industrial-agricultural aqueduct, because it was built downstream of a water dam to deliver water at a certain height elevation to a watermill for flour production. This watermill has two drop shafts, which is evidence that it used to work with two rotating stones. Using a stone construction style, the entire watermill structure had been built in several stages. Soda straw carbonates were visible along the wall of the aqueduct (Figure 30).

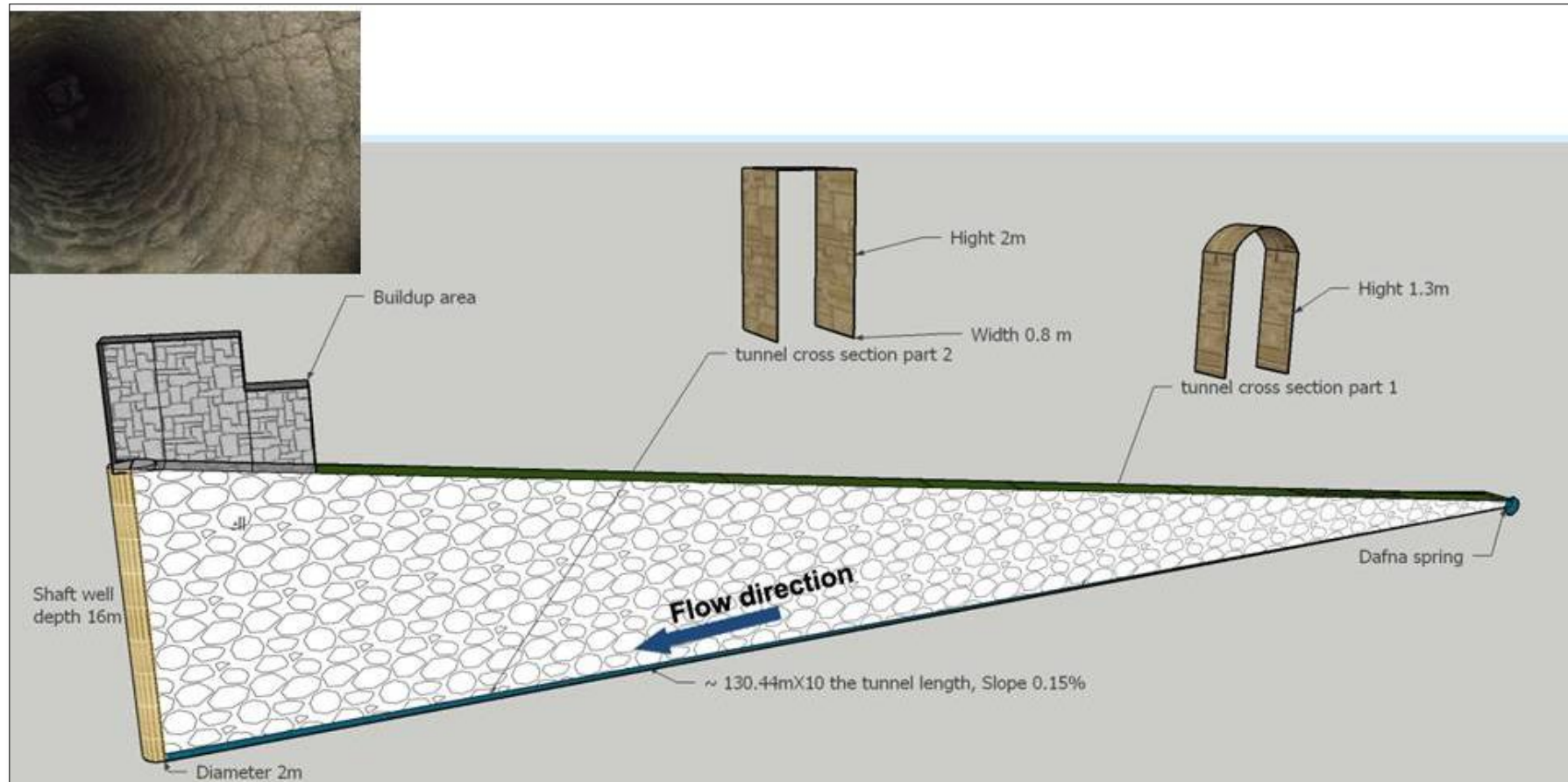


**Figure 27:** Section of the tunnel from Dafna spring to the extraction well, *corner left* shows the view to the drop shaft looking upwards (Photo taken by Raghid Sabri 2011)



**Figure 28:** *Right:* Wadi Tufah aqueduct (A-4), *left:* part of Masudiah aqueduct (A-3), where no trace of carbonate was found (Photos taken by Raghid Sabri 2011)

A-5: The aqueduct in Al-Bezrah is located at 414 m a.s.l.; the total length and path of the aqueduct cannot be traced because it is now surrounded by buildings (Figure 29). The carbonate sinter in the aqueduct was not thick—one layer of sinter (Figure 30)



**Figure 29:** Aqueduct Beit Iba A-5 (Photo taken by Raghid Sabri 2011)

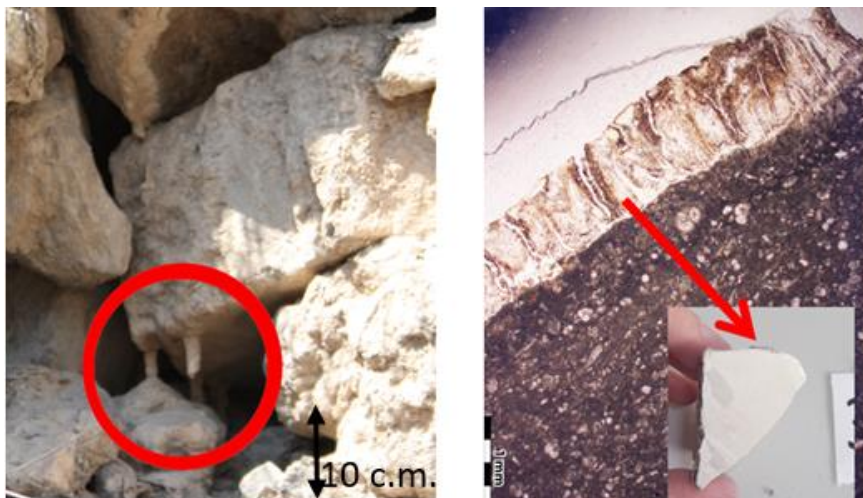


**Figure 30:** *Left:* Part of Wadi Tufah Aqueduct shows the soda straw sampled; *right:* thin section of sample from Al-Bezrah aqueduct shows the dimension of the sinter

## 4.2 Water sample results and discussion

Water analysis of this study agrees with previous studies (Figure 31 and Figure 32). The two groups of springs at Nablus and Sebestia are both calcium hydrogencarbonate types with calcium as the predominant cation. There is linear trend toward the north-west decreasing calcium and increasing sodium concentrations. The water in tunnel at A1 and A2 differs significantly with high sodium concentration, which can be explained by wastewater contamination.

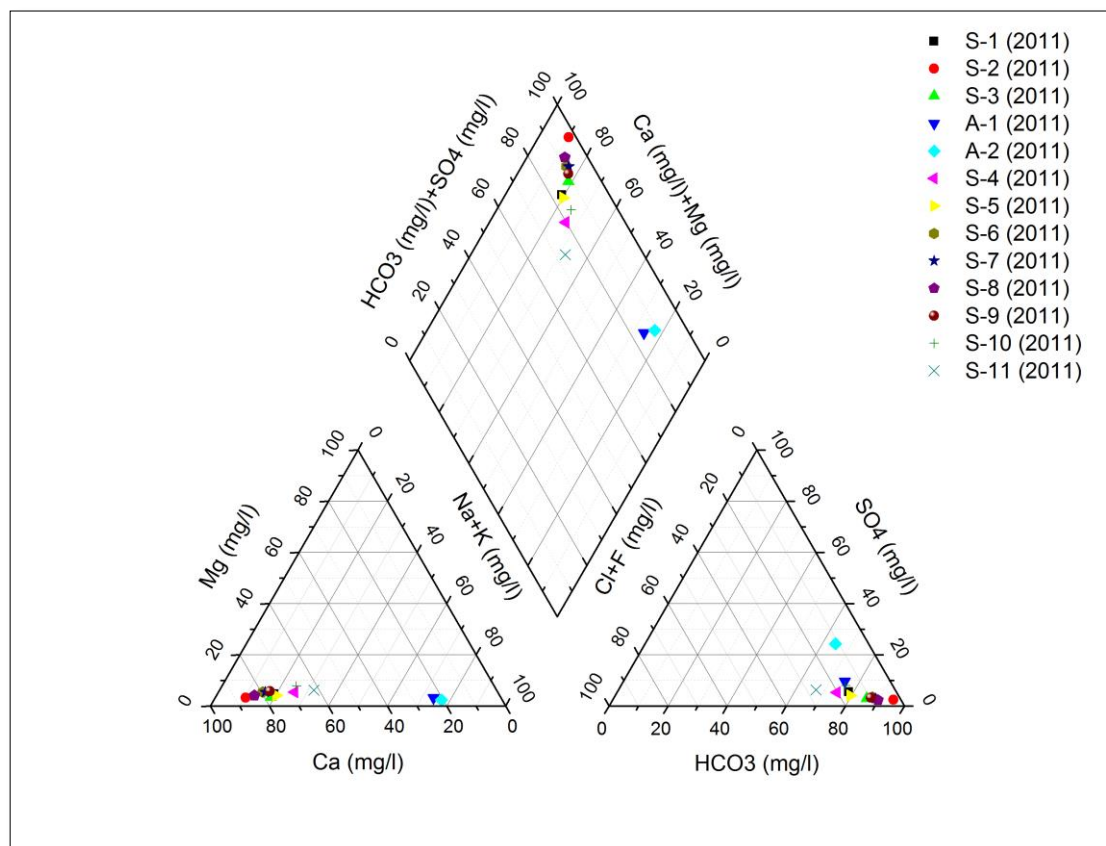


**Figure 31:** Piper diagram shows springs distributions (water sampling conducted August 2011)

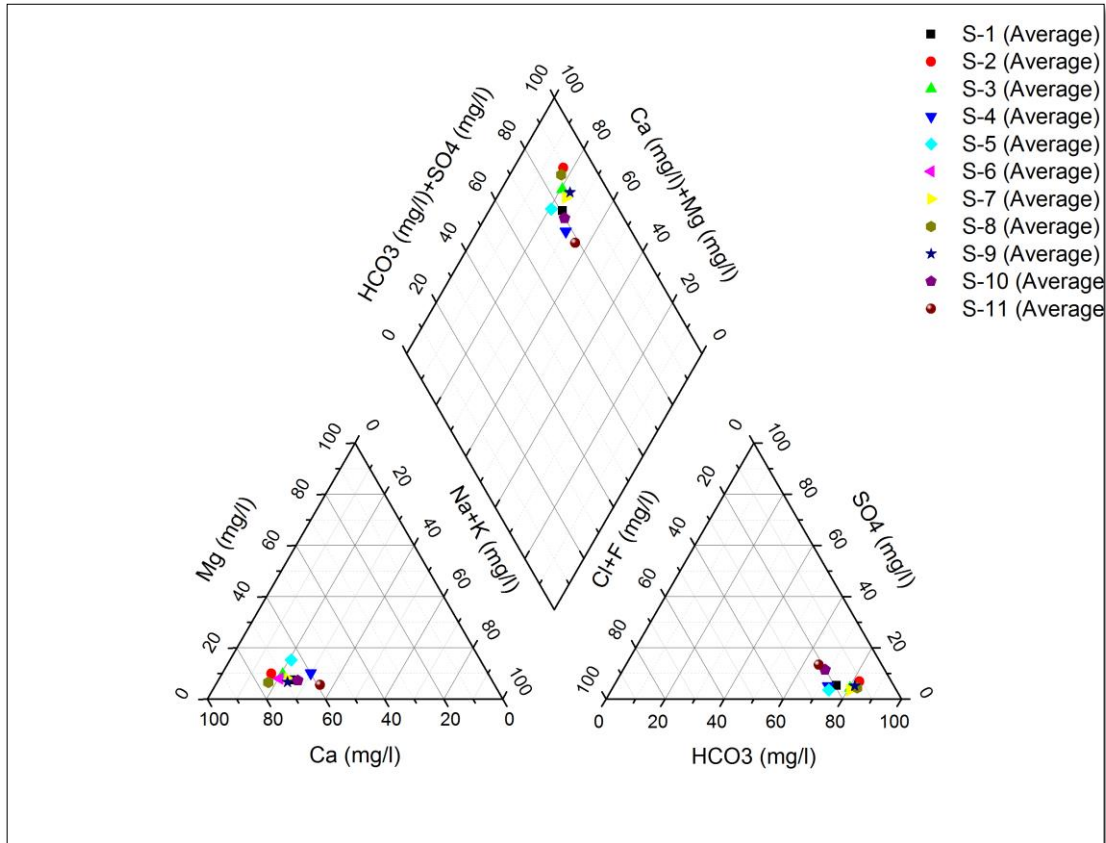


**Figure 32:** Piper diagram shows distribution of springs, an average during 1954–2009 (modified after Rofe and Raftery Consulting Engineers 1965; Palestinian Water Authority 2011b; Alawi et al. 2015)

Arsenic levels for all analyzed water samples are less than 1 ppb, except for the sample A-1 (tunnel water), which is 22 ppb. Samples A-1 and A-2 also have elevated levels in P, S, K, V, Cr, Ni and Cu (Figure 33), which also proves that the water from the tunnel is polluted from different sources such as: coal use, wastewater and industrial waste in the city.

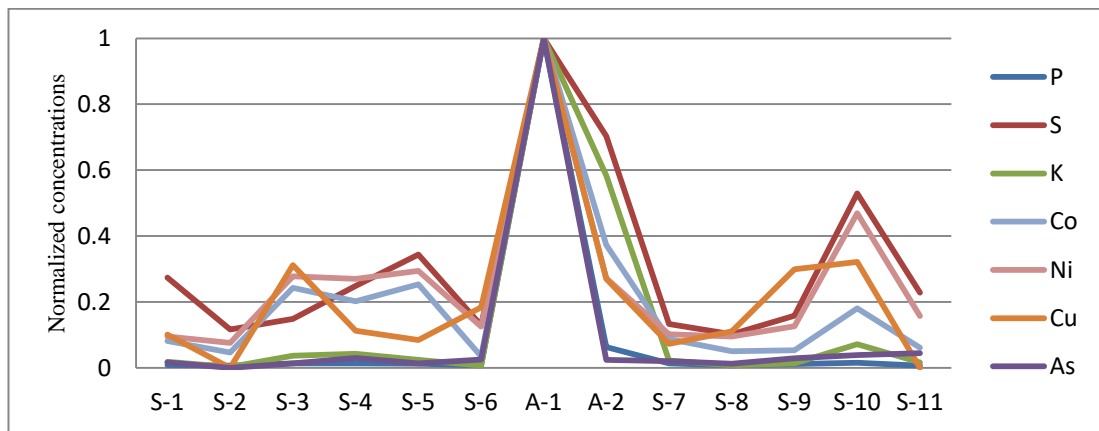


**Figure 33:** Normalized values to (A-1) trace element concentration in water samples

In the Nablus group, sites S-1 to S-5, it is observed that the total dissolved solid concentrations decrease with the increase in elevation. This is related to the water–rock interaction time; at greater depth, the water has more time to interact with rocks (Figure 34). This was also observed by Rofe and Raferty Consulting Engineers in a 1965 study. Yet, in the Sebestia group S-6 to S-11 the total dissolved solid concentrations increase with the increase of elevation (Figure 35). This is due to direct contact between meteoric and host rock; this means the recharge area is at a distance from the infiltration zone (Rofe and Raferty Consulting Engineers 1965).

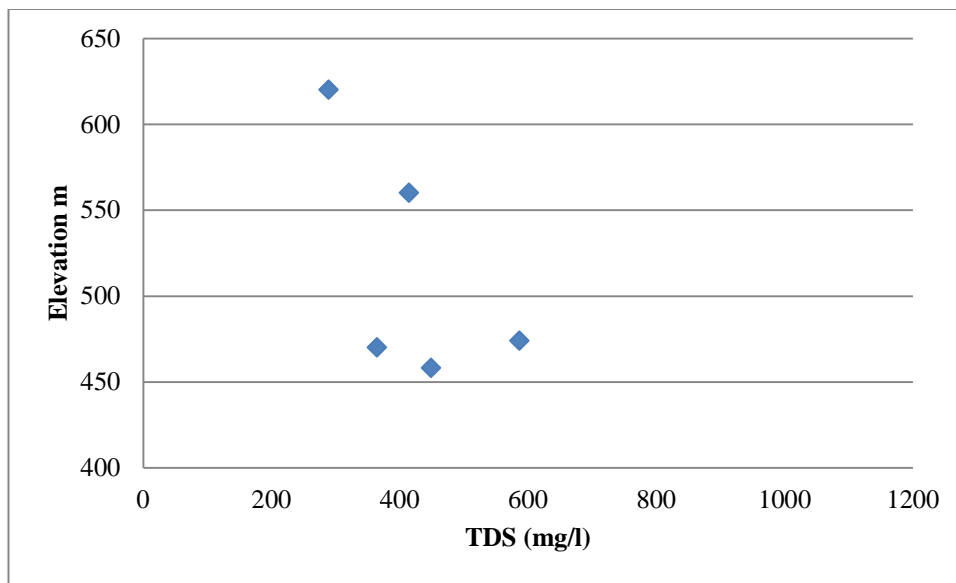


**Figure 34:** Total dissolve solids (TDS) trends with elevation (Nablus group springs)

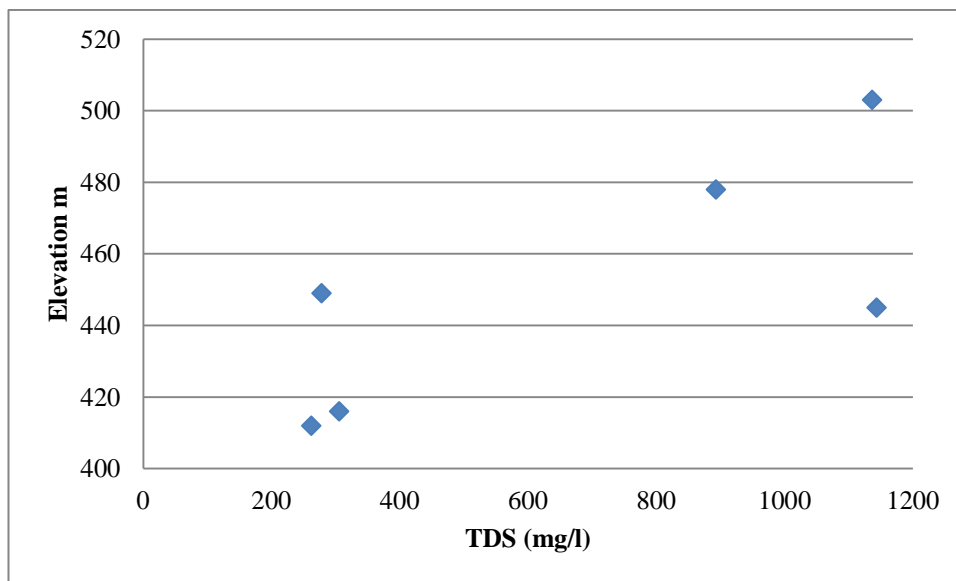


**Figure 35:** Total dissolve solids (TDS) trends with elevation (Sebestia group springs)

For better visualization of trace elements, the spider pattern method (Möller et al. 2009b) was applied using normalized trace elements concentrations (Bruland et al. 2014). This method shows that  $K^+$  and  $SO_4^{2-}$  are the most spatially dependent. This is due to the application of  $K_2SO_4(s)$  as fertilizers. Due to the fluctuation of elements concentrations, two recharge zones can be identified for the Nablus group: Ras al Ein spring (S-2) is the closest to the recharge zone and Al Subyan (S-5) is the furthest away. However, for the Sebestia group, the closest spring to the recharge zone is Zawata (S-6) and the furthest is Ein Al Hud (S-10) (Figure 36).

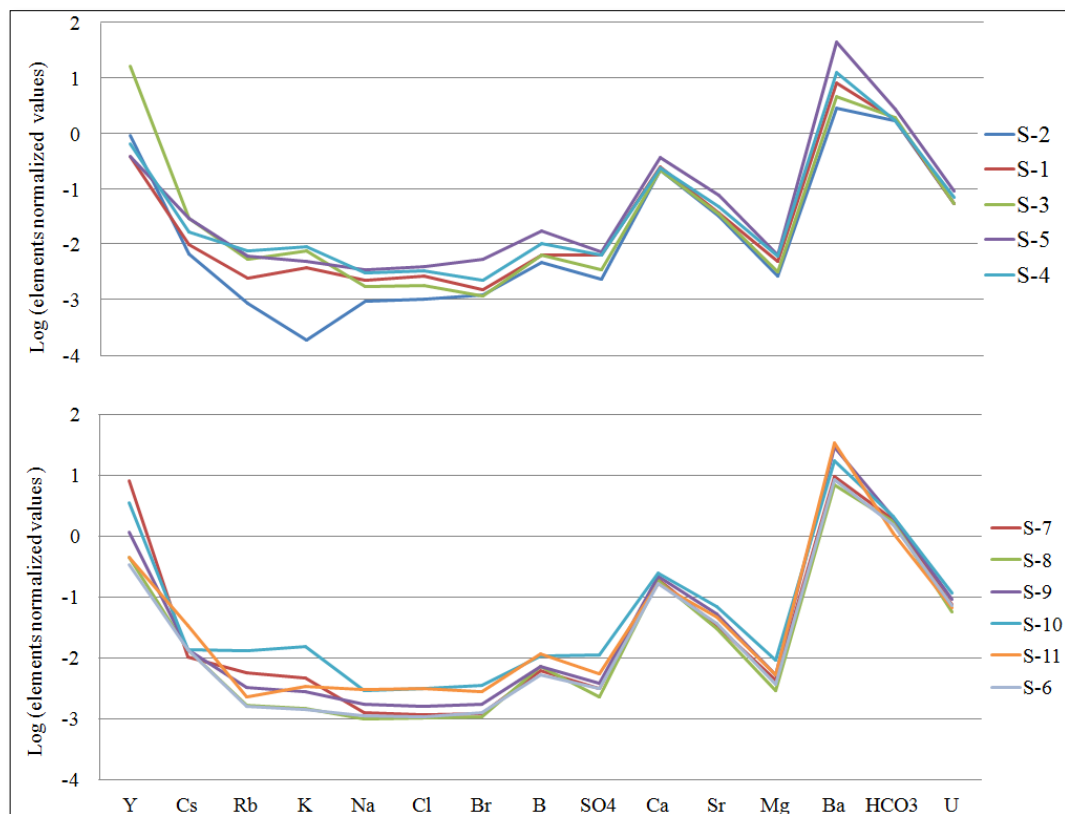


**Figure 36:** Spider patterns of groundwater are similar to patterns between the two groups, *above*: Nablus group, *below*: Sebestia group

The Mann-Whitney test was applied to compare the differences between the two spider patterns groups; there is no statistically significant difference between the two distributions at the 95.0% confidence level.

In terms of rare earth element and yttrium (REY), groundwater bodies can be grouped according to their REY normalized distribution patterns (Möller 2000). The REY results were normalized to C1 chondrite value (Anders and Grevesse 1989). The sampled springs could be divided into groups in terms of REY normalized

patterns. The first group, S-5, S-6 and S-11, shows in general lower REY values under the detection limit and were excluded from the analysis. There are clearly two different detectable groups of REY patterns: (1) S-2, S-3, S-7, S-10, and (2) S-1, S-4, S-8, S-9. REY has a memory effect with respect to the recharge zone (Möller 2000; Möller 2009c), thus it can be concluded that two recharge areas with different REY patterns exist. The difference is that regarding the negative Ce anomaly is more pronounced in the first group (S-2, S-3, S-7, S-10). The water in the tunnel has two different REY patterns. Thus one may speculate that A-1 had a more reduced condition in comparison to A-2 (Figure 37). To include all the springs, Ce anomaly was calculated based on this formula:

$$Ce \text{ anomaly} = \frac{3 * Ce_{normalized}}{2 * La_{normalized} + Nd_{normalized}}$$

Equation 3

The Ce anomaly calculation shows that the springs in the area are divided into two groups; one with positive anomaly (>1) and one with a negative anomaly (<1). The negative anomalies are a result of oxidation conditions along the pathway and positive anomalies are result of superficial fixed  $Ce^{4+}$  leaching into the water by reducing conditions (Möller 2000).

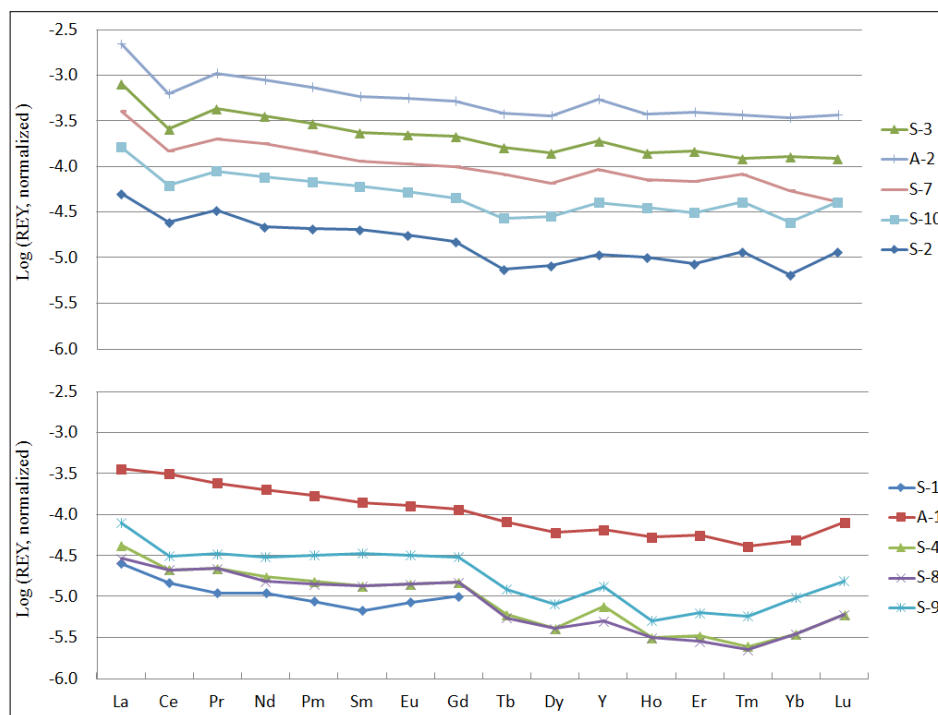
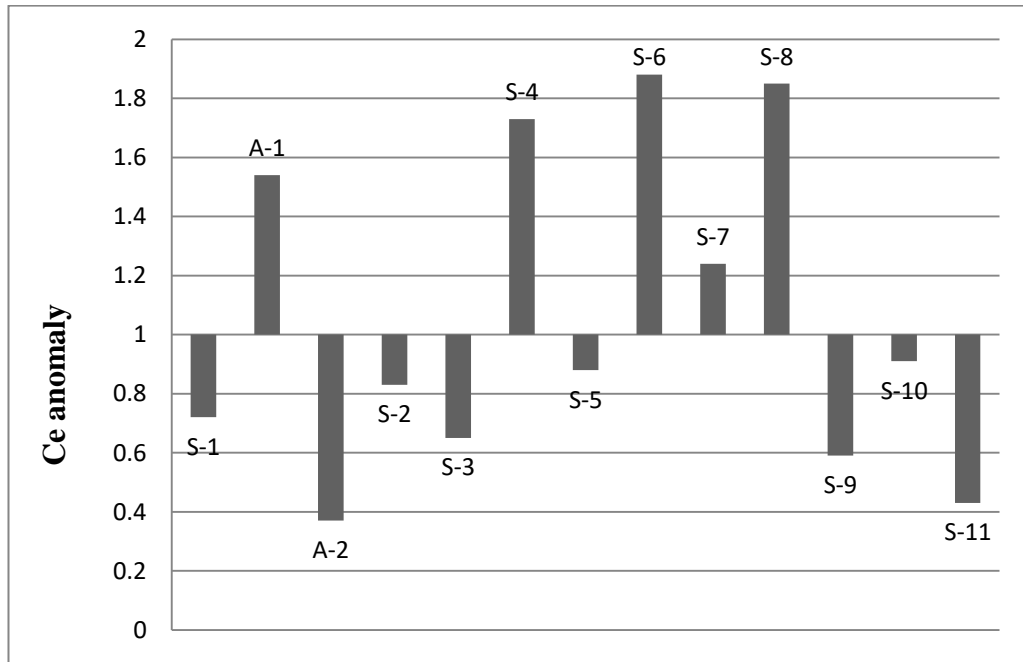


Figure 37: REE patterns show two different spring groups



**Figure 38:** Ce anomaly values for springs show positive anomalies for water samples (A-1, S-4, S-6, S-7, S-8) and negative anomaly for water samples (S-1, A-2, S-2, S-3, S-5, S-9, S-10, S-11) depending on oxidation condition along the pathway of the groundwater

#### 4.2.1 Stable isotope

It is known the Mediterranean basin has deuterium excess of 22‰ (Gat and Carmi 1970; Gat 1983) and the Sebestia spring group (S-6, S-8, S-9, S-10, and S-11) has a deuterium excess above 20‰, which means that these springs show an impact from the Mediterranean Sea. On the contrary, the Nablus group of S-1, S-2, S-3, S-4, and S-5, along with the tunnel water of A-1 and A-2, has a lower deuterium excess. This is due to evaporation before infiltration. Moreover, there are two mixing lines (two different slopes): the Sebestia group samples can be plotted on a straight line crossing both the Paleo-eastern Mediterranean Water Line (PMWL:  $\delta^2\text{H}=8 \delta^{18}\text{O}+7$ ; Gat 1983) and the Eastern Mediterranean Meteoric Water Line (EMWL:  $\delta^2\text{H}=8 \delta^{18}\text{O}+22$ ; Gat and Carmi 1970; Gat 1983). This means that the water is a mixture between recent precipitation and Pleistocene paleowater. The Paleo meteoric water line is derived from the stable isotopic composition for large continental confined aquifers with long residence times and the long residence time measured should relegate the recharge to the Pleistocene (Gat 2010). During Pleistocene, mature karst was developed containing water (Rofe and Raftery Consulting Engineers 1965).

On the contrary, Nablus group samples plot in a straight line that runs rather parallel between PMWL and EMWL. It appears that at the recharge zone for the Nablus group springs, the infiltration process takes more time and thus is subject to evaporation (Figure 39).

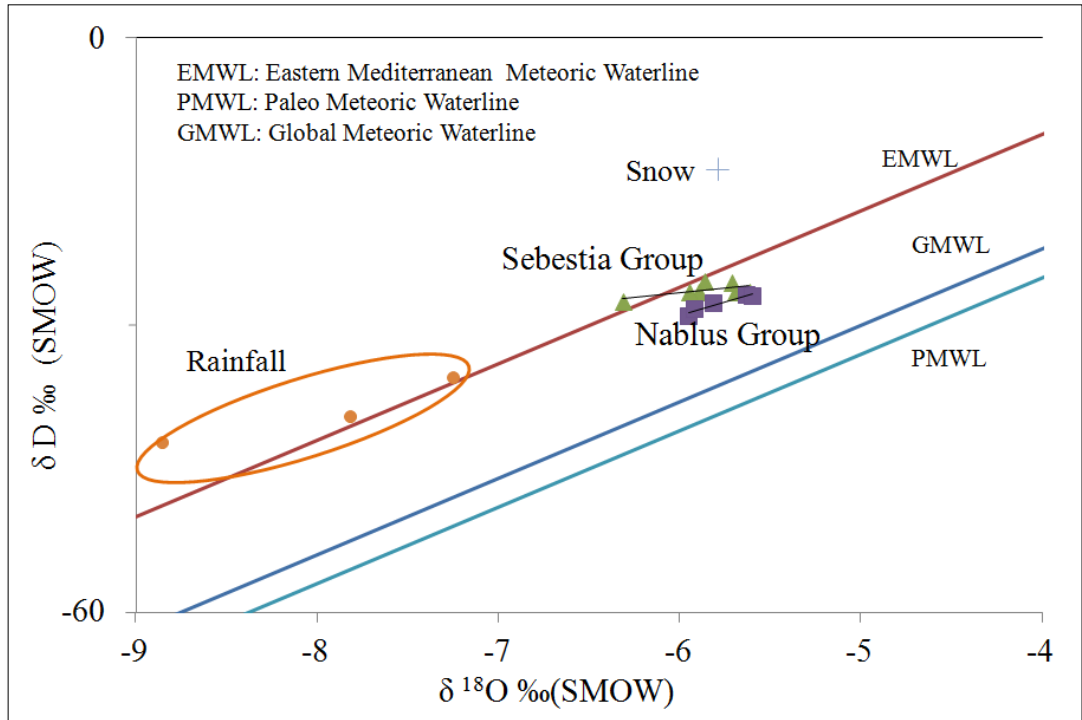


**Figure 39:** Distributions of the stable isotopes  $\delta^{18}\text{O}$  and  $\delta^2\text{H}$  in different water bodies in the study area; Eastern Mediterranean Meteoric Water Line ( $\delta^2\text{H}=8 \delta^{18}\text{O}+22$ ; Gat and Carmi 1970; Gat 1983), Global Meteoric Water Line ( $\delta^2\text{H}=8 \delta^{18}\text{O}+10$ ), Paleo Meteoric Water Line ( $\delta^2\text{H}=8 \delta^{18}\text{O}+7$ ; Gat 1983)

#### 4.2.2 Strontium isotope analysis ( $^{87}\text{Sr}/^{86}\text{Sr}$ )

In terms of Sr isotope results, it appears that water of the Nablus group along with the tunnel water (S-1, S-2, S-3, S-4, S-5, A-1, A-2) has at least two Sr sources. The same applies to the Sebestia group (S-6, S-7, S-8, S-9, S-10, and S-11). Accordingly, the water system in the area can be divided into two Sr isotope groups, one with a lower Sr ratio (0.7079) and one with a higher (0.7081) as shown in Figure 40.

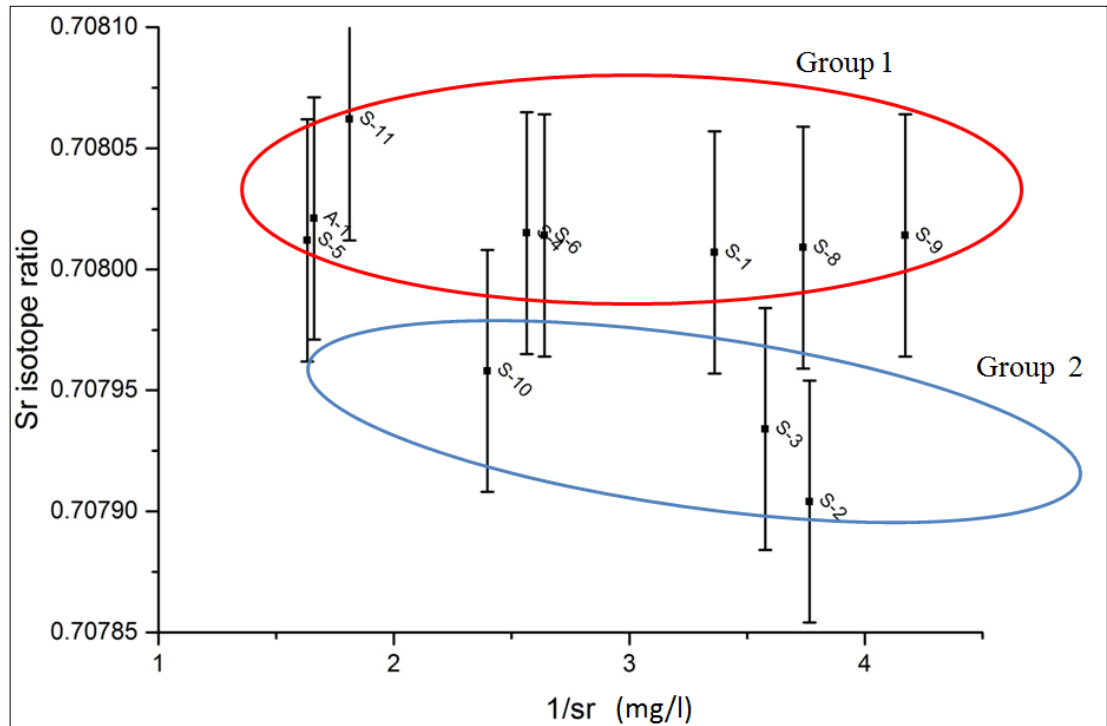


**Figure 40:** Sr isotope ratios  $^{87}\text{Sr}/^{86}\text{Sr}$  vs. mean reciprocal Sr concentrations (mg/l) for the springs shows two Sr sources in the aquifer (Error of 0.00005 is derived by replicate analysis of standard)

The two groups differ significantly based on the Mann-Whitney test at the 95.0% confidence level ( $P= 0.01604$ ) and is visualized by means of a box-and-whisker plot (Figure 41).

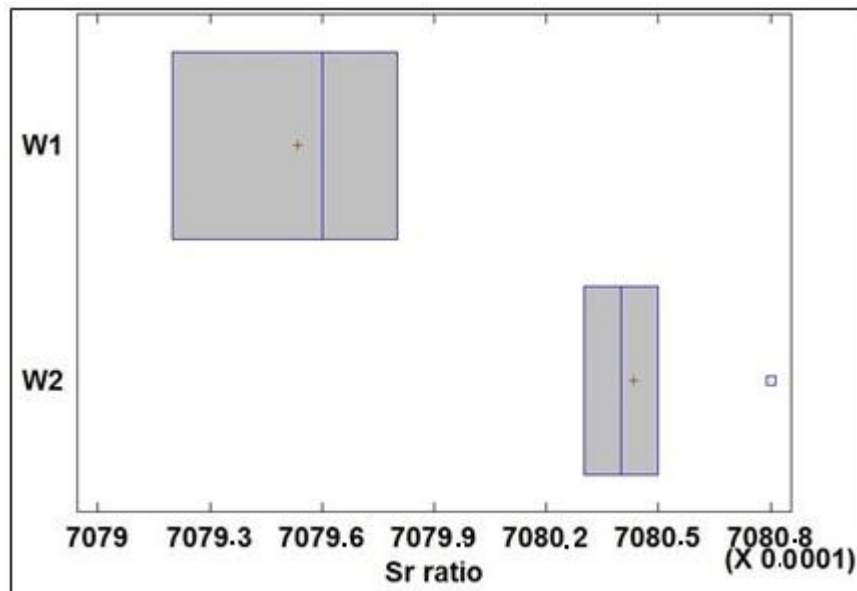


**Figure 41:** Box-and-whisker plot of the Sr ratio values of the two water groups show a significant difference between the two groups

Sr isotope analysis for rainfall, snow and runoff samples showed higher isotope ratios than groundwater samples (springs). Precipitation samples were collected from the study area (Nablus) and Ramallah (60 km south of the study area). Samples collected from the Nablus area have even higher values over 0.71. This is because the water contained clay collides and usually clay has a higher Sr isotope value.

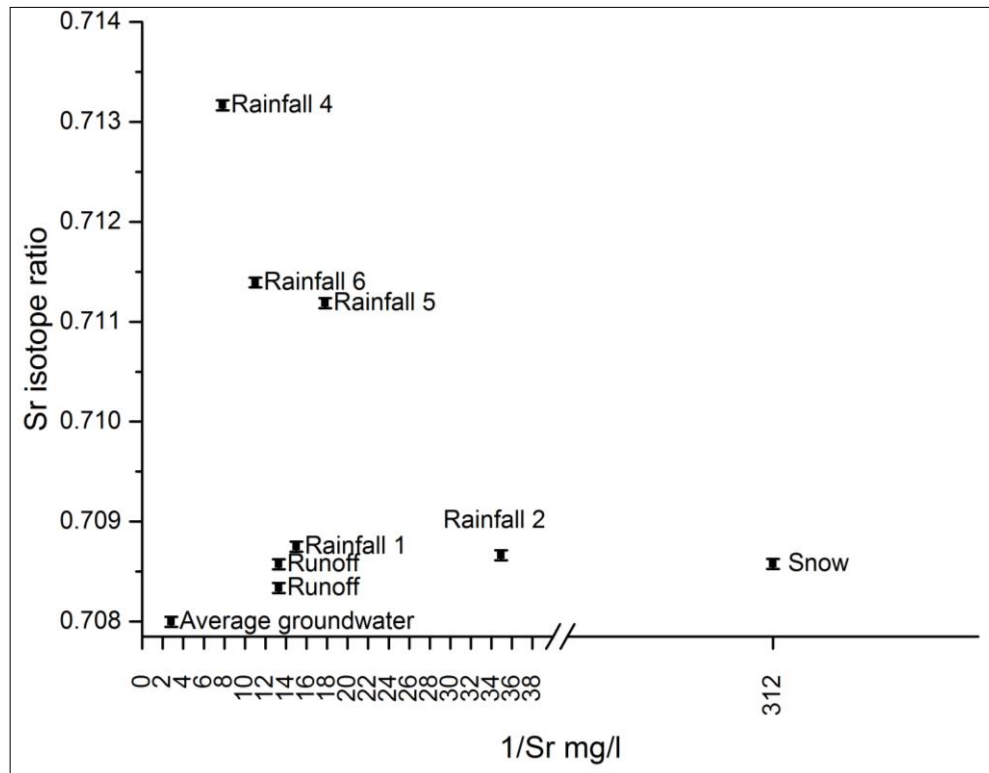


**Figure 42:** Sr isotope ratios  $^{87}\text{Sr}/^{86}\text{Sr}$  vs. mean reciprocal Sr concentrations (mg/l) for springs and rainfall samples show a wide variation in the isotopic Sr value for rainfall (Error of 0.00005 derived by replicate analysis of standard)

#### 4.2.3 Saturation index

Using PHREEQC, the saturation indices of the sampled springs were calculated (Table 7). At Ras al Ein (S-2), Qaryon (S-3) and Beit Al-Ma (S-4) the saturation indices for calcite are close to saturation and undersaturated for dolomite, aragonite, halite and gypsum. This explains why there is little to no carbonate deposits at these spring houses.

On the other hand, calcite is over saturated at Dafna (S-1), Al Subyan (S-5), tunnel water A-1, Zawata (S-6), Kfar Farat (S-7), Harun (S-8), Ijnisinya (S-9), Ein Al Hud (S-10) and Qabu (S-11). Thus, secondary calcite precipitates are found on the walls of the tunnel and springs houses.

**Table 7:** Saturation indices for springs selected minerals

	<i>si_Calcite</i>	<i>si_Dolomite</i>	<i>si_Aragonite</i>	<i>si_Halite</i>	<i>si_Gypsum</i>
S-1	0.2819	-0.3762	0.1333	-7.4522	-2.6614
S-2	0.0632	-1.0288	-0.0857	-8.2507	-3.2826
S-3	0.1507	-0.7784	0.0023	-7.6142	-2.9665
S-4	0.0277	-0.7582	-0.1199	-7.2256	-2.6988
S-5	0.8562	0.7401	0.7084	-7.1086	-2.5433
A-1	0.4803	0.3794	0.3322	-6.2141	-2.2482
S-6	0.2594	-0.3448	0.1127	-8.1377	-2.8584
S-7	0.2856	-0.291	0.1386	-8.0488	-3.0575
S-8	0.2326	-0.5539	0.085	-8.2113	-3.2053
S-9	0.2211	-0.3903	0.0737	-7.7907	-2.9399
S-10	1.0808	1.5626	0.9357	-7.2965	-2.4713
S-11	0.377	0.3139	0.2308	-7.2577	-2.8948

#### 4.2.4 Discussion

It can be seen, in terms of major cations, anions and trace elements, it is not possible to distinguish between the two different water bodies. Yet, it is possible to define two recharge zones. The Sebestia group, S-6, S-8, S-9, S-10, and S-11, has a deuterium excess of more than 20, which means that the groundwater is affected by Mediterranean rainfall.

Moreover, it was possible to establish at least two sources of Sr isotope and two different REY patterns in the water bodies. Concerning the water in the tunnel, two samples that were analyzed for Sr isotope ratios and proved that Dafna spring (S-1) is one source feeding the tunnel. Furthermore, these two samples were analyzed for REY pattern and indicate towards two different oxidation zones.

### 4.3 Carbonate analysis (host rock)

Host rock from some of the above-mentioned springs was sampled and analyzed. Calcite is the dominant mineral. Thin section and stable isotope analysis ( $\delta^{13}\text{C}$  (-1.52 ‰),  $\delta^{18}\text{O}$  (-2.54‰) (Veizer and Fritz 1976) revealed that the host rocks are marine carbonates (Figure 43).

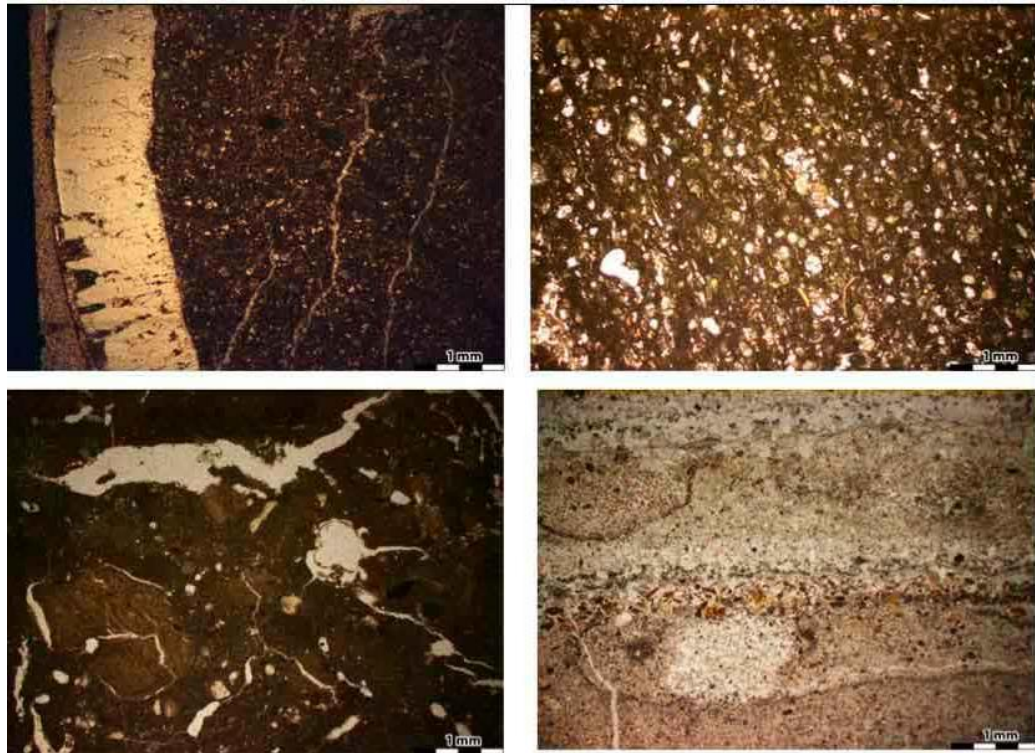


**Figure 43:** Different thin sections show carbonate rocks in the study area, *upper left:* calcite micrite mudstone at S-8, *lower left:* intrasparite rock including foraminiferal wackestone at S-10, *upper right:* calcite micrite mudstone at S-2, *lower right:* limestone (oolitic) at S-3

Sr isotope ratios ( $^{87}\text{Sr}/^{86}\text{Sr}$ ) for marine carbonate reflect the isotopic ratio of the origin marine water. Therefore, based on Sr isotope variation for the Phanerozoic graph developed by Veizer et al. (1999), it is possible to estimate the age of rock based on their isotopic value. For Qaryon spring, the host rock contains four laminations and Ras al Ein, one lamination. The isotope ratio for the samples is 0.708 that means that the host rock belongs to the Tertiary/Cretaceous. This matches the previous findings (Rofe and Raferty Consulting Engineers 1965; Alawi et al. 2015)

Normalized REE values to North American Shale composite (NASC, Gromet et al. 1984) for the host rock of S-2 (Ras al Ein) and S-3 (Qaryon) show a difference between the two samples in Ce anomaly. The Gd anomaly in both samples are a result of the high salinity of marine water during carbonate rock formations (Möller et al. 2009c).

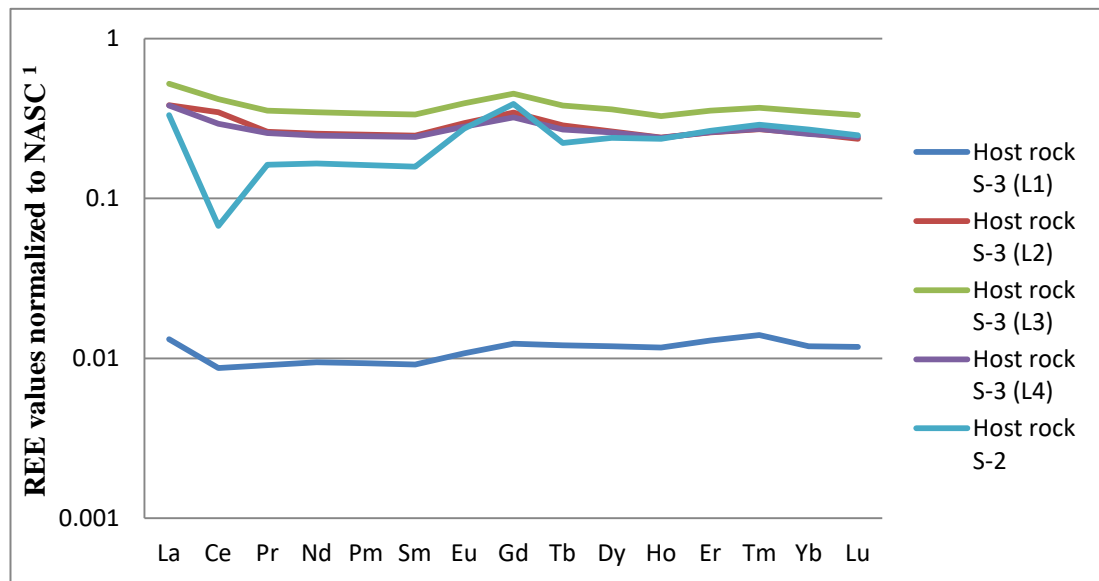


**Figure 44:** REE normalized values patterns normalized to NASC<sup>1</sup>(Gromet et al. 1984) show different Ce and Gd anomalies in host rocks

#### 4.4 Aqueduct building material

Several samples were collected from different aqueducts containing building materials. Some samples contain secondary carbonate; others had no traces of carbonate. Here, a brief description of the building material is discussed.

The Theater in Nablus was also included in the Nablus study location, because it was mentioned in the work of Fanni (1999) that the theater stage was used to store water. Hence, a carbonate deposit would probably be present. However, the thin sections show only a diminutive amount of carbonate growing above the plaster. Limestone from the region was used as building blocks for aqueducts A-3, A-4 and A-5 (Figure 45). The plaster used in both the theater and A-4 is uniform red mortar. The use of red mortar that included terracotta started around 400 A.D. and continued until 700 A.D. (Porath 2002).

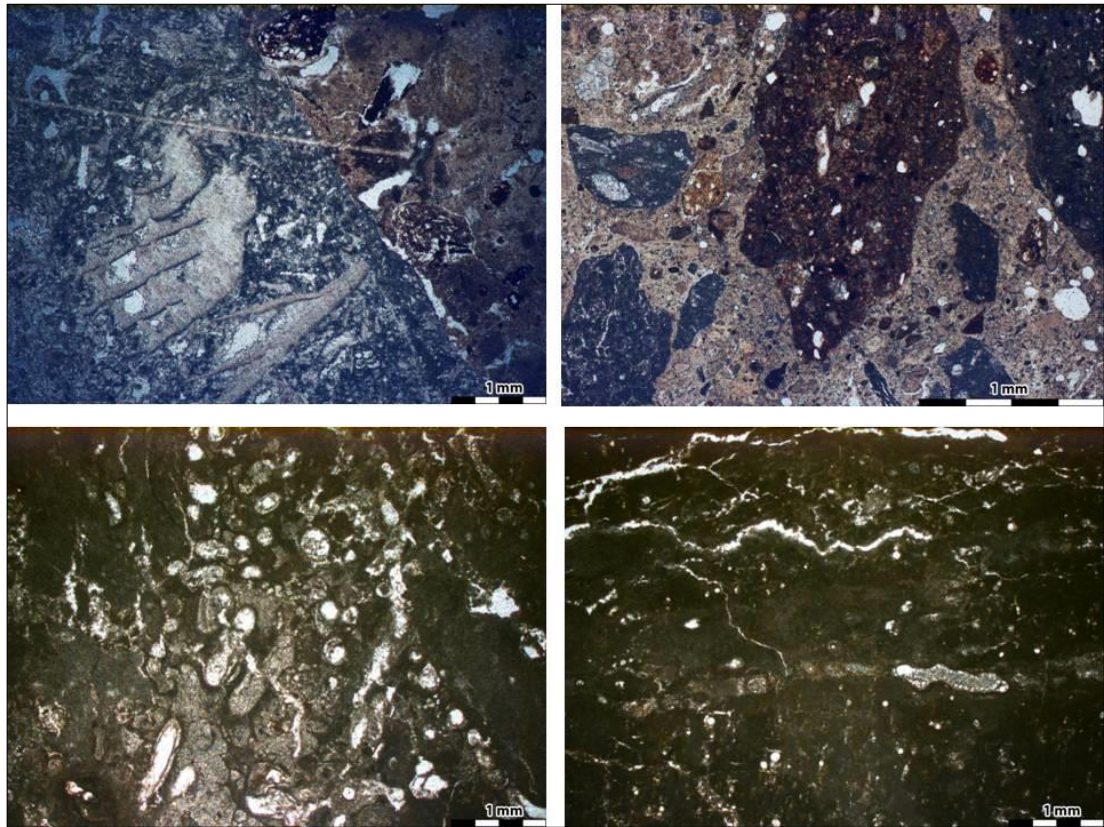


**Figure 45:** Different thin sections of the building material and plaster applied on the aqueducts and theater; *upper left*: thin section from theater shows diminutive growth of carbonate above the pinkish plaster material, *lower left*: thin section from A-4 shows the building material limestone rock including foraminiferal wackstone similar to outcrop rocks in the area, *upper right*: thin section from A-5 shows pinkish plaster material, *lower right*: thin section from A-3 shows the building material limestone rock including foraminiferal wackstone similar to outcrop rocks in the area

## 4.5 Secondary carbonate analysis

As mentioned before, different carbonate samples were collected from different sites. Each sample has its own story to tell: different microstructure, different lamination, and different growth rate and of course, different geochemical and isotopic content. Nevertheless, all samples have optical lamination with alternation in color (light and dark).

### 4.5.1 Ras Al Ein location (S-2)

At Ras Al Ein springs, several samples were collected, however, one represented secondary carbonate (Figure 46). This carbonate sinter was sampled from the wall of the dewatering tunnel leading to the spring. The sample thin section length is 1.3 cm. No water was visible at the surface so it can be assumed that scale formation is

recently not happening. Most probably the dewatering tunnel underwent rehabilitation and expansion, and thereby the youngest layers were removed.

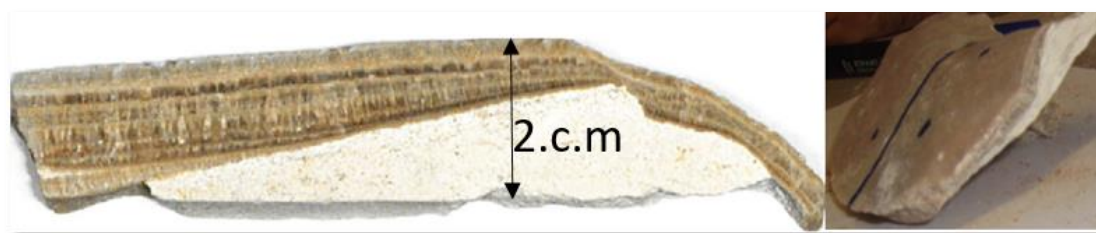


**Figure 46:** Sample S-2, *left*: cross section of the sample shows laminations, brown, light brown dark brown, *right*: sample before cutting

This sample contains 90 layers. The crystal type and dimension alter within each layer, mainly between columnar (2mm), microsparite (0.1mm) and Mosaic calcite (0.5). The Mg–Ca molar ratio in the current water and in the carbonate is very low (Figure 47); microsparite and mosaic crystal shapes are not due to diagenesis but due to different flow rates and biological growth. Normally, columnar crystal forms under a slow constant flow rate, while microsparite and mosaic form under a variable flow rate and the growth of carbonate is induced by biological activity (Frisia 2015). Mosaic laminations contain silica within the calcite lamina and microsparite contain silica and Fe-minerals. Accordingly, these layers were formed due to flash floods that contained more collides than normal spring flow.

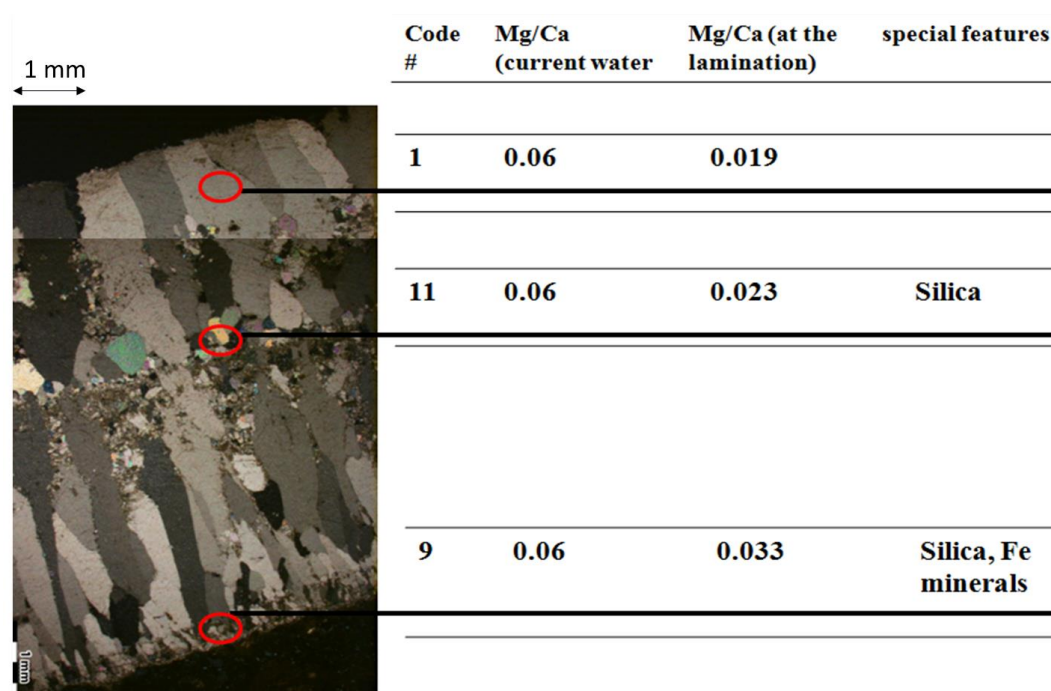


**Figure 47:** Sample S-2 thin section shows main crystals type code and their features: crystal type code are based on Frisia (2015) classification shown in section 2.4.3

**Source identification: strontium isotope analysis  $^{87}\text{Sr}/^{86}\text{Sr}$ ,  $\delta^{234}\text{U}$  (S-2)**

Three laminations were chosen from this sample for Sr isotope analysis: L1 the most recent lamination (0 mm from the top), L2 lamination in the middle of the sample (6.4 mm) and L3 the oldest lamination at (7.4 mm). The host rock and spring water were also analyzed.

There is no significant difference between the three laminations in terms of Sr isotope ratio (0.708), however, the ratio is higher than the host rock (0.7078). The Sr isotope ratio for the spring Ras Al Ein (S-2) is lower than the carbonate samples and higher than the host rock (0.7079). Furthermore, looking at the Sr concentration, it seems that the Sr isotope ratio for the spring is a mixture between the host rock and the carbonate layer (Figure 48). This means that the carbonate film above the host rock has a consistent Sr isotope ratio.

As mentioned in Section 2.4.3,  $^{234}\text{U}$  analysis can be also used to trace the water sources. In this case,  $\delta^{234}\text{U}$  values range from 365 to 405 (Table 8). To conclude, the spring water quality (through water–rock interaction) did not change during the precipitation of this carbonate.

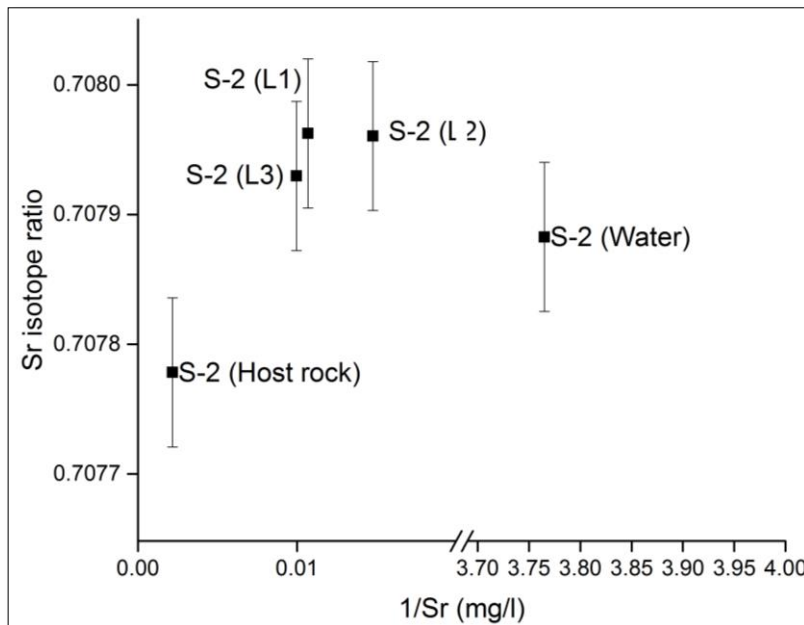


**Figure 48:** Sr isotope ratio  $^{87}\text{Sr}/^{86}\text{Sr}$  vs. mean reciprocal Sr concentrations (mg/l) shows no significant difference between the three laminations at S-2 and a significant difference between the laminations and the host rock. The water sample Sr value is influenced by both host rock and the carbonate layer, (Error of 0.00005 is derived by replicate analysis of standard)

***Uranium Thorium disequilibrium dating***

Three laminations were chosen for U–Th disequilibrium dating. The lamina was cut with a micro sawing drill and then analyzed as described in section 3.3.3. The  $^{238}\text{U}$  concentration is relatively low  $< 1 \mu\text{g/g}$ . The initial concentrations of  $^{230}\text{Th}$  were identified as being high from the measured  $^{230}\text{Th}/^{232}\text{Th}$  ratio (Table 8). Thus, the resulting age had to be corrected using an algorithm called STRUTages that combines the isochron techniques and stratigraphical constraints (Roy-Barman and Pons-Branchu 2016).

**Table 8:** U–Th data measured for sample S-2 (Ras al Ein)

mm		$^{238}\text{U}$ ( $\mu\text{g/g}$ )		$^{232}\text{Th}$ (ng/g)		$\delta^{234}\text{U}$		$^{230}\text{Th}/^{238}\text{U}$		$^{230}\text{Th}/^{232}\text{Th}$	
L1	0–2.73	0.69	$\pm 0.0004$	4.98	$\pm 0.031$	404.83	$\pm 1.5$	0.078	$\pm 0.0005$	5.15	$\pm 0.033$
L2	2.73–5.36	0.41	$\pm 0.0005$	88.75	$\pm 0.094$	365.64	$\pm 1.07$	0.22	$\pm 0.0006$	3.13	$\pm 0.009$
L3	5.36–7.53	0.42	$\pm 0.0003$	27.61	$\pm 0.034$	393.94	$\pm 0.83$	0.156	$\pm 0.0004$	7.3	$\pm 0.019$

The corrected ages of the lamination of the carbonate sinter ranges from 3.8 k.a. (the youngest) to 9.7 k.a. (the oldest). As previously before, the youngest formation has probably been removed during expansion of the channel. It should be pointed out that the dewatering channel is not man-made but part of the karst system. The age range was evaluated with stable isotope values of  $^{18}\text{O}$  and  $^{13}\text{C}$  from the Soreq cave isotope data (Bar-Matthews et al. 1998).

**Table 9:** Measured ages before 2011 for S-2 (Ras al Ein)

<sup>1</sup>algorithm developed (Roy-Barman and Pons-Branchu 2016), <sup>2</sup>(Bar-Matthews et al. 1998),

<sup>3</sup>(Bar-Matthews et al. 1999)

mm		Corrected age k.a. using STRUTages <sup>1</sup>		$\delta^{13}\text{O}$ ‰VPDB	$\delta^{13}\text{C}$ ‰VPDB	Equivalent age k.a. from Soreq cave data <sup>2,3</sup>	Period
L1	0–2.73	3.8	$\pm 1.34$	–6.18	–11.16	4	Bronze
L2	2.73–5.36	7.1	$\pm 3.5$	–5.79	–10.78	7	Pottery Neolithic
L3	5.36–7.53	9.7	$\pm 1.97$	–5.61	–10.95	9	Pre Pottery Neolithic

### ***Laminae, peak counting and trace element variation***

The age results verify that the laminations here are not annual; 90 layers represent around 6 k.a. If the growth rate is continuous, then 1 mm of growth represents around 450 years. The saturation index for the present-day water S-2 is lower than the surrounding springs (Table 7). That explains the slow growth rate and the discontinuity of growth. Moreover, Mg, Fe and Sr peaks are not regular, Fe peaks are pronounced when the crystal type is 9 (microsparite) or 11 (mosaic calcite). The Sr concentration increases with the growth axis of the sinter (Figure 49). The increase of Sr concentration in water can decrease the calcite growth rate (Tai et al. 2012). It is uncertain to say that concentration of Sr increased or the fractionation factor changed in the origin water, but if it increased it can be the reason for the carbonate growth rate retardation.

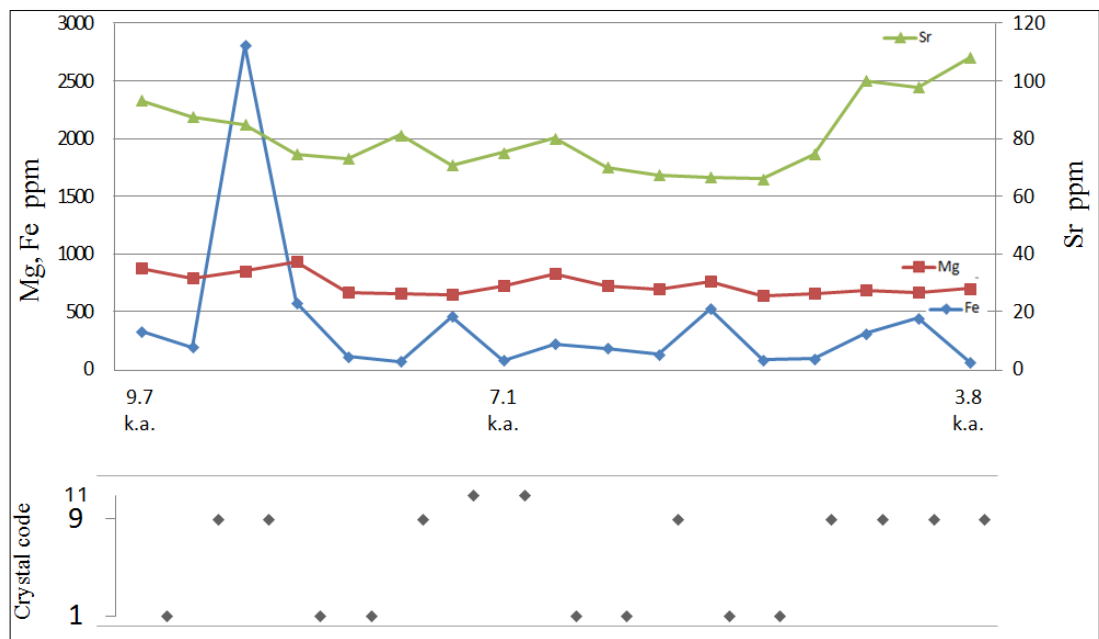


**Figure 49:** *Top:* Mg, Fe, Sr peaks along the growth axis of the sinter (k.a. before 2011) show an increase in Sr concentrations towards the recent growth, *bottom:* crystal variation along the growth axis of the sinter: 9 (microsparite), 11 (mosaic calcite) and 1 (columnar). Fe concentrations are high at crystal types 11, 9

### ***Rare earth elements and yttrium***

Rare earth elements (REE) and yttrium (REY) concentrations in sinter normally start with elevated values and then decline gradually along the growth axis of the sinter (Figure 50). This is normal behavior, as the dissolution of REY from rocks at the beginning will be high and then would reach its equilibrium over a period of thousands of years (Möller et al. 2009c).

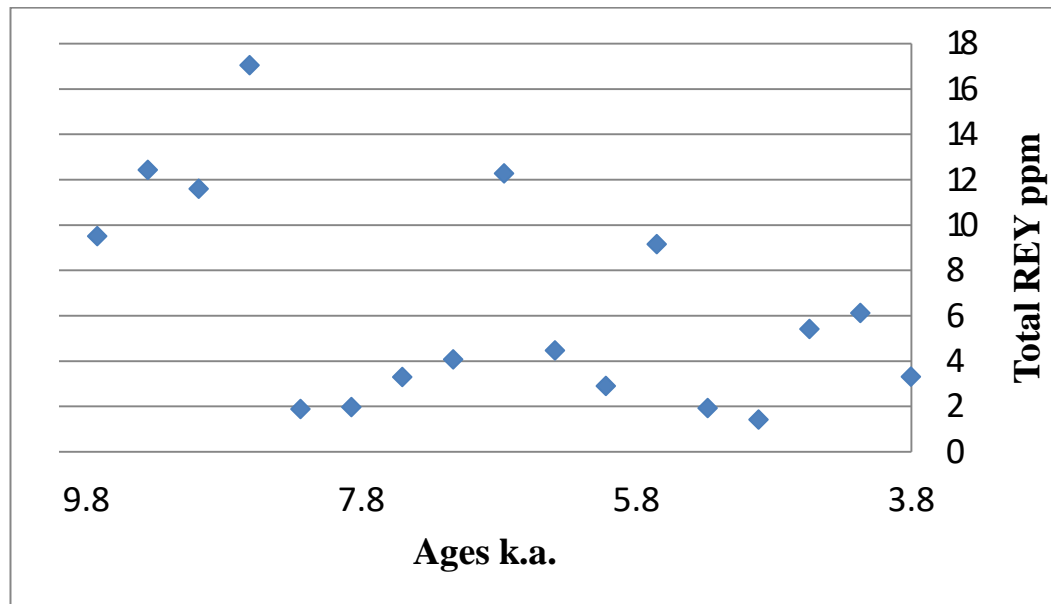


**Figure 50:** Total REY concentration for sample S-2 versus age (before 2011 A.D.) shows a decreasing trend

The REE patterns for the sequence laminations are similar to the host rock with Ce anomaly, until the last lamination. At this point, the water conditions of the water change from oxidizing to reducing conditions.  $Ce^{3+}$  is oxidized to  $Ce^{4+}$ , and  $Ce^{4+}$  is adsorbed to clay minerals and this causes the negative Ce anomaly in water (Möller 2000; Pons-Branchu et al. 2014).

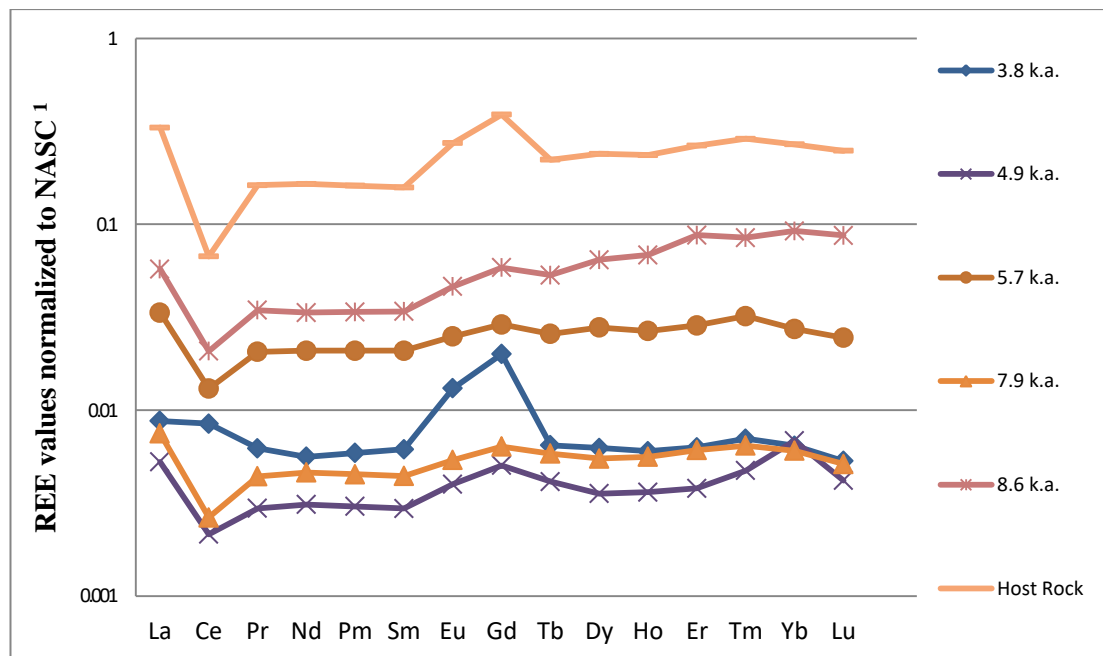


**Figure 51:** REE values patterns normalized to NASC for selected lamination and the host rock show similarity between the lamination and the host rock except for the last lamina 3.8 k.a. due to a change of the oxidizing conditions, <sup>1</sup>(Gromet et al. 1984)

As it is known, the first documented utilization of this spring was during the Roman period. However, any changes in the entrance of the spring could have caused aeration and consequently a change in oxidation conditions (in the last lamination). Around the study area, the excavation of horizontal spring with tunnels to increase the discharge began during the Iron Age (Frumkin 2002b). So, it may have been during the Bronze period that people started to enlarge the entrance of the spring.

#### 4.5.2 Ijnisinya location (S-9)

At Ijnisinya springs, several samples were collected; two are considered in this section. Sample S-9 (a) is a laminated carbonate sinter that was collected from the walls near the spring head (Ijnisinya). The outer shape of this sample is spherical and its laminations are following the shape (Figure 52).

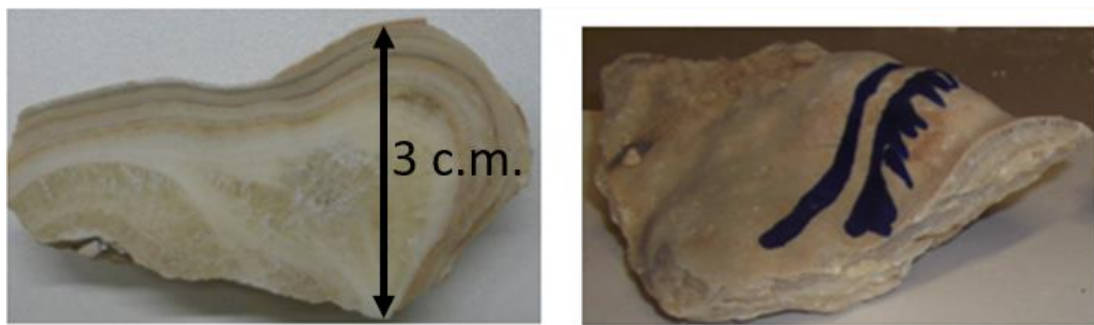


**Figure 52:** Samples S-9 (a): *left:* polished cross section shows different lamination colors (white, gray and brown), *right:* sample before cutting

The average thickness of the sample is 37.88 mm (23.4 mm thickness where the thin section was taken). The growth is not continuous; there are three growth periods and in total comprised of 113 layers. The first growth part is homogenous white crystal growth. The same crystal type continues after a visible line of interruption. Then the third growth part is distinguished by the alternating layers from white, grey, brown to dark tones. The first growth (ca. 13.9 mm) has uniform crystal type, columnar micro crystalline (2 mm). This is referred to as variable flow rate (Frisia 2015). The crystal shape in the second growth part (5 mm) is similar to the first part. The third growth is more diverse; it starts with 1-mm thickness of several micrite laminations, then mosaic calcite crystals follow. After that, there are subsequent alternating layers from columnar micro crystalline (0.25mm) and mosaic calcite crystals (

Figure 53).

Sample S-9 (b) has no lamination; it is assumed that its growth rate was rapid and based on biological activity. The sample is a maze of calcite tubes overlapping (Figure 54). These tubes are hollow from the inside and probably were organic solution vugs; black dots are signs of algal growth. Cyanobacteria might be the basis of these structures but additional analysis is needed.

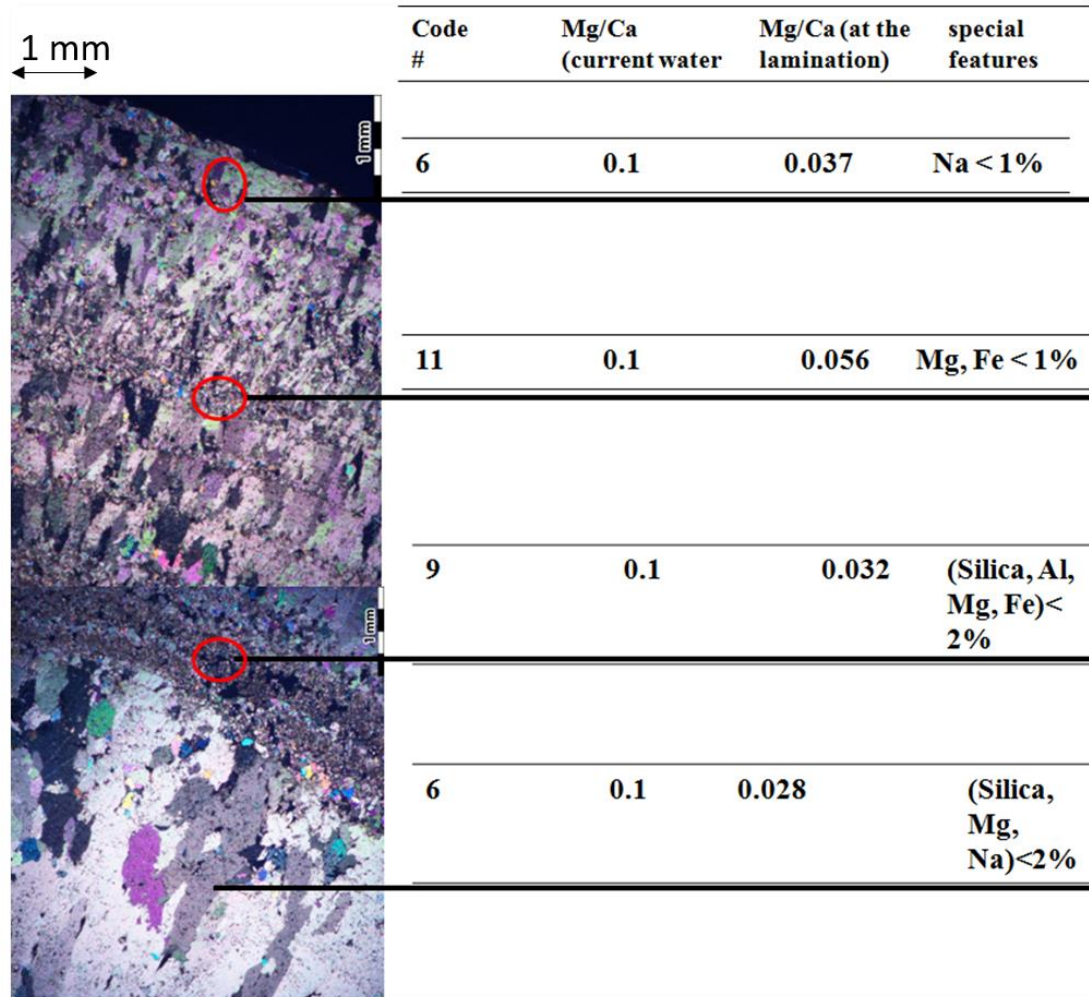


**Figure 53:** Sample S-9 thin section shows main crystals type code and their features crystal type code are based on Frisia (2015) classification shown in section (2.4.3)



**Figure 54:** Sample S-9(b) a block of overlapping calcite tubes

***Source identification: strontium isotope analysis  $^{87}\text{Sr}/^{86}\text{Sr}$ ,  $\delta^{234}\text{U}$  (S-9)***

Sr isotope ratio for laminated carbonate samples S-9(a) have the same signature as the groundwater delivering the Sr and U. Yet, S-9(b) has lower Sr isotope ratio (Figure 56). This means that two sources of Sr have fed the growing secondary carbonate. Four laminations were chosen for  $\delta^{234}\text{U}$  analysis. The younger most recent lamination has lower  $\delta^{234}\text{U}$  values (441) in comparison to the other laminations (527-543) (Table 10). This means that the water quality feeding the carbonate altered due to geological events.

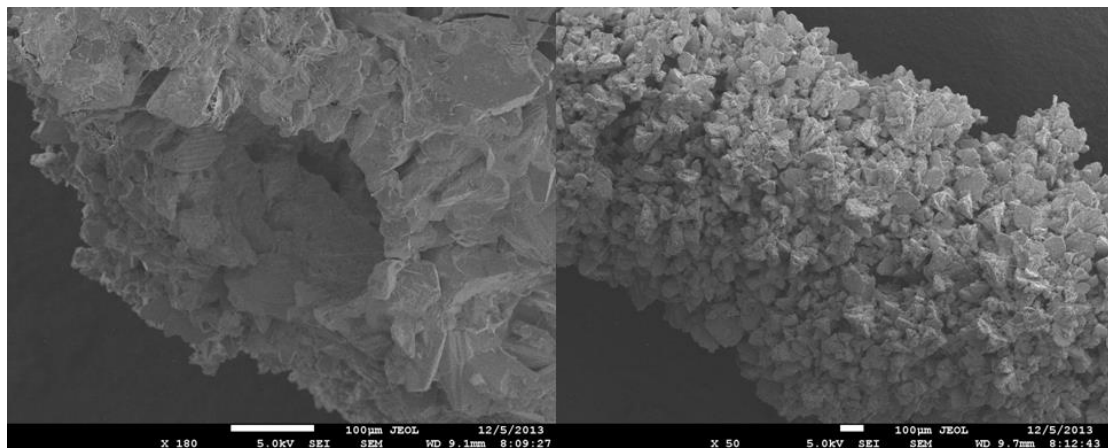


**Figure 55:** SEM image S-9(b), *left*: view to the tube opening, *right* tube structure

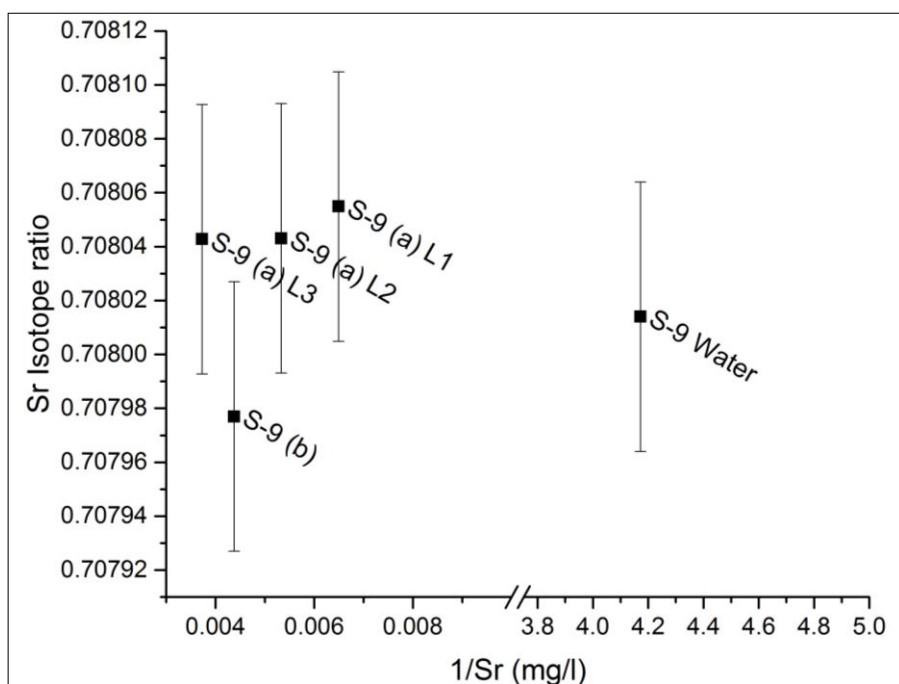


**Figure 56:** Sr isotope ratio  $^{87}\text{Sr}/^{86}\text{Sr}$  vs. mean reciprocal Sr concentrations (mg/l) shows no significant difference between the three laminations of S-9(a) and the water sample but different Sr value for sample S-9(b), (Error of 0.00005 is derived by replicate analysis of standard)

#### *Uranium Thorium disequilibrium dating*

Four laminations were chosen for U/Th disequilibrium dating. Each lamina was cut with a micro sawing drill and then analyzed as described in section 3.3.3. The  $^{238}\text{U}$  was relatively low with  $< 1 \mu\text{g/g}$  (Table 10). For the first growth (L3 and L4) the initial concentrations of  $^{230}\text{Th}$  are low and for the second growth are high (L1 and L2). Thus, the resulted age was corrected by means of STRUTages (Roy-Barman and Pons-Branchu 2016) for the second growth part, while the first growth part showed no significant difference in the corrected and uncorrected age.

**Table 10:** U–Th data measured for S-9 (a) (Ijnisiya spring)

mm		$^{238}\text{U}$ ( $\mu\text{g/g}$ )		$^{232}\text{Th}$ (ng/g)		$\delta^{234}\text{U}$		$^{230}\text{Th}/^{238}\text{U}$		$^{230}\text{Th}/^{232}\text{Th}$	
L1	1–3	0.359	$\pm 0.0002$	35.64	$\pm 0.026$	441	$\pm 1.01$	0.105	$\pm 0.0004$	3.26	$\pm 0.012$
L2	5–7	0.423	$\pm 0.00024$	22.51	$\pm 0.011$	527	$\pm 1.14$	0.055	$\pm 0.00029$	3.18	$\pm 0.017$
L3	11–14	0.425	$\pm 0.00009$	0.876	$\pm 0.0005$	542	$\pm 0.92$	0.025	$\pm 0.00024$	37.91	$\pm 0.364$
L4	22–27	0.456	$\pm 0.00009$	1.455	$\pm 0.0008$	542	$\pm 0.81$	0.0256	$\pm 0.00016$	24.77	$\pm 0.151$

The ages of the lamination of the carbonate sinter ranges from recent precipitation to 1.7 k.a (oldest formation) as shown in Table 11. The stable isotope data ranges are

different from Soreq cave, therefore, it was not used for age evaluation. The difference in the stable isotope values between this location and Soreq cave is due to the differences in plantation type and in amounts of precipitation. Applying the Hendy test also revealed that there is no kinetic fractionation for the stable isotope.

**Table 11:** Measured ages for S-9 a, <sup>1</sup>(Roy-Barman and Pons-Branchu 2016)

Distance from the top mm		Corrected age k.a. using STRUTages <sup>1</sup>		$\delta^{13}\text{O} \text{ ‰ VPDB}$	$\delta^{13}\text{C} \text{ ‰ VPDB}$	Period
L1	1–3	0.137	±0.072	–5.50	–9.26	Recent
L2	5–7	0.6	±0.4	–5.32	–8.67	Islamic period
L3	11–14	1.676	±0.93	–5.93	–9.33	Byzantine period
L4	22–27	1.73	±0.73	–6.30	–10.55	Roman–Byzantine transition period

### *Laminae, peak counting and trace element variation*

Lamina counting for the first growth revealed 65 laminae. This means, each lamina represents 1 year of carbonate growth. The lamina counting revealed a 65-year time span and U–Th dating revealed a 60-year span. It is clear the growth discontinued prior to 1676 years ago, subsequently resumed growth up until  $600 \pm 400$  years ago at which it stopped again. Then recently continued growth. As previously mentioned,  $\delta^{234}\text{U}$  is also altered, so the hypothesis here is: the water of this spring was diverted around 340 B.C. by a pipe and then the destruction of this pipe triggered the second growth period. An earthquake hit the area in 363 A.D. (Russell 1980) and this could be the cause of the pipe destruction.

The second growth period L2 has a large age error, therefore, it can be assumed that this layer started to grow again during the periods before 1000–800, and/or 500–100 years ago amid the cold humid periods that were first outlined in Issar's work (1998). With 20 layers, each layer represents one year. The laminations are annual and not seasonal because the sample is located above the spring base flow.

A hot dry period followed, and growth might have ceased again. Then a geological event happened and the feeding source of carbonate started flowing again with an altered  $\delta^{234}\text{U}$  value for the third growth. It might be a result of the recent destructive

earthquake happened in 1929. Based on this hypothesis, 52 layers in the third growth represent 52 years from 1927–1979.

Moreover, Mg concentration peaks appear every 10 years. Thus, during these wet periods when the sample scale was growing, a dry phase occurred more or less every 10 years. On the other hand, Sr is not totally coupled with Mg as reported in literature (Mattey et al. 2010; Orland et al. 2014). It is speculated that high Mg concentrations inhibited Sr incorporation in calcite crystals. The concentration peak of Sr is correlated with Al and Fe, and Fe peaks are pronounced when the crystal type is 9 (microsparite) or 11 (mosaic calcite).

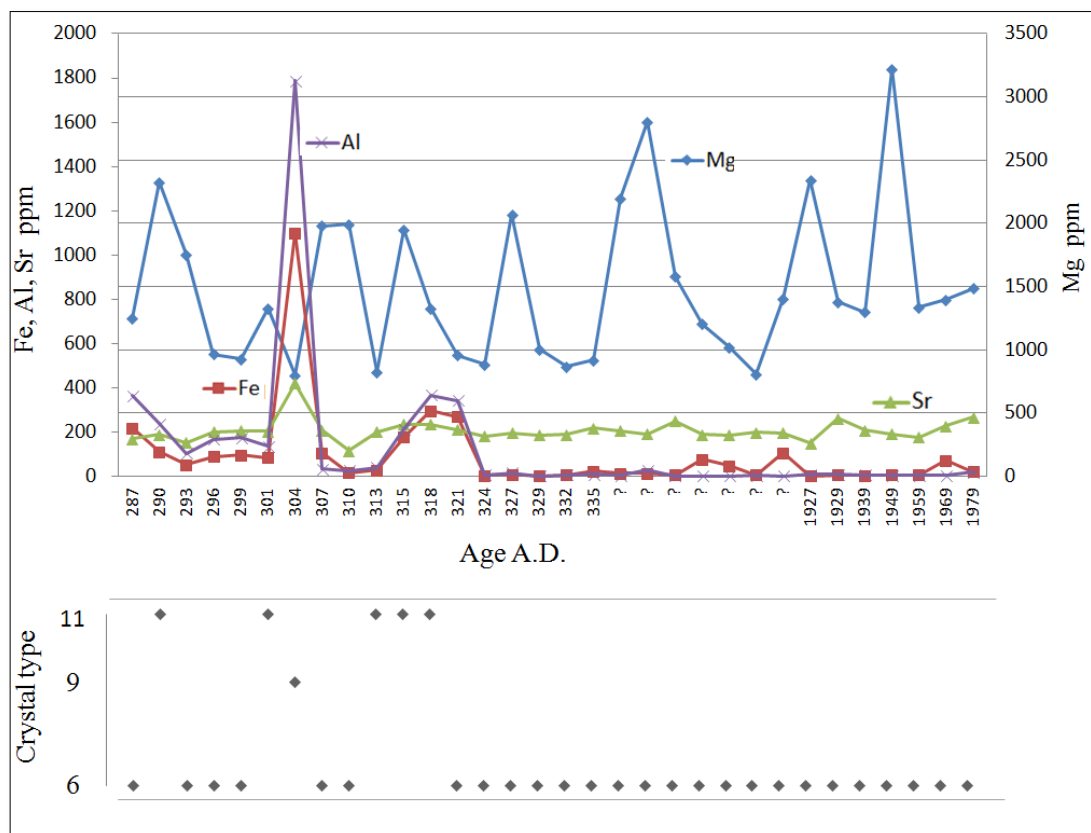


**Figure 57:** *Top:* Mg, Fe, Sr and Al peaks along the growth axis of the sinter from 287–1979 A.D. show frequent Mg peaks and less frequent Fe, Sr and Al. Question sign (?) indicates that the age was not determined, *bottom:* Crystal variation along the growth axis of the sinter: 9 (microsparite), 11 (mosaic calcite) and 6 (columnar microcrystalline). Fe concentrations are high at crystal type 11, 9

### ***Rare earth elements and yttrium***

Rare earth elements (REE) and yttrium (REY) concentration increase with time (Figure 58). Light REE elements are present in REE phosphate minerals, clays, Fe-Mn Oxides and organic matter (Tachikawa et al. 2004; Marchandise et al. 2014) The overall increase in light REE represented in (Nd) is correlated with Mn, however, the

most recent increase is not (Figure 59). This means that there are individual input sources for REY and Mn from anthropogenic activities. The REE patterns for the sequence laminations are variable. From 290 to 335 A.D. there is no detected REE. After 1929 A.D. the patterns of REE show an enrichment of heavy REE with Ce anomaly. In 1979 the Ce anomaly and heavy REE were not observed (Figure 60). The absence of Ce anomaly could have been caused by a flooding event which caused reducing conditions. Looking into the rainfall data, January 1974 (within the age error of year 1979) had the highest precipitation in 50 years (324 mm) according to VASCLimO precipitation data (Beck et al. 2004).

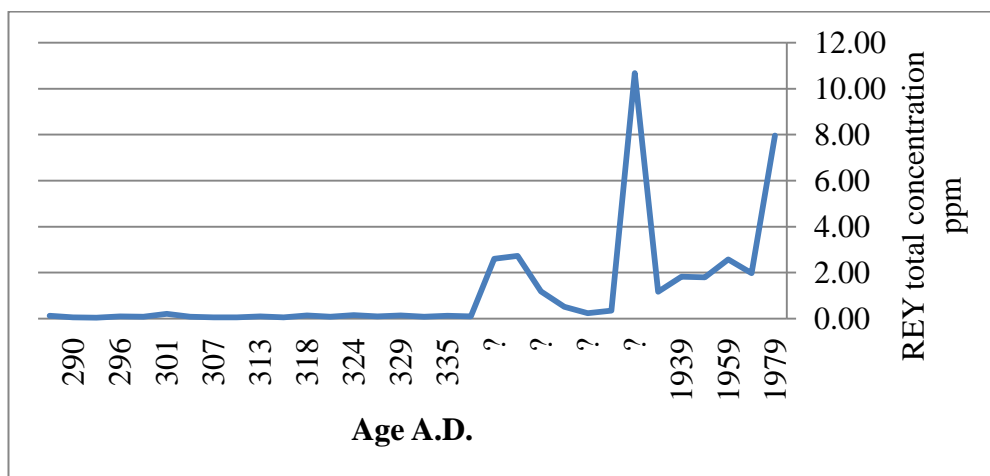


**Figure 58:** Total REY concentration for sample S-9 (a) along the growth axis of the sinter from 290–1779 A.D., shows robust increase after 1929 A.D. Question sign (?) indicates that the age was not determined

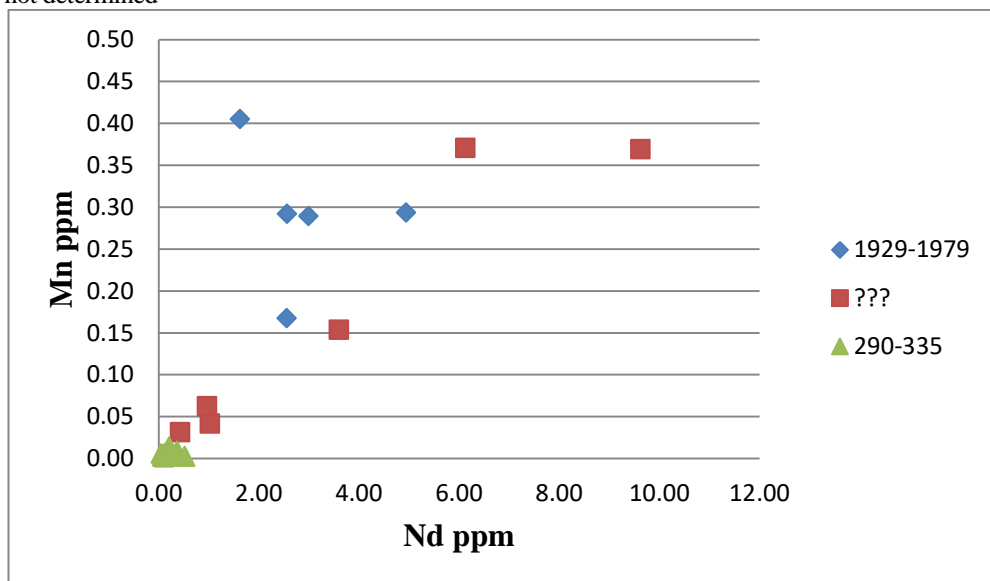


**Figure 59:** Mn vs. Nd show a linear relation in the first growth 290–335 A.D. and second growth, and a nonlinear relation for the third growth 1929–1979 A.D.

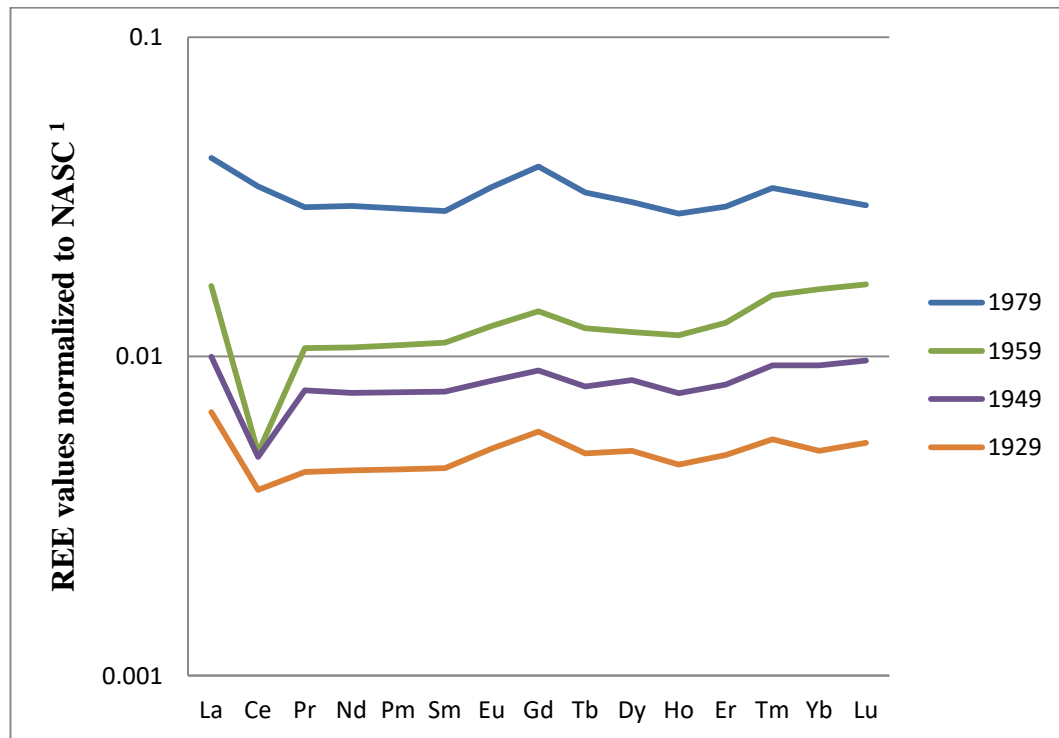


**Figure 60:** Selected REE values patterns normalized to NASC, <sup>1</sup>(Gromet et al. 1984) with corresponding age. From 1929 to 1979 A.D show a change in the oxidation condition in 1979 A.D.

#### 4.5.3 Harun Location (S-8)

Harun spring has a long dewatering tunnel that was connected to an additional source probably to increase the water flow. The carbonate deposit was collected at this connection point (Figure 24). The sample is laminated (372 lamiae) with gray being the dominant color (Figure 61).



**Figure 61:** *Left:* polished cross section shows different lamination colors (gray, black, white and brown), *right:* sample before cutting

The dominating crystal type is mosaic calcite, yet, columnar (open and microcrystalline) and micrite crystals are also common. Micrite contain high Fe > 1%, which means that iron bacteria were influencing the growth (Figure 62). The present

of open columnar and microcrystalline indicates that the flow rates vary from constant flow rate to variable flow (Frisia 2015). Therefore the flow rate feeding this carbonate was variable.

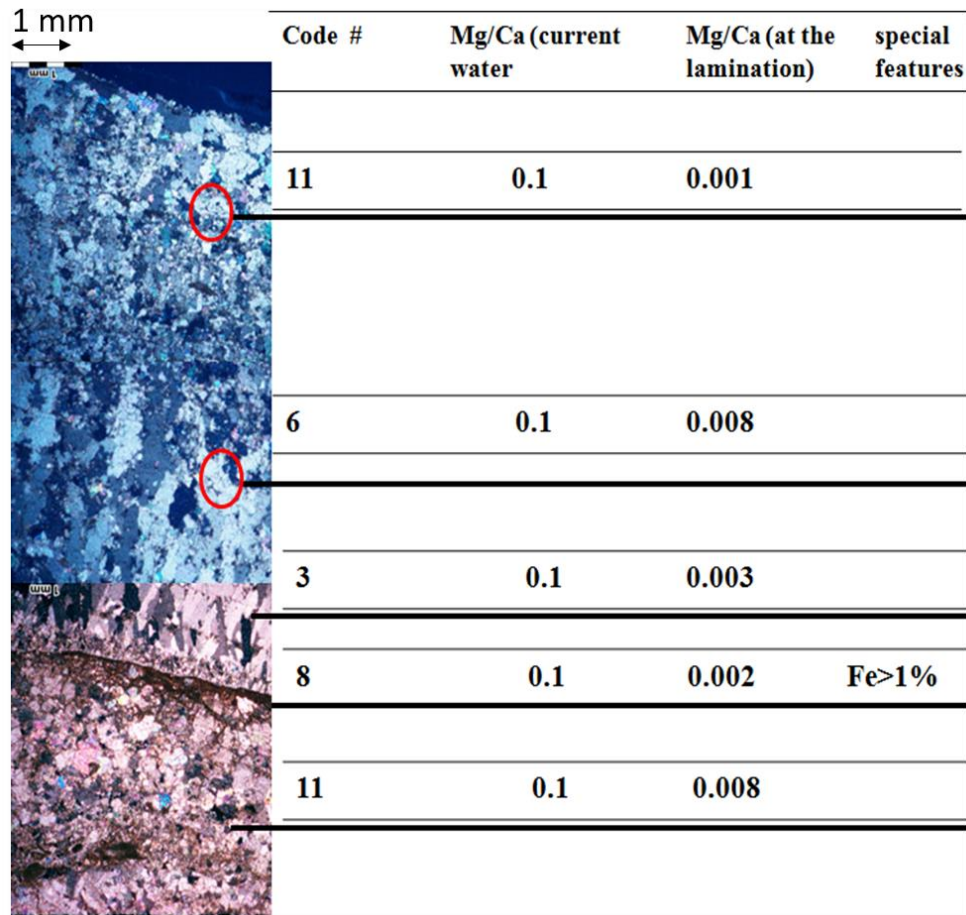


**Figure 62:** Sample S-8 thin section shows main crystals type code and their features crystal type code are based on Frisia (2015) classification shown in section 2.4.3

**Source identification: strontium isotope analysis  $^{87}\text{Sr}/^{86}\text{Sr}$ ,  $\delta^{234}\text{U}$  (S-8)**

In order to identify the sources of this carbonate sample, strontium isotope ratio  $^{87}\text{Sr}/^{86}\text{Sr}$  and  $\delta^{234}\text{U}$  analysis were done. It is shown in Figure 63 that the carbonate sample (S-8) has the same Sr isotope signature of S-9 and it is higher in S-2.  $\delta^{234}\text{U}$  results also agree with Sr isotope ratio results, as shown in Figure 64, sample S-2 have different  $\delta^{234}\text{U}$  values from (S-9) and (S-8). In the previous section, it was mentioned that S-9 sample has interrupted growth. Thus, we can conclude that the water spring S-9 was diverted and connected to the water tunnel of spring S-8. The two groups in Figure 64 differ significantly based on the Mann–Whitney test at the 95.0 % confidence level ( $P=0.00811$ )

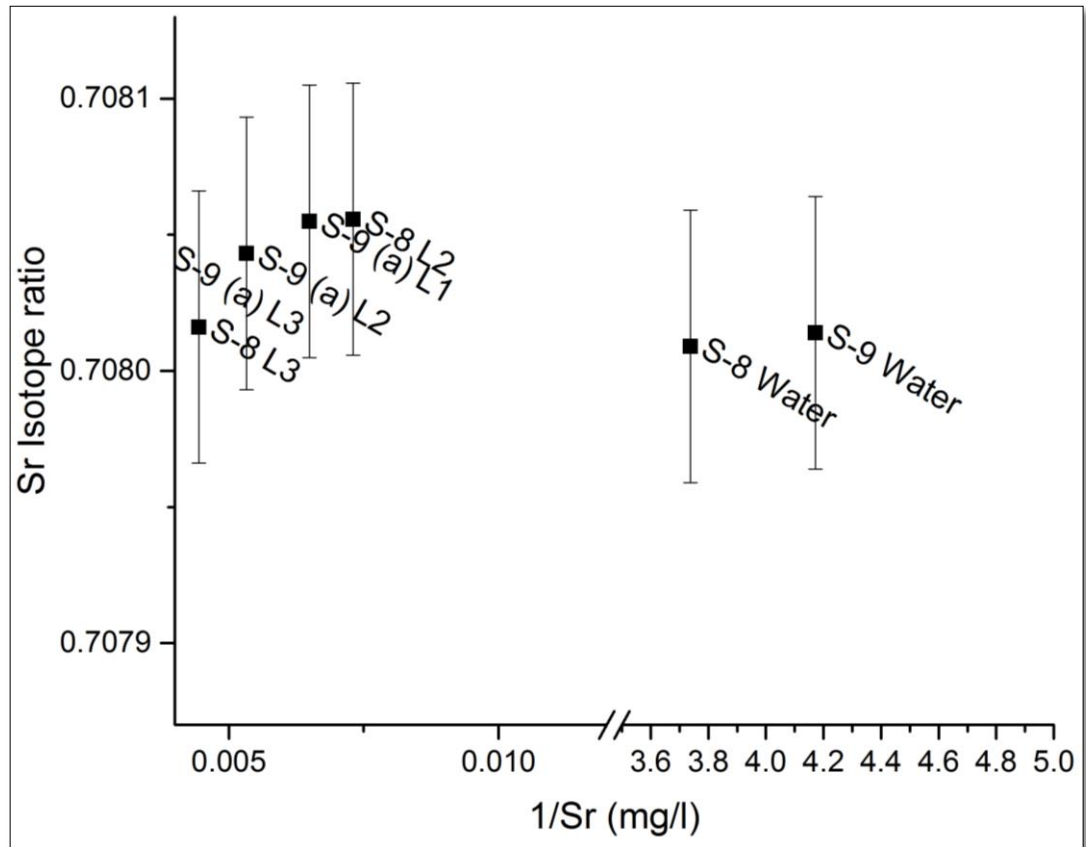


**Figure 63:** Strontium isotope ratio  $^{87}\text{Sr}/^{86}\text{Sr}$  vs. their reciprocal Sr concentrations show no significant different between sample S-8, S-9 and the origin water (Error of 0.00005 is derived by replicate analysis of standard)

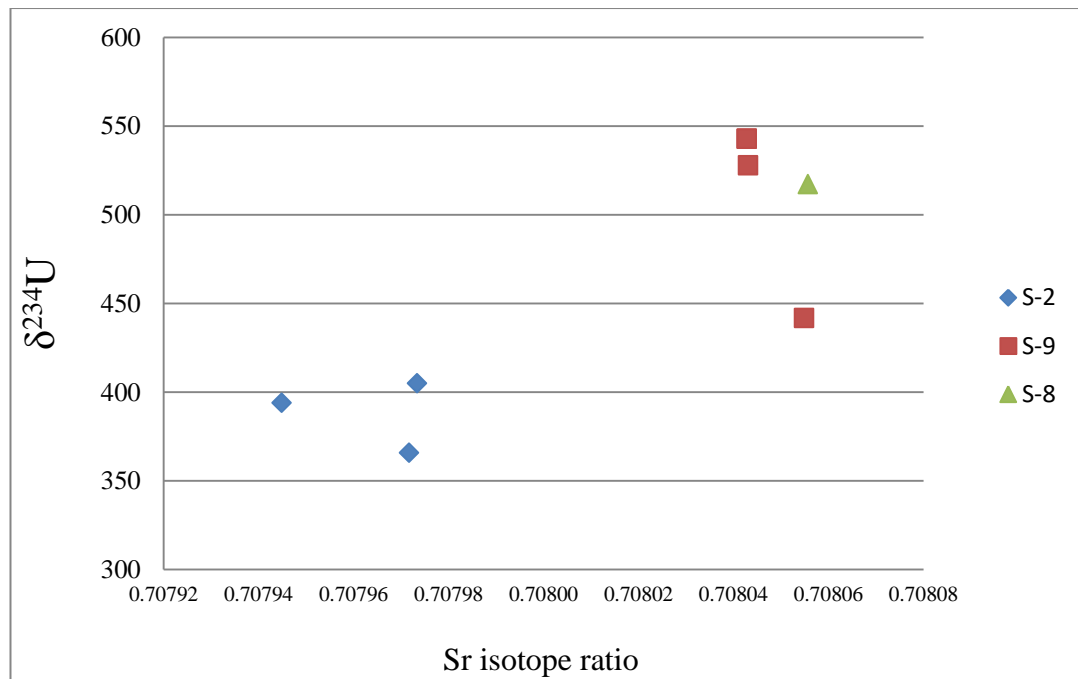


**Figure 64:** Variations of Sr isotopic ratios ( $^{87}\text{Sr}/^{86}\text{Sr}$ ) and  $\delta^{234}\text{U}$  in carbonate sinter samples provide a means to identify two different groups

***Uranium Thorium disequilibrium dating***

One sample was chosen for dating. Yet, in order to be able to correct the initial concentrations of  $^{230}\text{Th}$ , this sample was aliened within sample S-8 because this sample is part of S-9 stratigraphically; any lamination from sample S-8 will lie between the first, second growth and third growth. The  $^{238}\text{U}$  concentration is relatively low  $< 1 \mu\text{g/g}$  and with a rather high initial concentration for  $^{230}\text{Th}$  (Table 10). Accordingly, the resulted age was corrected using the algorithm STRUTages (Roy-Barman and Pons-Branchu 2016).

**Table 12:** U–Th data measured for samples S-9 and S-8

Sample	$^{238}\text{U}$ ( $\mu\text{g/g}$ )		$^{232}\text{Th}$ (ng/g)		$\delta^{234}\text{U}$		$^{230}\text{Th}/^{238}\text{U}$		$^{230}\text{Th}/^{232}\text{Th}$	
S-9 (L1)	0.359	$\pm 0.0002$	35.64	$\pm 0.026$	441	$\pm 1.01$	0.105	$\pm 0.0004$	3.26	$\pm 0.012$
S-9 (L2)	0.423	$\pm 0.00024$	22.51	$\pm 0.011$	527	$\pm 1.14$	0.055	$\pm 0.0003$	3.18	$\pm 0.017$
S-8	0.158	$\pm 0.0017$	1.517	$\pm 0.0023$	517	$\pm 1.55$	0.158	$\pm 0.0017$	1.51	$\pm 0.0023$
S-9 (L3)	0.425	$\pm 0.00009$	0.876	$\pm 0.0005$	542	$\pm 0.92$	0.025	$\pm 0.00024$	37.91	$\pm 0.364$
S-9 L4)	0.456	$\pm 0.00009$	1.455	$\pm 0.0008$	542	$\pm 0.81$	0.0256	$\pm 0.00016$	24.77	$\pm 0.151$

**Table 13:** Measured ages for S-8,  
<sup>1</sup> algorithm developed by (Roy-Barman and Pons-Branchu 2016)

Distance from the top mm		Corrected age k.a. using STRUTages <sup>1</sup>		$\delta^{13}\text{O}$ ‰ VPDB	$\delta^{13}\text{C}$ ‰ VPDB	Period
L1	1–3	0.137	$\pm 0.071$	–5.50	–9.26	Recent
L2	5–7	0.6	$\pm 0.4$	–5.32	–8.67	Islamic period
S-8		0.953	$\pm 0.029$	–6.30	–11.03	Byzantine period
L3	11–14	1.67	$\pm 0.93$	–5.93	–9.33	Byzantine period
L4	22–27	1.73	$\pm 0.73$	–6.30	–10.55	Roman–Byzantine transition period

***Laminae, peak counting and trace element variation***

The collected carbonate sample was taken at the connection point between this tunnel and the water diverted from Ijnisinya spring (S-9). Therefore, if its flow was continuous throughout the year, carbonate growths would be also continuous. Hence, in this case, the laminations in this sample are seasonal. In total, 371 laminae represent 180 years and the dated lamina represents the last growth. Based on that,

the last lamination dates back to 1053±29 A.D. and the first precipitation to around 880 ±29 A.D.

The peaks in element concentrations do not represent annual or event peaks because the water carrier (clay pipe) was influencing the water quality. The concentrations of Al, Fe, and Pb of the earliest laminations were rather high and decreased gradually due to the accumulation of carbonate scale inside the pipe. At one point the concentrations increased enormously and then decreased again. Such a change in concentration is evident when the scaling inside the pipe blocked it and thereafter the pipe was replaced (Figure 65). It was also observed that Sr and Mg concentrations do behave differently: extreme high Mg concentrations are correlated with minimum concentrations of Sr. It is speculated that when Mg concentrations are above 1500 ppm this inhibited Sr incorporation in calcite crystals.

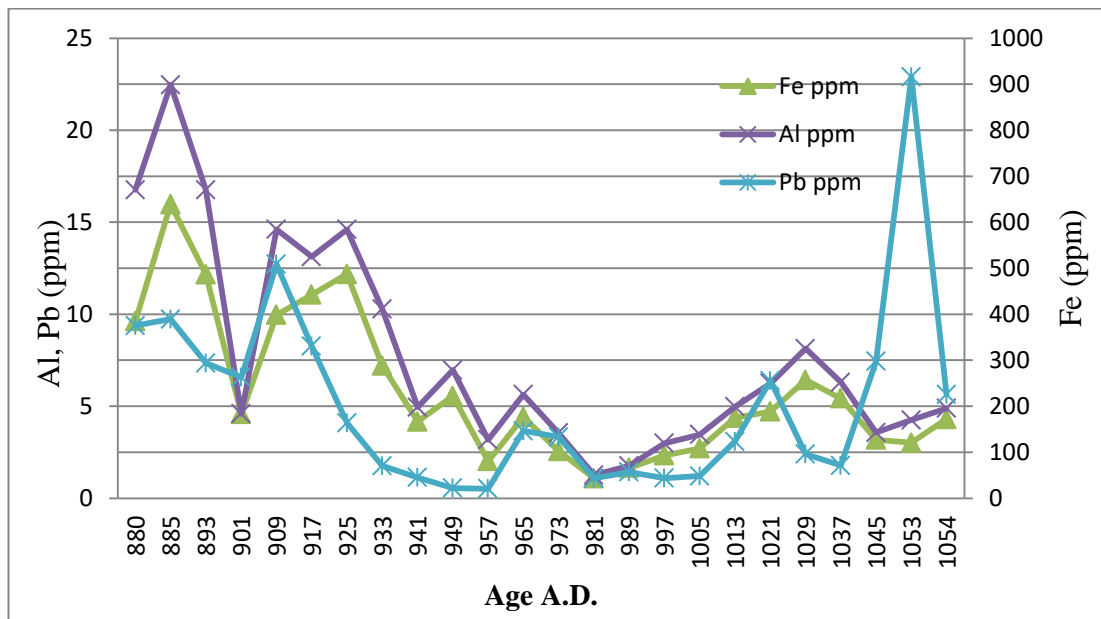


**Figure 65:** Al, Pb and Fe variation within the growth of the S-8 sinter from 880–1054 A.D.

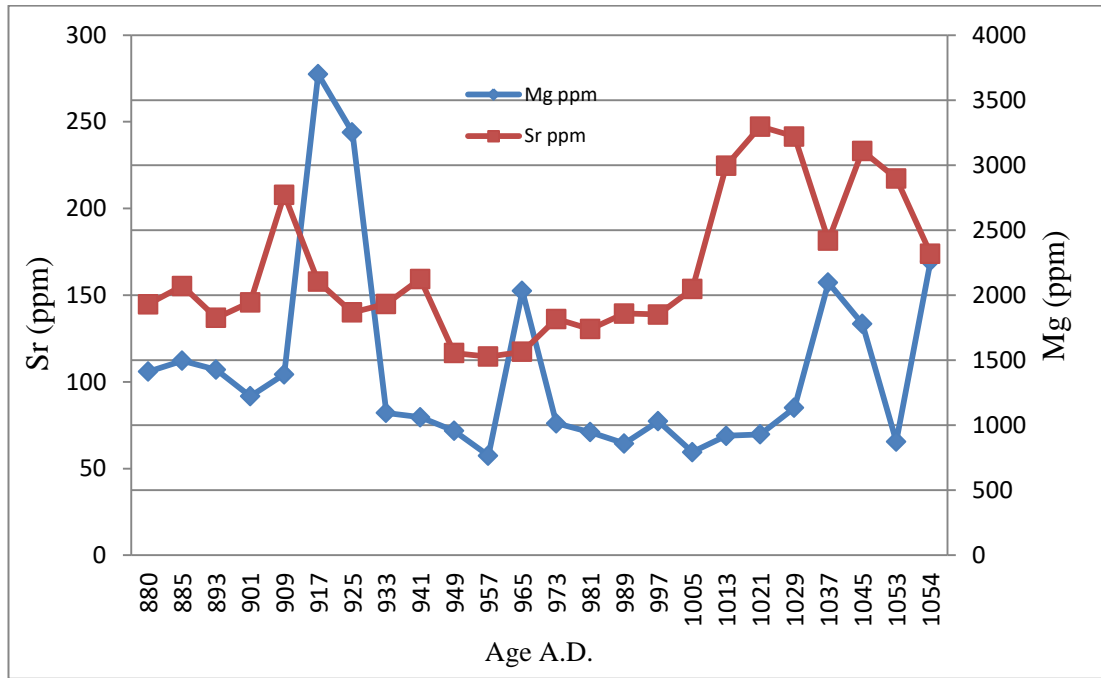


**Figure 66:** Sr and Mg variation within the growth of S-8 sinter from 880–1054 A.D.

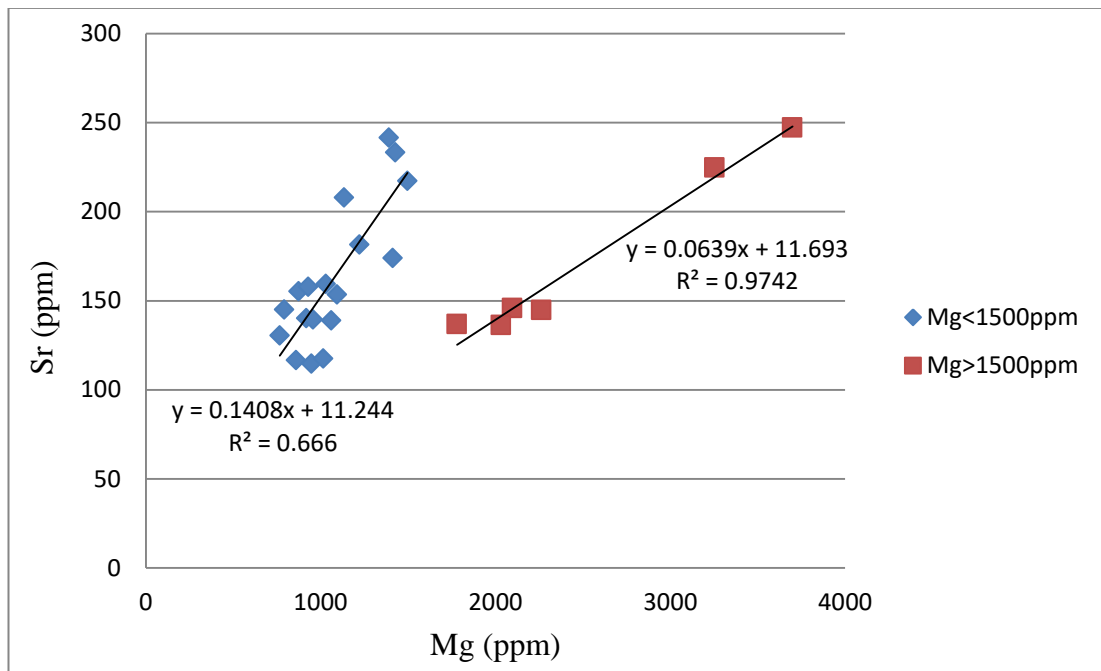


**Figure 67:** Mg concentration vs. Sr concentration show two different trends depending on Mg concentration in the S-8 sinter

***Rare earth elements and yttrium***

REY concentrations vary in the same pattern of trace elements (Fe, Al and Pb) (Figure 65), decreasing along the growth axis until it reaches a point and began to increase again. This is also due accumulation of carbonate scale inside the pipe. At

the time of the earliest laminations with no scale, the pipe material was leaching into the water. With time, however, scale accumulation covered the material and decreased the leaching (Figure 68). A correlation between Nd and Mn (0.88) implies that the water carrier was made of clay (Figure 69) because light REE and Mn are present in clays (Tachikawa et al. 2004; Marchandise et al. 2014). The REE patterns are identical with pronounced Ce anomalies indicating oxidizing conditions (Figure 70), unlike S-9 REE patterns. This means that during water transport aeration took place and the heavy REE were enriched in comparison to the light REE.

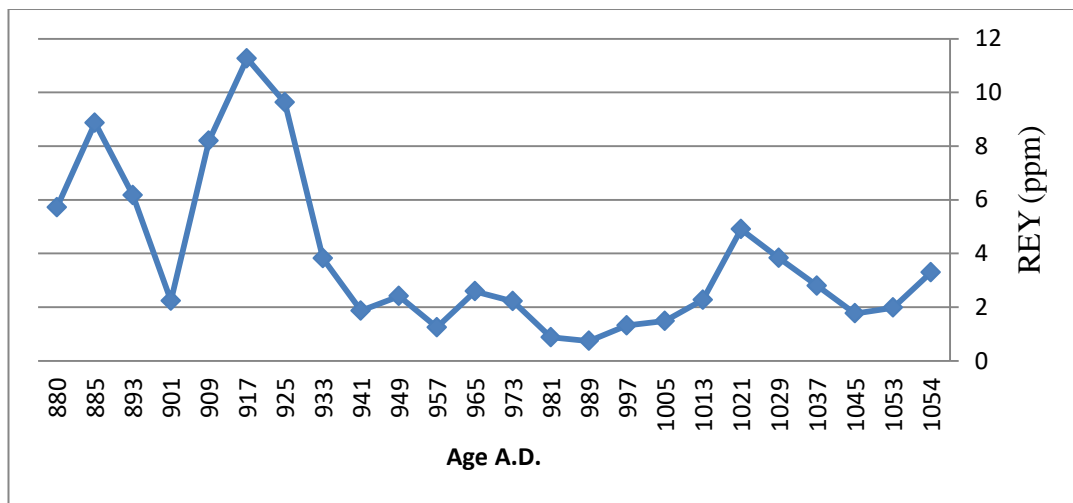


**Figure 68:** Total REY concentrations along the growth axis of the sinter from 880–1054 A.D. for sinter S-8, show an increase of REY in the first 20 years, then a decrease

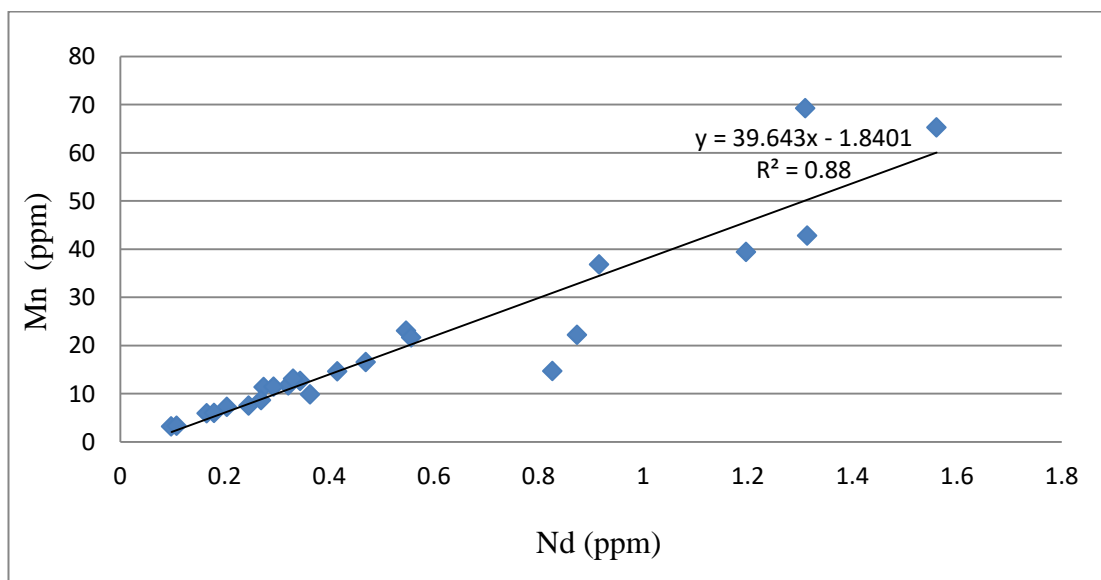


**Figure 69:** Mn vs. Nd in sample S-8, show a linear relationship, which suggests that the input of the both elements is from the same source

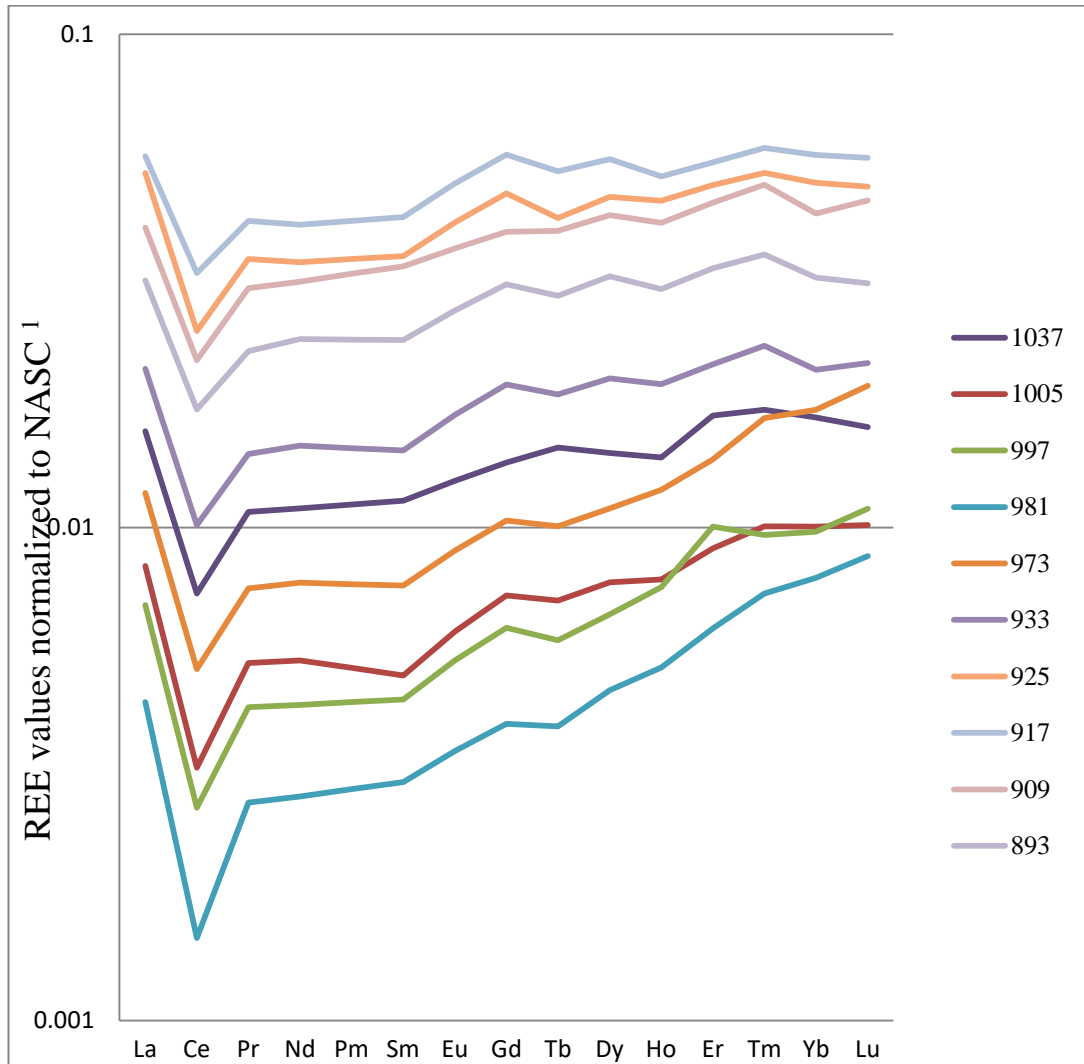


**Figure 70:** Selected REE values patterns normalized to NASC in sample S-8<sup>1</sup>(Gromet et al. 1984) and corresponding age A.D. show similar patterns along the growth axis of the sinter

#### 4.5.4 Water tunnel Location (A-1)

Four samples were collected from different locations; two of these samples were collected from the wall of the tunnels at different elevation A-1(a), A-2(b) (Figure 71, Figure 72). Because both samples provided similar results, one was chosen for further dating analysis. Sample A-1(c) (Figure 73) was taken from the floor of the tunnel. A-1(d) (Figure 74) was sampled from the roof of the inspection window.



**Figure 71:** Sample A-1(a) cross section shows the lamination and outer side of the sample



**Figure 72:** Sample A-1(b) cross section and the sample before cutting

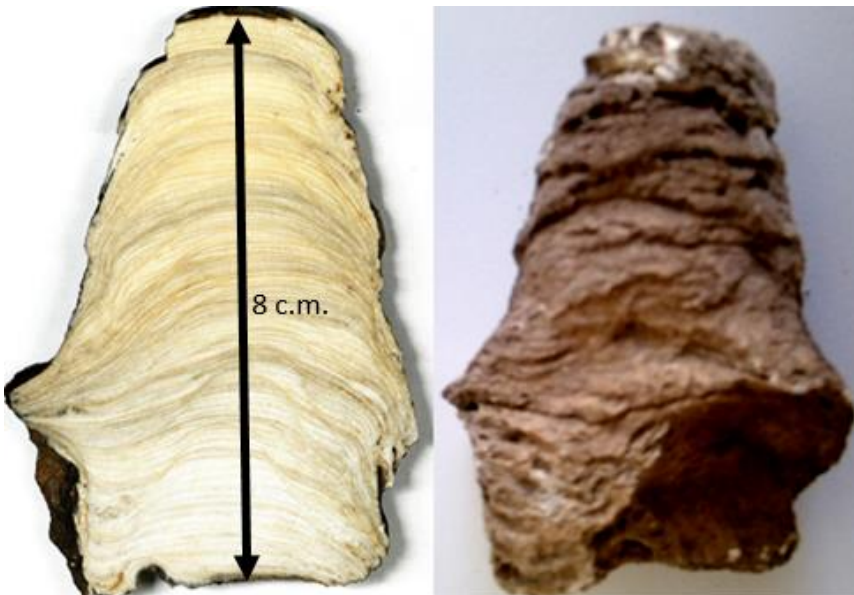


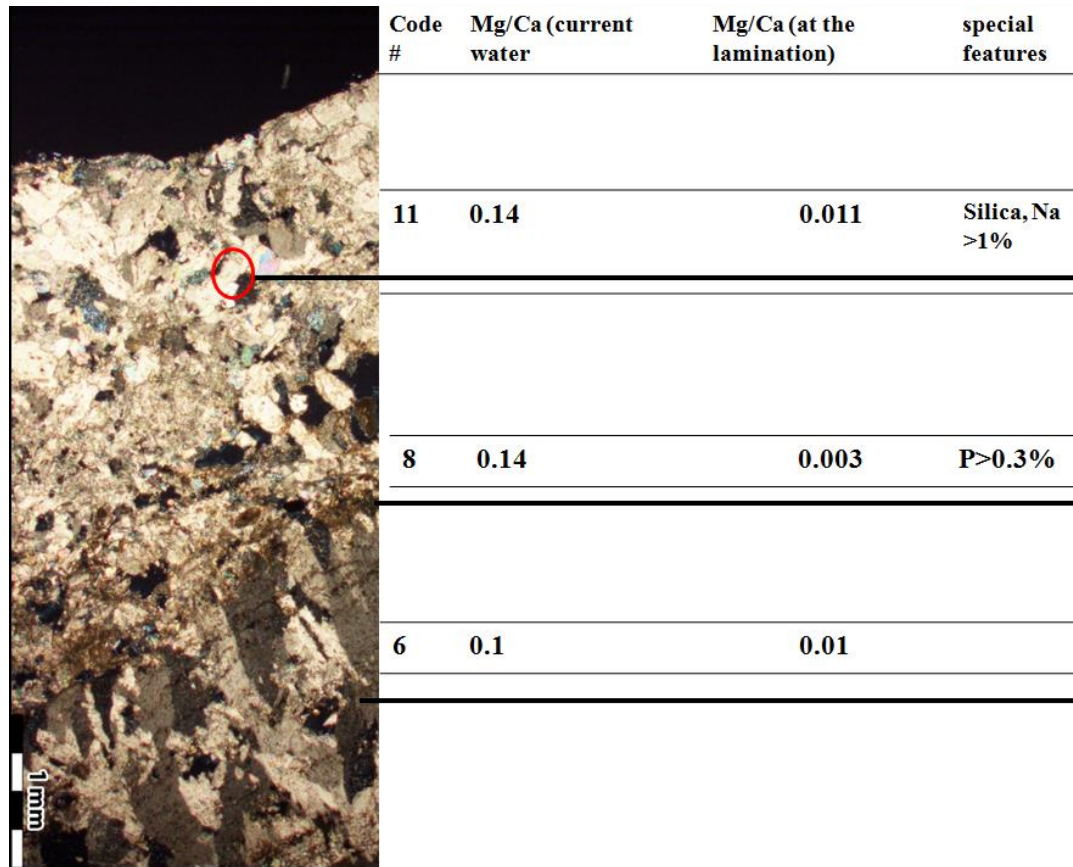
**Figure 73:** Sample A-1(c) cross section and the sample before cutting



**Figure 74:** Sample A-1(d) cross section and the sample before cutting

Sample A-1 (b) has 163 laminations within 34 mm. The colors of the laminations varied from white, brown to gray. The crystal types are similar. Throughout the

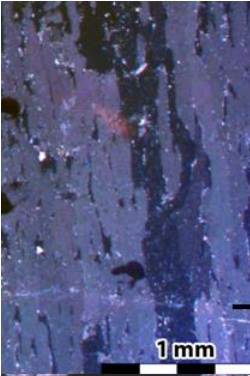
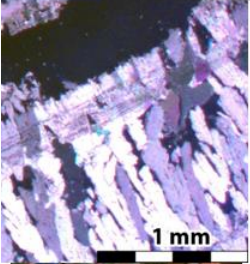
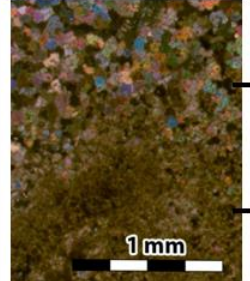
growth of this carbonate, it remains columnar microcrystalline up until the last 3 mm, where it changes to micrite and then to mosaic calcite, which indicates that the flow rate was variable (Figure 75).



**Figure 75:** Sample A-1(b) thin section shows the main crystal type codes and their features. Crystal type codes are based on Frisia (2015) classification shown in section 2.4.3

Sample A-1(c) is around 8 cm with 271 laminations. The colors of laminations alternate from white to gray. With the earliest laminations, a micrite crystal type was observed, thereafter mosaic and after that, the crystal type changed into columnar with lateral overgrowths and columnar elongated.

A micrite crystal type is triggered by biological activity and columnar elongated reflect a constant drip rate (Frisia 2015). Therefore, it is clear that biological conditions (bacteria) had enhanced the rapid initial growth of this carbonate sample, and thereafter in a brief transition period, the crystal changed into mosaic calcite. After that, the crystal type changed into columnar elongated, which signified a constant drip rate.

	Code #	Mg/Ca (current water)	Mg/Ca (at the lamination)	special features
	3	0.14	-----	S>0.14%
	4	0.14	-----	S>0.14%
	11	0.1	-----	
	8	0.1	-----	

**Figure 76:** Sample A-1(c) thin section shows main crystals type codes and their features. Crystal type codes are based on Frisia (2015) classification as shown in section 2.4.3

**Source identification: strontium isotope analysis  $^{87}\text{Sr}/^{86}\text{Sr}$ ,  $\delta^{234}\text{U}$  (A-1)**

As already mentioned in section 4.2.2, the water in tunnel has one source: Dafna spring (S-1). The carbonate analysis, however, revealed different results. Samples A-1 (a), A-1 (b) and A-1 (c) have the same Sr isotope signatures 0.7081 for all laminations. That means all these samples are fed from Dafna spring (S-1). However, sample A-1 (d) has different isotopic ratio for each lamination (Figure 77: ). This means an additional Sr source with an isotope ratio of 0.7079 is infiltrating into the tunnel and probably from Ras al Ein (S-2) and Qaryon (S-3).

From sample A-1 (b), four laminations were chosen for  $\delta^{234}\text{U}$  analysis and from sample A-1 (c), two samples were chosen. Despite the similarity of the Sr isotope ratio, the lamination differs significantly in respect to  $\delta^{234}\text{U}$ . The three groups in Figure 78 differ significantly based on the Kruskal-Wallis test at the 95.0 % confidence level (P= 0.00126). It seems that the newer two laminations from sample A-1 (b) were feed

from Ras al Ein spring (S-2) as shown in Figure 78. One can assume that the higher isotope ratio is a result of mixing groundwater with rainfall (Figure 42).

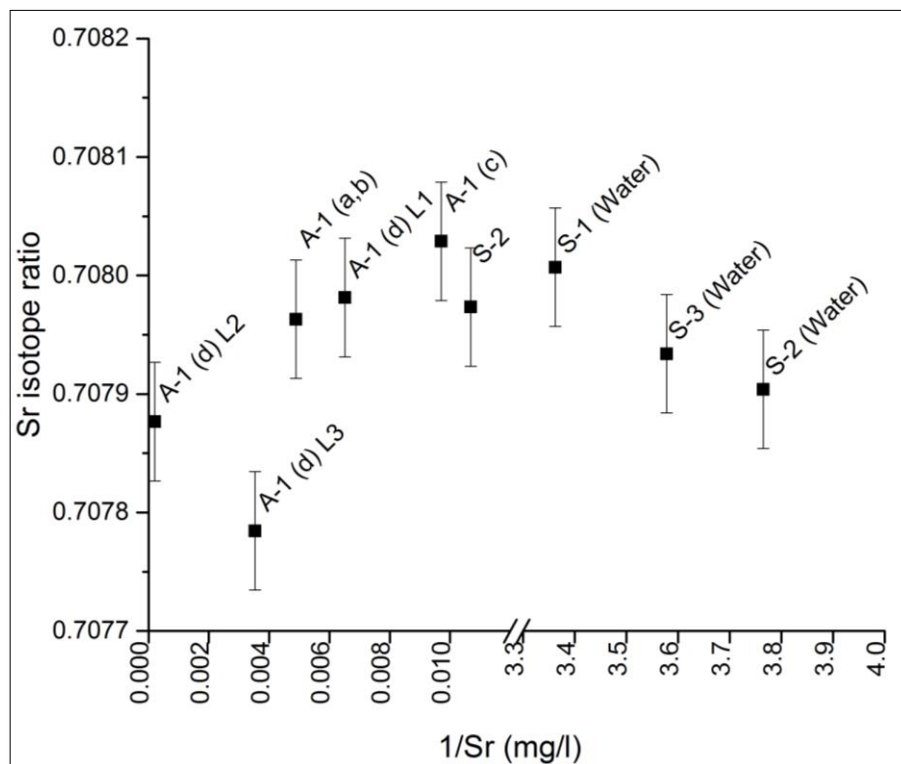


**Figure 77:** Sr isotope ratio  $^{87}\text{Sr}/^{86}\text{Sr}$  vs. mean reciprocal Sr concentrations for samples in tunnel, shows the carbonate in the tunnel has different sources: S-1, S-2 and S-3 and rainfall (Error of 0.00005 is derived by replicate analysis of standard)

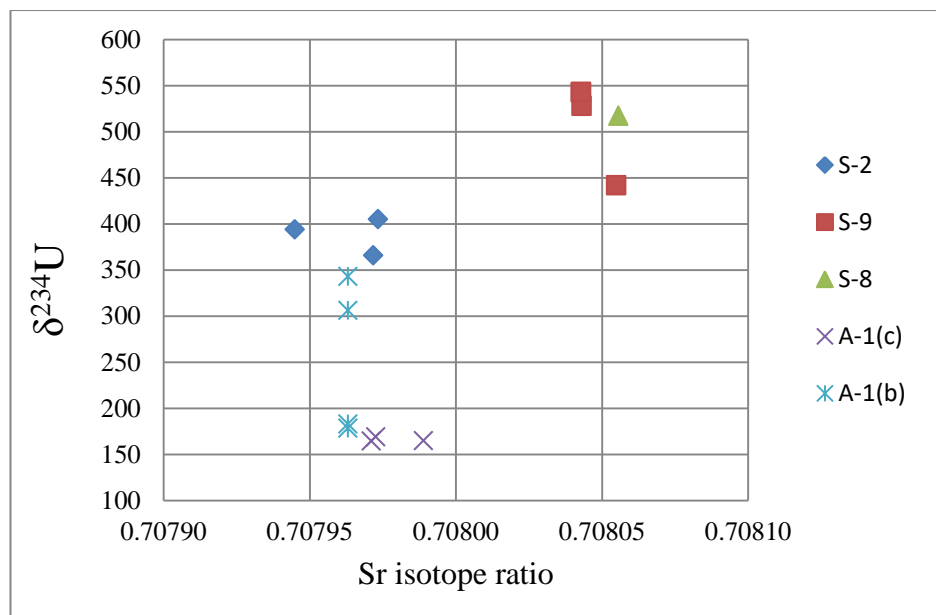


**Figure 78:** Variations of Sr isotopic ratios ( $^{87}\text{Sr}/^{86}\text{Sr}$ ) and  $\delta^{234}\text{U}$  in carbonate sinter samples provide a means to identify three different groups

***Uranium Thorium disequilibrium dating***

For sample A-1 (b), four laminations were chosen for U–Th disequilibrium dating. The lamina was cut with a micro sawing drill and then analyzed as described in section 3.3.3. The  $^{238}\text{U}$  content is  $< 1 \mu\text{g/g}$ . The initial concentrations of  $^{230}\text{Th}$  are identified to be high, taking into account the measured ratio of  $^{230}\text{Th}/^{232}\text{Th}$  (Table 14). Thus, the age was corrected by means of STRUTages (Roy-Barman and Pons-Branchu 2016).

**Table 14:** U–Th data measured for A-1(b)

Sample	$^{238}\text{U}$ ( $\mu\text{g/g}$ )		$^{232}\text{Th}$ (ng/g)		$\delta^{234}\text{U}$		$^{230}\text{Th}/^{238}\text{U}$		$^{230}\text{Th}/^{232}\text{Th}$	
A-1b(L1)	0.0226	$\pm 0.0069$	6.62	$\pm 3.174$	343	$\pm 0.94$	0.023	$\pm 0.0069$	6.749	$\pm 2.053$
A-1b(L2)	0.0118	$\pm 0.0002$	2.61	$\pm 0.004$	306	$\pm 0.806$	0.012	$\pm 0.0002$	8.446	$\pm 0.133$
A-1b(L3)	0.0134	$\pm 0.0003$	1.88	$\pm 0.002$	178	$\pm 0.767$	0.013	$\pm 0.0003$	9.566	$\pm 0.196$
A-1b(L4)	0.0139	$\pm 0.0005$	8.24	$\pm 0.278$	183	$\pm 1.196$	0.014	$\pm 0.0005$	8.378	$\pm 0.288$

**Table 15:** Measured ages for A-1 (b),  
<sup>1</sup> algorithm developed by (Roy-Barman and Pons-Branchu 2016)

Distance from the top mm		Corrected age (years before 2011) using STRUTages <sup>1</sup>		$\delta^{13}\text{O}$ ‰VPDB	$\delta^{13}\text{C}$ ‰VPDB	Period
L1	1–3	6	$\pm 5$	–5.39	–7.86	Recent
L2	5–7	110	$\pm 30$	–5.20	–7.84	British
L3	11–14	400	$\pm 20$			1611/ Islamic
L4	22–27	540	$\pm 15$	–5.46	–8.00	1471/ Islamic

Sample A-1 (c) has an U concentration less than  $0.1 \mu\text{g/g}$ , so it was difficult to detect  $^{230}\text{Th}$  with the same method. Increasing the sample size to 1 g increased the matrix effect. Therefore, the error was high and did not give evaluable results for the age of the sample (Table 16 and Table 17).

**Table 16:** U–Th data measured for A-1(c)

Sample	$^{238}\text{U}$ ( $\mu\text{g/g}$ )		$^{232}\text{Th}$ (ng/g)		$\delta^{234}\text{U}$		$^{230}\text{Th}/^{238}\text{U}$		$^{230}\text{Th}/^{232}\text{Th}$	
		$\pm$		$\pm$		$\pm$		$\pm$		$\pm$
A-1c(L1)	0.01899	$\pm 0.00001$	2.55	$\pm 0.05$	164.6	$\pm 1.4$	0.336	$\pm 0.006$	2.62	$\pm 0.05$
A-1 c(L2)	0.03055	$\pm 0.00001$			164.2	$\pm 1.0$				
A-1c(L3)	0.03376	$\pm 0.00001$	2.72	$\pm 0.02$	168.6	$\pm 0.9$	0.386	$\pm 0.003$	2.81	$\pm 0.02$

**Table 17:** Measured ages for A-1 (c),

<sup>1</sup> algorithm developed by (Roy-Barman and Pons-Branchu 2016)

Distance from the top mm		Corrected age k.a. using STRUTages <sup>1</sup>		$\delta^{13}\text{O}$ ‰ VPDB	$\delta^{13}\text{C}$ ‰ VPDB	Period
L1	1–3	12.3	15	–19.88	–34.91	Non evaluable
L2	5–7			–20.03	–34.46	
L3	11–14	24	13	–19.64	–33.00	Non evaluable

#### ***Stable isotope classification and its correlation with age (A-1)***

The stable isotope results for the sinter sample A-1 (c) differ completely from the other carbonate samples in the tunnel and the normal range of secondary carbonate in Palestine. Therefore, it is important to discuss this section in detail. As shown in Figure 79, sample A-1 (c) has light isotopic ratios. Methane has a light  $\delta^{13}\text{C}$  value of  $-60\text{‰}$  (Panchuk et al. 2008) and therefore, the light  $\delta^{13}\text{C}$  value in the sample indicates the presence of methane in the origin water and this is a sign of wastewater contamination. This also denotes that the carbonate in sample A-1(c) started to accumulate after the installation of the water network (around 100 to 150 years ago, as discussed in section 1.2.2) and following the increase of the water consumption and therefore wastewater discharge.

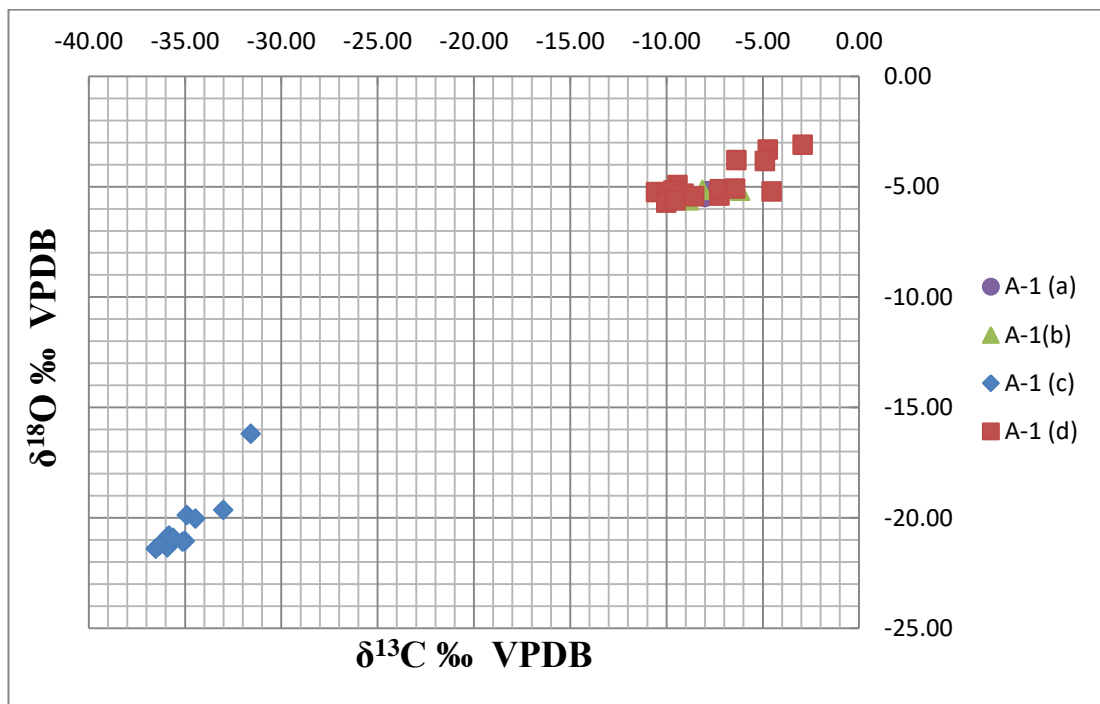


**Figure 79:** Stable isotope variation,  $\delta^{18}\text{O} \text{ ‰ VPDB}$  versus  $\delta^{13}\text{C} \text{ ‰ VPDB}$  for the tunnel samples (A-1), show sample A-1(c) having lighter isotope ratio than A-1(a), A-1(b) and A-1(d) due to wastewater influence on sample A-1(c)

#### *Sample dating using lamina counting and S/Ca method*

U–Th dating was not successful with sample A-1 (c) due to low U content, and the stable isotope values indicate a 100-year-old sample. An alternative method was used to determine the age of the sample: lamina counting coupled with S/Ca peaks counting. S and Ca concentrations were measured using SEM–EDS to have a better resolution than the CNS analyzer. S/Ca peaks reflect the emissions of S in the air in wintertime. The first S/Ca peak occurred in 1953 (Frisia et al. 2008). The sulfur peak increased as a result from the use of diesel in the heating system. The sinter was still growing during sampling in 2011. The counting reveals 271 laminae, for seasonal growth it means 135 years. For the youngest 117 laminae, 59 S/Ca peaks are observed. Each two lamination layers correspond to one peak, which means that the first S/Ca peak in this sample happened in the middle of the 20<sup>th</sup> Century (Figure 80). S/Ca was only observed in the thin section of sample A-1.

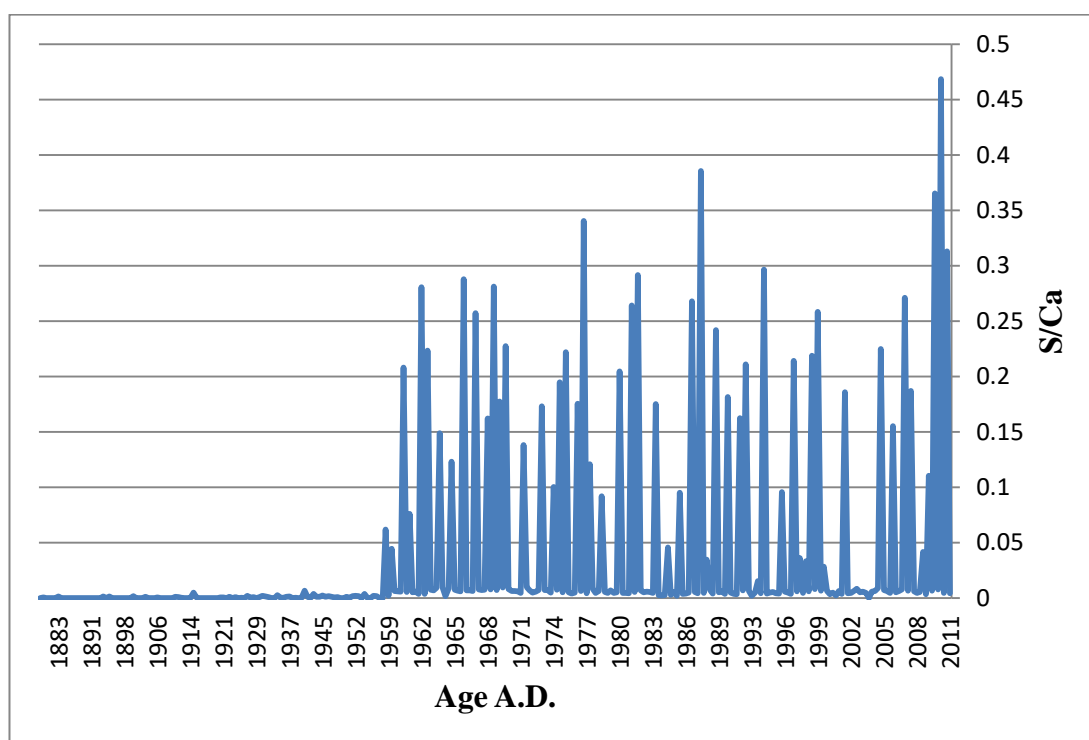


**Figure 80:** S/Ca ratio for sample A-1 (c) show an increase of the ratio after 1959 with seasonal frequency due to the increase of S emissions in water with the use of diesel heating

#### *Trace element variation*

The seasonality in sample A-1(c) is also observed in the concentration of Mg, Sr and Fe (Figure 81). Mg concentrations are low and in the same range of Sr and Fe. This means the high salinity of the water reduced the Mg activity ratio and thus reduced its incorporation in the calcite. It is speculated that Sr is the dominant element and it limits the incorporation of Mg concentration (Figure 82).

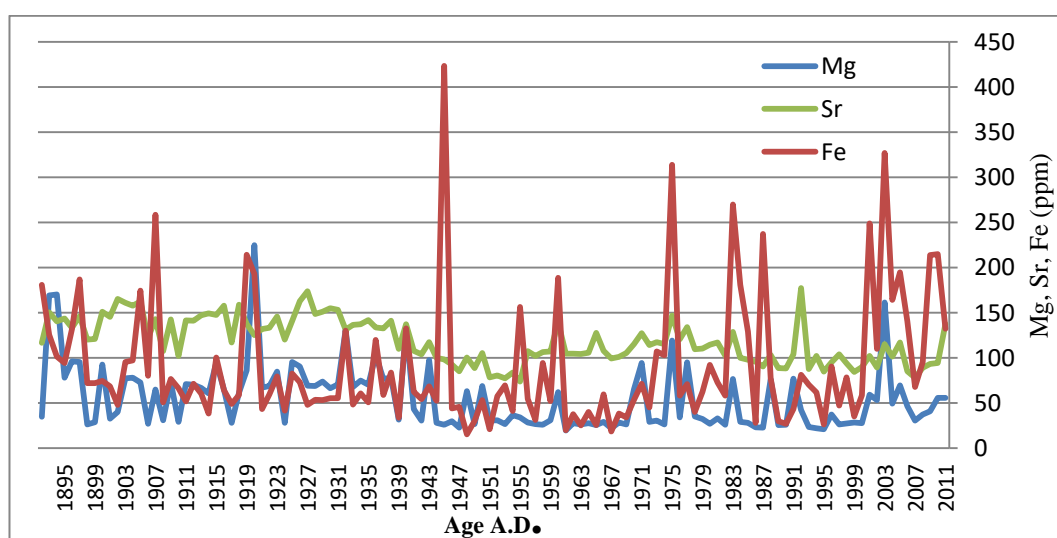


**Figure 81:** Mg, Sr and Fe concentrations along the growth axis (A.D. calendar year) sample A-1 (c) with low concentrations of Mg shown at the same scale as Fe and Sr

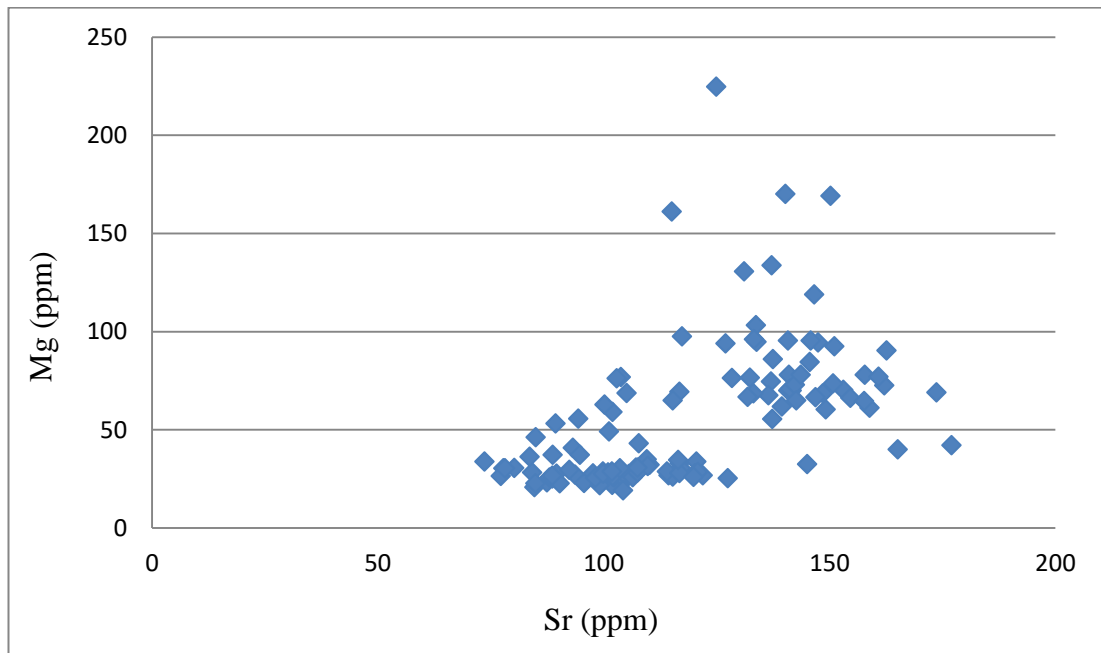


**Figure 82:** Mg concentrations versus Sr concentration in the sinter A-1 (c), shows no correlation

Elevated arsenic concentrations are observed in sample A-1 (c), in comparison to the other samples where concentration did not exceed 2 ppm. Furthermore, the concentrations for both samples A-1 (c) and A-1 (b) increase after 1991 (Figure 83, Figure 84).

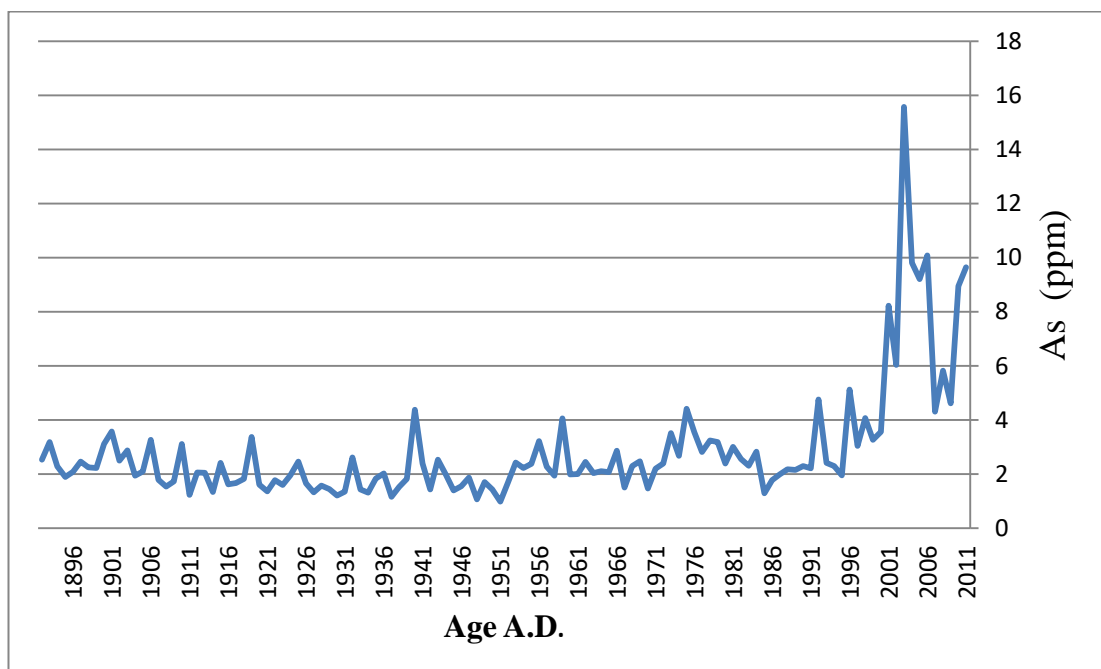


**Figure 83:** As concentration along the growth axis (calendar year) of sample A-1 (c), shows an increase after 1991



**Figure 84:** As concentration along the growth axis (calendar year) of sample A-1 (b), shows an increase after 1920

#### *Rare earth elements and yttrium*

The REY concentration increases in the same way as As in both samples A-1 (c) and A-1 (b). In sample A-1 (c) there is a point increase after the 20<sup>th</sup> Century, however, the recent increase is more pronounced (Figure 85). A peak in the same year is also observed in sample A-1 (b) (Figure 86).

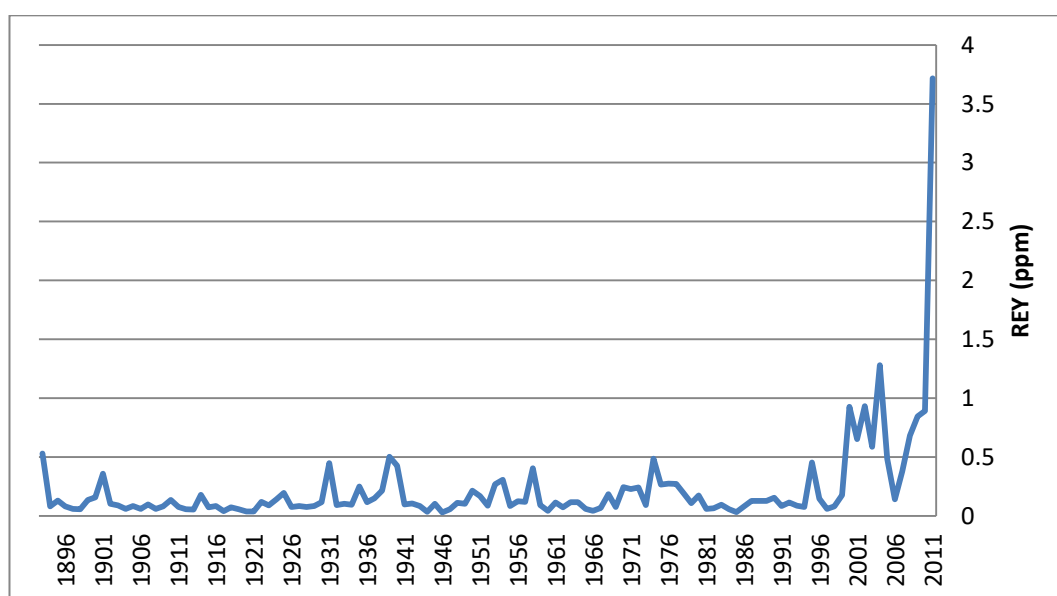


**Figure 85:** REY concentration along the growth axis (calendar year) in sample A-1 (c), show an increase after 1991



Regarding REE patterns in sample A-1 (c), Ce anomalies vary along the growth axis of the sinter due to the change of oxidation conditions during precipitation (Figure 88).

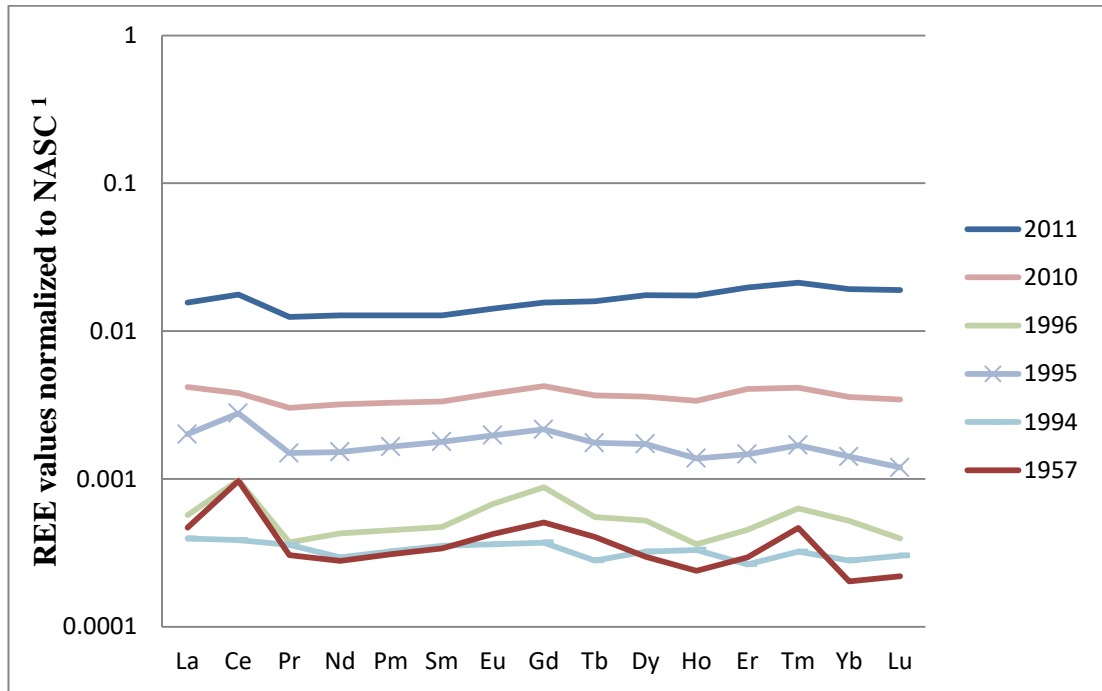


**Figure 88:** REE patterns for selected years normalized to NASC, <sup>1</sup>(Gromet et al. 1984) in sample A-1 (c), show a change in the patterns in Gd and Ce, a Gd positive anomaly due to high salinity and a Ce positive anomaly due to reducing conditions

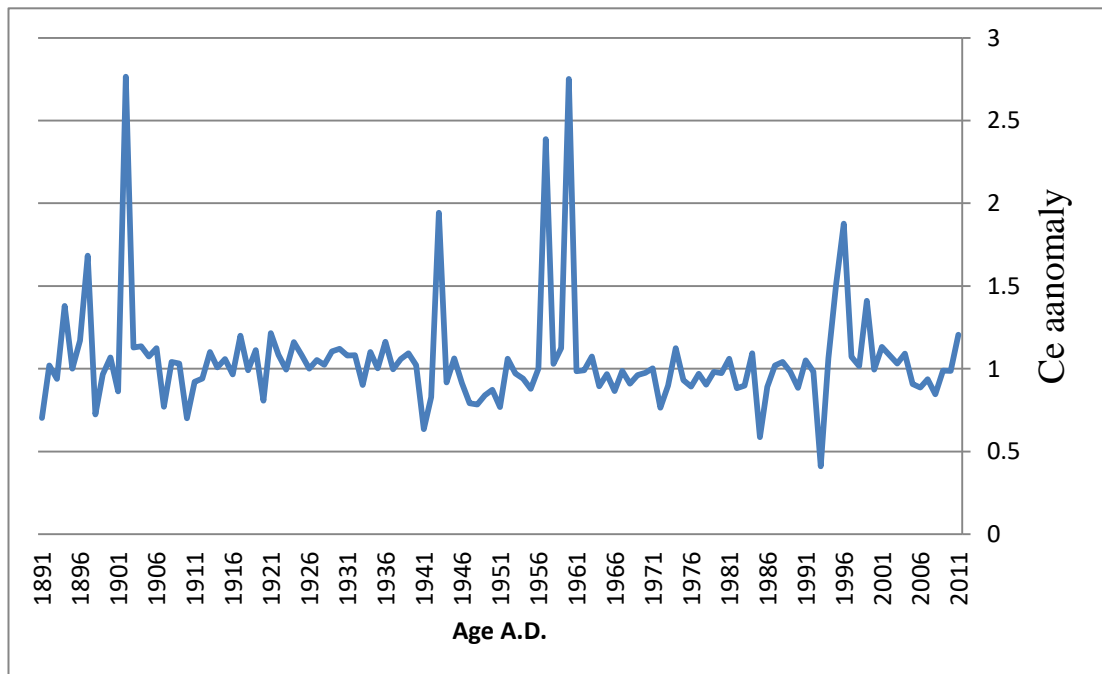


**Figure 89:** Ce anomaly values along the growth axis (A.D. calendar years) calculated according to formula 3 on page 58. Sample A-1 (c) shows a frequent change from a positive to negative anomaly that indicates a variation in oxygen level in the water

On the other hand, sample A-1 (b) exhibits a negative Ce anomaly all along the growth axis, except for the first growth (Figure 90).

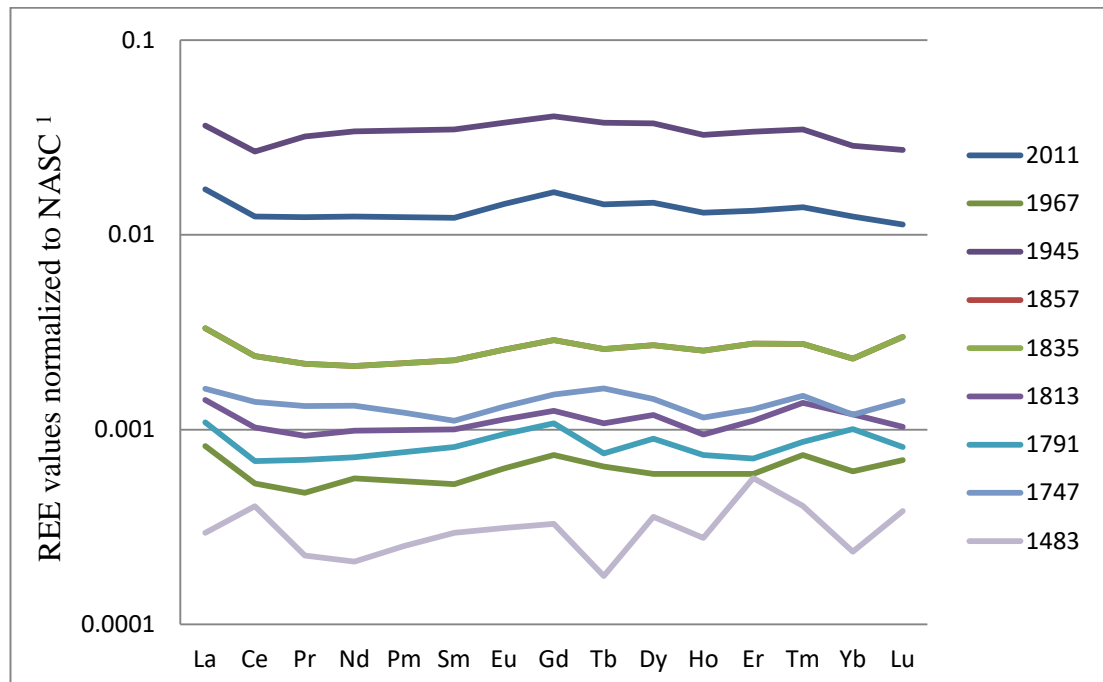


**Figure 90:** REE patterns normalized to NASC, <sup>1</sup>(Gromet et al. 1984) sample A-1 (b), show a different pattern for the first growth at 1483 A.D. than the rest with a positive Ce anomaly

#### 4.5.5 Water aqueduct Location (A-4)

Five samples were collected from the outside wall of the aqueducts (Figure 30, Figure 91). These carbonate samples are a result of seeping water from the aqueduct. Sample A-4(a) soda straw carbonate has circle laminations (Figure 92) of around 7 cm in length.

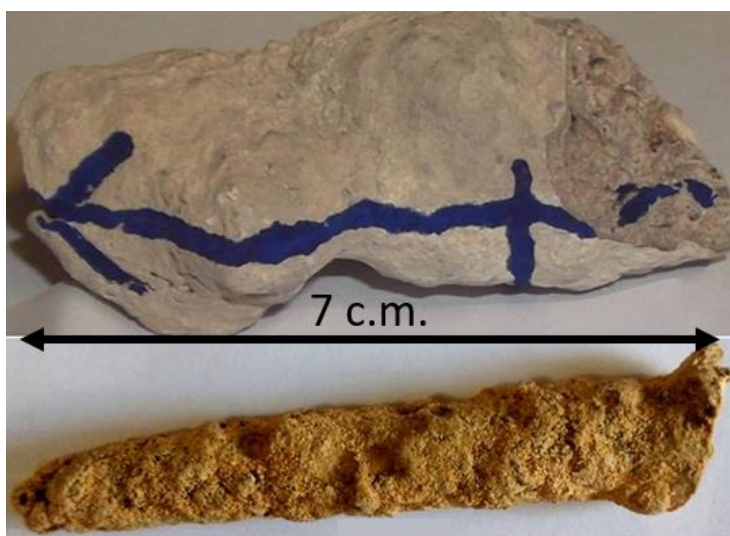


**Figure 91:** Samples collected from location A-4, *top*: A-4(b), *bottom*: A-4(a)

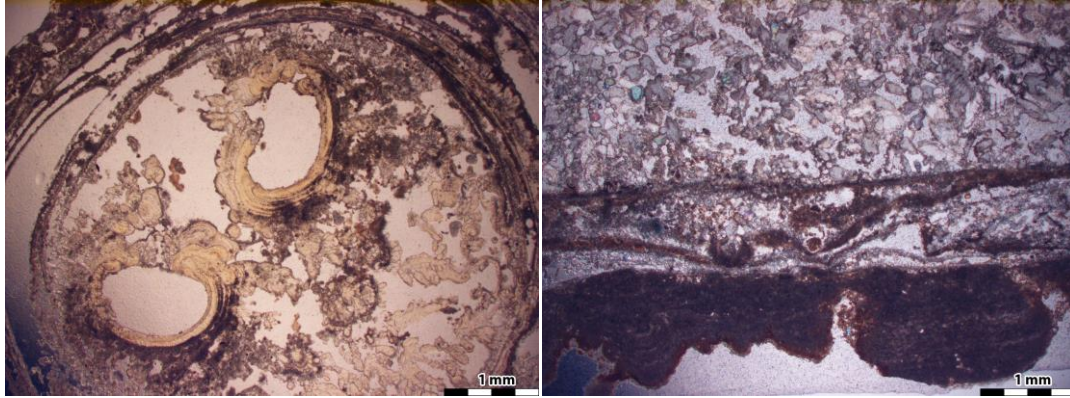


**Figure 92:** Thin section images for sample shows circular lamination calcite with voids not suitable for dating A-4 (a), *left*: cross section, *right*: longitudinal section

Sample A-4(b) is also hanging from the outside aqueduct wall like stalactites but its dimensions are different (Figure 91) at around 8 cm in length and 4 cm in diameter. The sample has circular and longitudinal laminations.

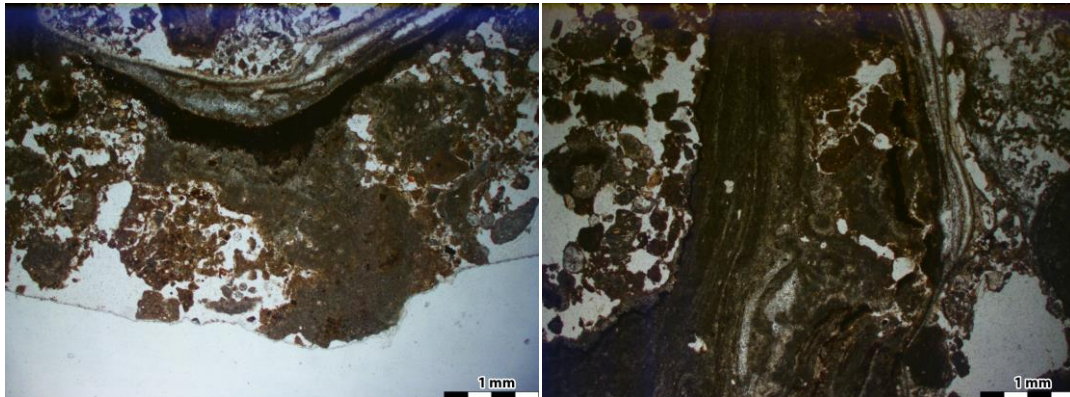


**Figure 93:** Thin section sample shows circular lamination calcite with voids not suitable for dating A-4(b), *Left*: tip of the sample, *right*: along the side of sample

The samples are not suitable for dating because the laminations are not in sequential order and due to the presence of voids (Dorale et al. 2004) Nevertheless, they are suitable for identifying water sources.

**Source identification: strontium isotope analysis  $^{87}\text{Sr}/^{86}\text{Sr}$ , (A-5)**

This aqueduct was likely once fed by collected water before (upstream of) the dam, which is today a ruin. Sr isotope ratios were measured for samples A-4(a) and A-4(b). As shown in Figure 94, the sample A-4 (a) isotope ratio differs from that of sample A-4(b). Sample A-4(a) has the same isotopic ratio as S-4 (Beit Al-Ma) spring and S-4 (Al Subyan), while A-4(b) has the same isotopic ratio as S-2 (Ras Al Ein) and S-3 (Qaryon). Therefore, the dam was probably fed from the springs S-2, S-3, and S-4. Also S-5 could be an option but because of its small size it is less likely.

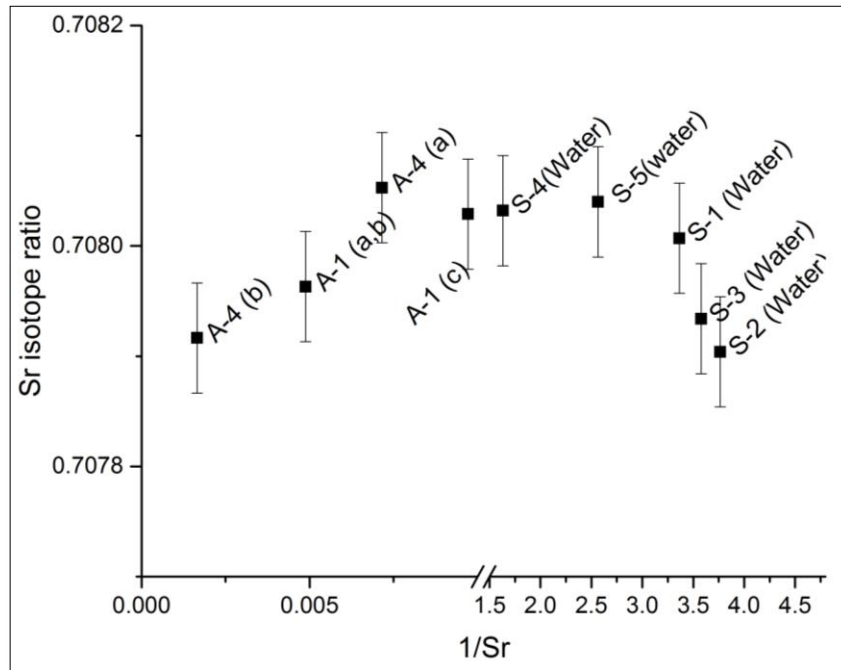


**Figure 94:** Sr isotope ratios  $^{87}\text{Sr}/^{86}\text{Sr}$  vs. mean reciprocal Sr concentrations in sample A-4 show a significant difference between samples A-4(a) and (b). Sample A-4(b) has the same isotopic signature as A-1(a, b) and the water samples S-2, S-3. A-4(a) has a higher isotopic ratio and is similar to A-1, S-4 and S-5 (Error of 0.00005 is derived by replicate analysis of standard)

## 4.6 Discussion

### 4.6.1 Is urbanization a source of groundwater quality degradation?

The city size of Nablus expanded after the Oslo agreement between the Palestine Liberation Organization (PLO) and the government of Israel in 1993 (Figure 95). Between 1991 and 1995 new building units increased by 187% in the West Bank (Sabri 1998). After 1999, the growth of the building sector fluctuated depending on the political situation. Nevertheless, between 1999 and 2015 the number of new building permits remained reasonably constant (PCBS 2015d).

By comparing satellite images for Nablus city and the surrounding area using NDVI (normalized difference vegetation index) from January 1973, August 1987, August 1999 and August 2015, the increase of the buildup area could be confirmed. A high NDVI index indicates more vegetation cover, while low NDVI indicates the buildup area (Figure 95).

Cement and stone production is one of main industrial activities in Nablus city (PCBS 2006) with 10 licensed establishments (Ministry of National Economy 2012).

Coal and diesel fuel is still widely used for heating in winter. There are many soap production factories distributed in the old city. Nablus city is connected to a sewer system, while the nearby cities and villages are still using septic tanks that are likely in many cases not watertight or not utilized in a proper manner.

It is clear through groundwater and carbonate analysis that for 100 years the groundwater is becoming polluted (see section 4.5.4). The water samples from the tunnel showed elevated concentrations of As, Cd, P, S, K, V, Cr, Ni and Cu (Figure 33). Each of the mentioned trace elements has its individual source. Yet, mainly the increase of detergent use, the increase of car repairing shops and the use of coal for heating are the sources of water pollution.

Carbonate sample A-1 (c) showed that the origin water has been definitely mixed with wastewater (section 4.5.4). Stable isotope analyses prove that the total 135 years growth has organic source (Figure 79). Furthermore, As and REY concentrations increased tremendously in the last 20 years (Figure 83, Figure 85, Figure 86).

The REE distribution in soil and groundwater is altered by contaminations from industrial and agricultural sources. REE are present in agricultural waste due to the use of fertilizer (Tyler 2004; Hu et al. 2006). Furthermore, fossil fuel use and cement factories will increase the concentration of REE in dust (Tyler 2004; Semhi et al. 2010) and the use of coal will increase As in dust and thus in percolation water. The ash produced by municipal solid waste incinerators is another known source of REE (Morf et al. 2013). In the Nablus governorate there are 16 dumping sites, of which 15 incinerate solid waste (PCBS 2002), where ash is dispersed in the air. Sewage sludge is also contaminated with REE (Kawasaki et al. 1998), which means that untreated wastewater is also contaminated. Wastewater and run-off water contain high concentrations of REE (Olmez et al. 1991).

Other carbonate deposits sampled in villages showed less influence by wastewater despite the use of septic tanks instead of a sewer system. The lessened effects can be a result of plant uptake of pollutants since many local plant Eucalyptus trees near septic tanks as a way to remediate wastewater. However, there is still increase in REY in the most recent carbonate growth. Earthquakes can also influence the groundwater quality in different situations such as effects due to water mixing between different aquifers (Environment Canterbury 2011) and due to wastewater pipelines damage.

#### 4. Results and discussion (Nablus area)

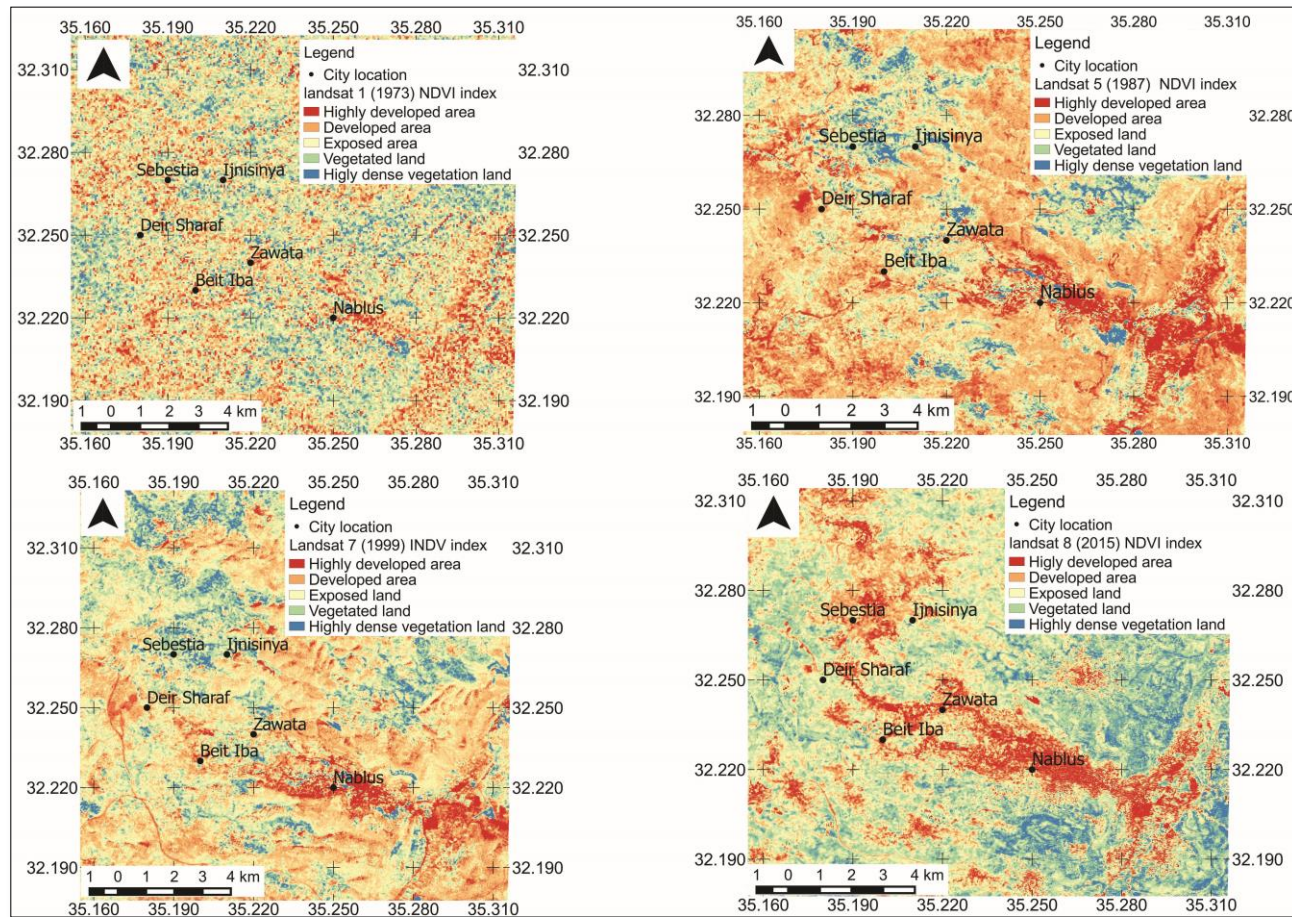


**Figure 95:** Land-use maps of the study area show an increase in building development.

*Top left:* 1973 map (generated from Landsat 1 satellite data USGS 1973 using QGIS 2015). *Top right:* 1987 map (generated from Landsat 5 satellite data USGS 1987 using QGIS 2015). *Bottom left:* 1999 map (generated from Landsat 7 satellite data USGS 2009 using QGIS 2015) and *bottom right:* 2015 map (generated from Landsat 8 satellite data USGS 2015 using QGIS 2015)

#### 4.6.2 Ancient water network Nablus–Sebestia

The probable connection between the three springs (Qaryon, Ras Al Ein and Harun) and the tunnel path starting from Dafna spring as suggested in the literature (Fanni 1999; Frumkin 2002a) are interpreted and shown in Figure 96. Based on the results of geochemical analyses, the hypothesis that Dafna spring (S-1) was the source for the water tunnel is confirmed. However, it was not the only source. Ras Al Ein spring (S-2) and Qaryon spring (S-3) could have been additional sources for the tunnel. On the other hand, the system is not linked with Sebestia. The Wadi Tufah aqueduct (A-4) is the last part in the system that can be proven to be linked to Nablus through geochemical analysis. The connection point at Harun spring (S-8) tunnel can only be linked with Ijnisinya spring (S-9). Thus, the water network route in Figure 96 that was solely based on the literature is revised in Figure 97 according to the geochemical results and takes into account the topography.

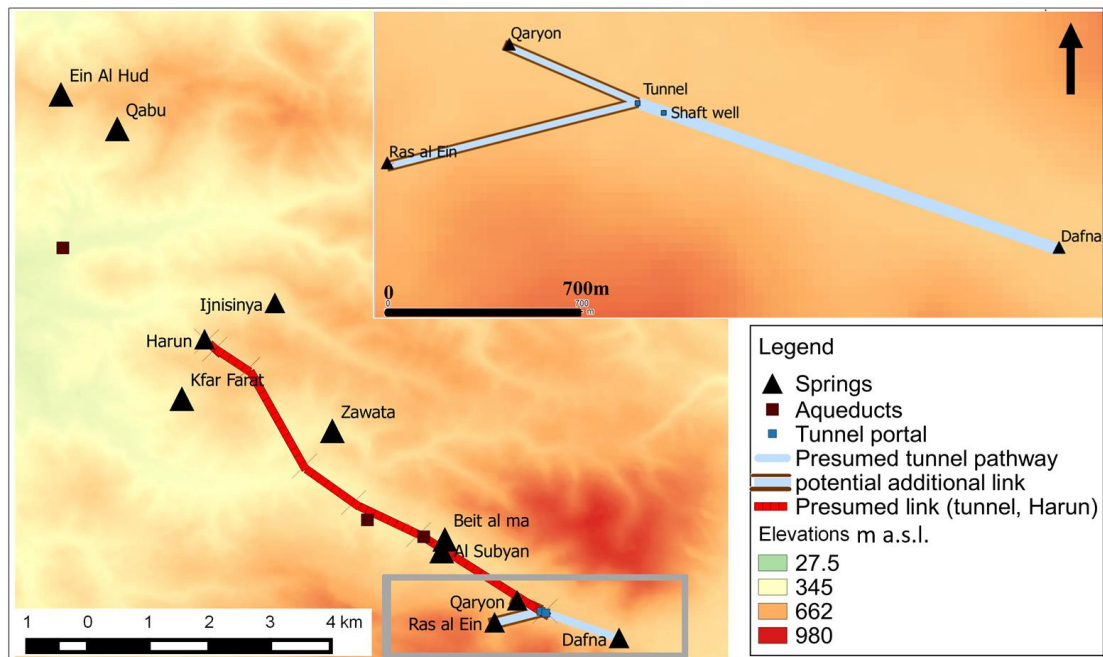


**Figure 96:** Probable connection between water system (modified after Sabri et al. 2015) (USGS 2011) with sampling locations generated by QGIS, shows presumed link between the tunnel and Harun spring as suggested by Frumkin (2002a). *Top right:* Map enlargement shows the presumed tunnel pathway as suggested by Fanni (1999) and a probable additional pathway to be examined

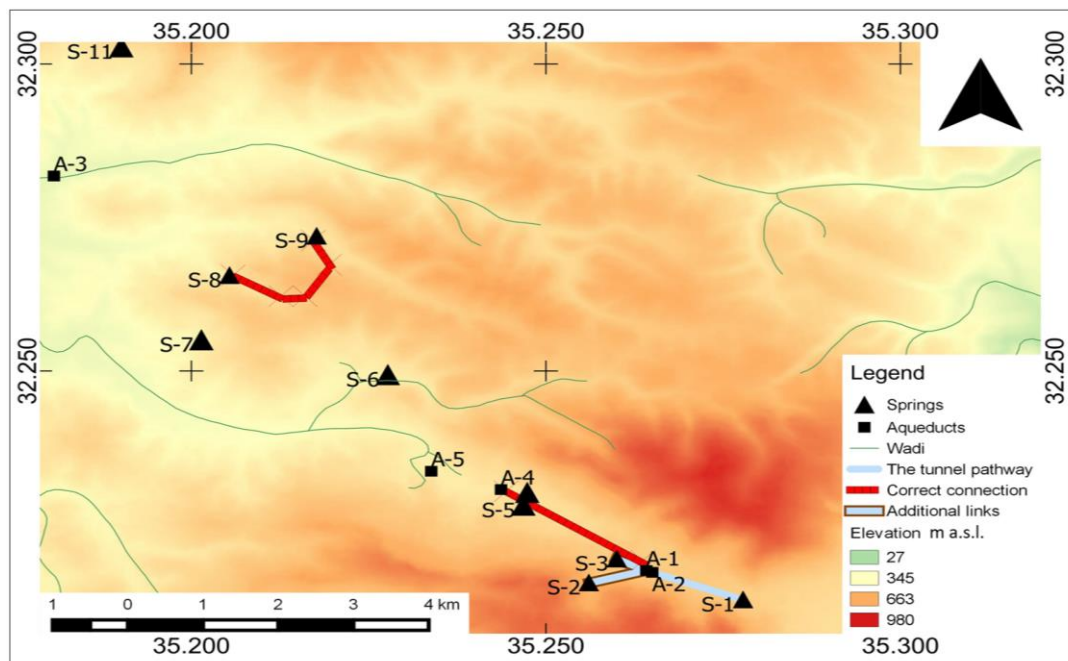


**Figure 97:** Actual connection between the water systems revised according to the geochemical analysis results, (USGS 2011) with sampling locations generated by QGIS

Unfortunately, the carbonate sample from A-5 was not sufficient for geochemical analysis. Thus, it was not possible to trace the water source for this aqueduct. The carbonate samples collected from the tunnel are rather young from Mamluk period and therefore it was not possible to determine if rainfall harvesting occurred in this period.

#### 4.6.3 Paleoclimate calculations

For paleoclimate calculations, sample S-9 was the best choice because of the low content of detritus material during the first growth as shown in section 4.5.2. The calculations are based on a method developed by Bar-Matthews et al. (1998). One assumption is assuming that the water temperature from which the carbonate sample S-9 precipitated is similar to the current temperature of 20 °C. Based on calcite–water fractionation equations (O'Neil et al. 1969),  $\delta^{18}\text{O}$  for spring water is calculated. The value  $\delta^{18}\text{O}$  for spring water is 1‰ higher than rainwater (Gat 1983; Bar-Matthews et al. 1998). The rainfall amount was calculated using the relationship between the current  $\delta^{18}\text{O}$  rainwater and annual rainfall amount developed by Bar-Matthews et al. (1998) (Table 18).

**Table 18:** Calculated rainfall amounts based on  $\delta^{18}\text{O}$  values

<sup>1</sup>algorithm developed by Roy-Barman and Pons-Branchu (2016), <sup>2</sup>based on calcite–water fractionation equations by O'Neil et al. (1969), <sup>3</sup>calculated using the relationship between the current  $\delta^{18}\text{O}$  rainwater and annual rainfall developed by Bar-Matthews et al. (1998) \*the current average rainfall amount 1954–1979 is 537 mm.

Distance from the top mm	Corrected age k.a. using STRUTages <sup>1</sup>		$\delta^{18}\text{O}$ ‰ VPDB	$\delta^{18}\text{O}$ ‰ VSMOW springs <sup>2</sup>	$\delta^{18}\text{O}$ ‰ VSMOW rainfall <sup>2</sup>	Calculated rainfall amount mm <sup>3</sup>
1–3	0.137	±0.072	–5.50	–4.58	–5.58	500 *
5–7	0.6	±0.4	–5.32	–4.39	–5.39	480
11–14	1.676	±0.93	–5.93	–5.02	–6.02	540
22–27	1.73	±0.73	–6.30	–5.40	–6.40	600

The rainfall amount calculation agrees with the age estimation for the recent growth (1929–1979). Based on this calculation, it appears that the average rainfall amount decreased by around 100 mm. Nevertheless, it is still in the range, as from year to year the rainfall quantity can vary up to 200 mm. This agrees with results from Soreq caves (Bar-Matthews et al. 1998) and Tiberias lake sediments (Issar 1998; Issar and Zohar 2004).

## 5. Results and discussion (Al Malih area)

### 5.1 Water system description

Within water system in Al Malih area in Palestine, there is a unique geological area located around 30 m below sea level. Besides the running Wadi, there are different types of springs with highly different ranges of salinity—a tenfold difference. Springs emerge from different fractures depending on the sequence of seasons (



Figure 98). Secondary carbonate is precipitated along the sides of the Wadi.

The water was once utilized to operate a watermill, thus, agricultural aqueducts transported the water to the drop shaft. After rotating the wheel, the water is directed back to the Wadi through the water outlet (Figure 99). Thick carbonate sinter (tufa) has accumulated on the walls of the outlet channel (

Figure 100).



Figure 98: Two different groundwater outlets (Photo taken by Raghid Sabri 2011)



**Figure 99:** Arrows represent the water flow through the aqueduct and millhouse at Al Malih, top left: view to the aqueduct (Photo taken by Raghid Sabri 2011)



**Figure 100:** Water outlet at the watermill at Al Malih, shows the accumulation of the carbonate (Photo taken by Raghid Sabri 2011)

## 5.2 Geochemical results (water)

As mentioned in section 1.5.1, there are two types of groundwater: thermal water and mineral water. Thermal water of S-12 and mineral water of S-13, along with the surface water of S-14 were sampled and analyzed. The results revealed that the dominant cation is Na in S-12 and S-14, and Ca in S-13. The dominant anion for S-12 and S-14 is Cl, and HCO<sub>3</sub> for S-13. Despite being few meters apart, both springs S-12 and S-13 differ significantly in terms of geochemistry. To visualize the results, a spider pattern diagram was plotted (Figure 101). Concentrations of Y, Cs, Ba and HCO<sub>3</sub> for samples S-12 and S-14 are above ocean concentrations and the Cl/Br mass ratio is ten times higher than S-13 (Table 19). This is an indicator that the recent precipitation is mixed with water in contact with halite evaporites. Stable isotope analysis also revealed that there is a mixing line between modern precipitation and brine water (Figure 102).

5. Results and discussion (Al Malih area)

**Table 19:** Selected cation and anion measured in Al Malih area

Sample no.	Li	Na	K	Ca	Mg	F	Cl	SO <sub>4</sub>	HCO <sup>3</sup>	Br	Cl /Br
	mg/l										
S-14	0.09	759	49	352.2	117.	2.3	1649	402	221	25	66
S-13	0.01	89	5.2	106.3	29	0.4	233	46	245	2.3	5
S-12	0.09	631	40	358.5	96.2	2.2	1567	336	298	26	60

**Table 20:** Selected parameters measured in Al Malih area

Sample no.	Salinity (ppm)	Temperature C°	Si Calcite	Si Dolomite	Si Aragonite	Dissolved O <sub>2</sub> (mg/l)
S-14	3628.8	35.0	1.30	2.60	1.10	7.78
S-13	734.72	29.5	0.34	0.53	0.20	6.25
S-12	3488.0	33.8	0.36	0.60	0.22	1.07

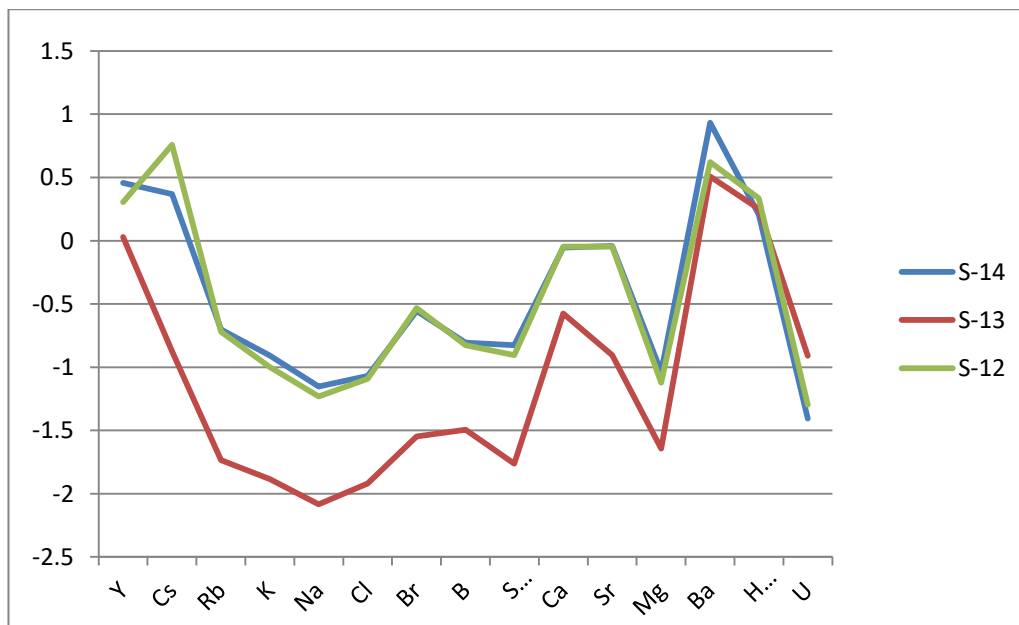


**Figure 101:** Spider patterns for groundwater bodies Al Malih area show similar patterns within the three water samples: Y, Cs, Ba and HCO<sub>3</sub> concentrations in S-12 and S-14 exceed sea level concentrations

There are at least three Sr resources in Al Malih area. As shown in (Figure 103), mineral water (S-13) had higher Sr isotope ratio than surface water (S-14) and thermal water (S-12). Despite the fact that thermal water and surface water have the same Sr concentration, they have different Sr isotope ratios. It can be assumed from Figure 103 that in S-14 the Sr isotopic value is a mixture between the thermal water and the mineral water.

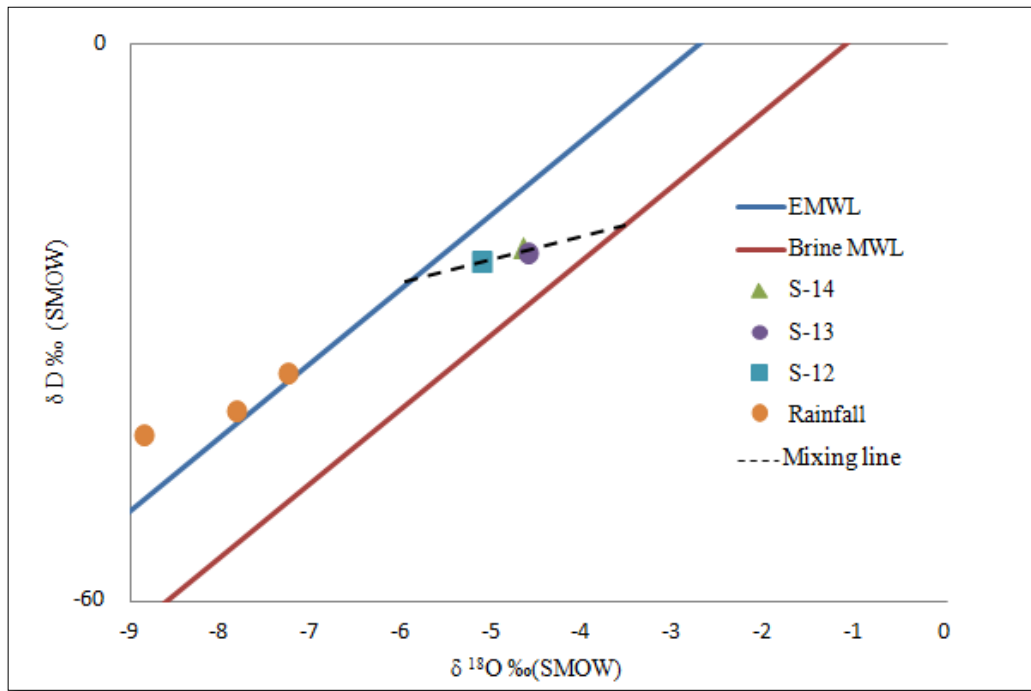


**Figure 102:** Distributions of the stable isotopes  $\delta^{18}\text{O}$  and  $\delta^2\text{H}$  at Al Malih shows a mixing line between brinewater in contact with halite and recent precipitation. **EMWL:** Eastern Mediterranean Meteoric Water Line ( $\delta^2\text{H}=8 \delta^{18}\text{O}+22$ ; Gat and Carmi 1970; Gat 1983), **Brine MWL:** Brine Meteoric Water Line ( $\delta^2\text{H}=8 \delta^{18}\text{O}+9$ ; Fontes and Matray1993)

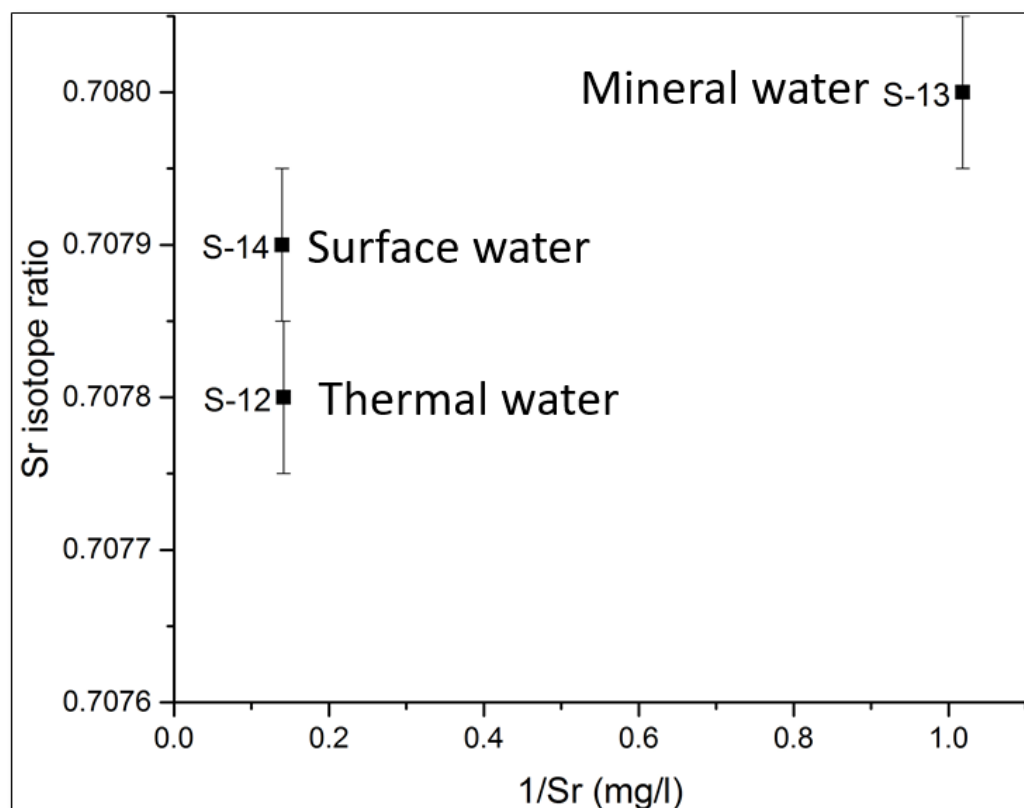


**Figure 103:** Sr isotope ratios  $^{87}\text{Sr}/^{86}\text{Sr}$  vs. mean reciprocal Sr concentrations (mg/l) for the springs show two Sr sources S-12 and S-14 and the Wadi's water is a mixture (Error of 0.00005 is derived by replicate analysis of standard)

### 5.3 Geochemical results (Carbonate)

Two sample carbonate samples (tufa) were collected from this location: the first from the watermill outlet (A-6) (Figure 99 and Figure 101) and the second from the surface water (S-14) as control sample.

Sample A-6 is laminated carbonate and consists of 205 laminae. If the mill process was carried out annually after harvesting the wheat, then it means that this watermill was operating at least for 200 years (Figure 104).



**Figure 104:** Sample A-6, *left*: cross section of sample, *right*: thin section shows lamination

The springs S-12 and S-13 have similar saturation indexes; both could be the source of carbonate. Therefore, to identify the source of the carbonate, the Sr isotope ratio was measured for both A-6 and S-14. It clearly evident that the watermill was operated with thermal water.

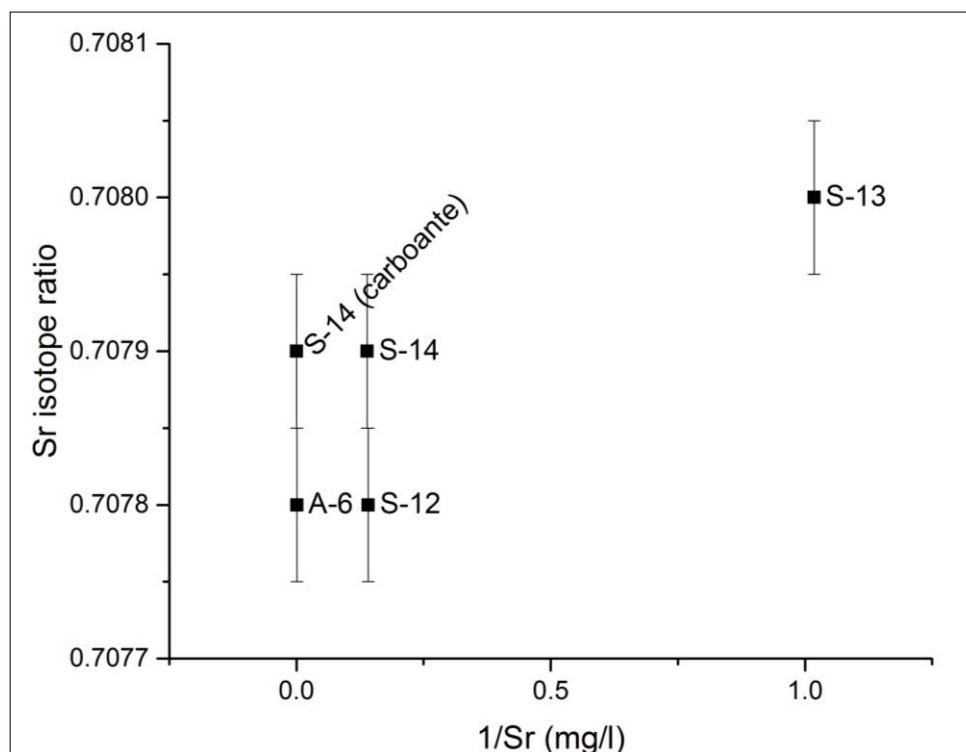


**Figure 105:** Sr isotope ratios  $^{87}\text{Sr}/^{86}\text{Sr}$  vs. mean reciprocal Sr concentrations (mg/l) show that the carbonate sample A-6 has the same isotopic signature as sample S-12, the carbonate sample for the Wadi has the same isotopic signature as the Wadi water. This indicates that S-12 water is the origin for the carbonate sinter in the watermill A-6 (Error of 0.00005 is derived by replicate analysis of standard)

To visualize the result, it was assumed that the last year of operation of the watermill was 1920 (similar to other locations). REE were measured for several laminations, and

showed a positive anomaly for the supplying water. The positive anomaly means that superficial fixed  $Ce^{4+}$  will leach out as  $Ce^{3+}$  if the passing water is reduced water (Möller 2000). This means for the initial lamination that the water was in oxidizing conditions, then this condition altered and the water became reduced and was not able to oxidize  $Ce^{3+}$  to  $Ce^{4+}$ , however, the previously superficial fixed  $Ce^{4+}$  leached out as  $Ce^{3+}$  under the new reduced conditions. This also in agreement with the low dissolved  $O_2$  levels of the thermal spring S-12. The carbonate sample S-14 shows no Ce anomaly, with higher dissolved  $O_2$  levels at S-14 (

Table 20).

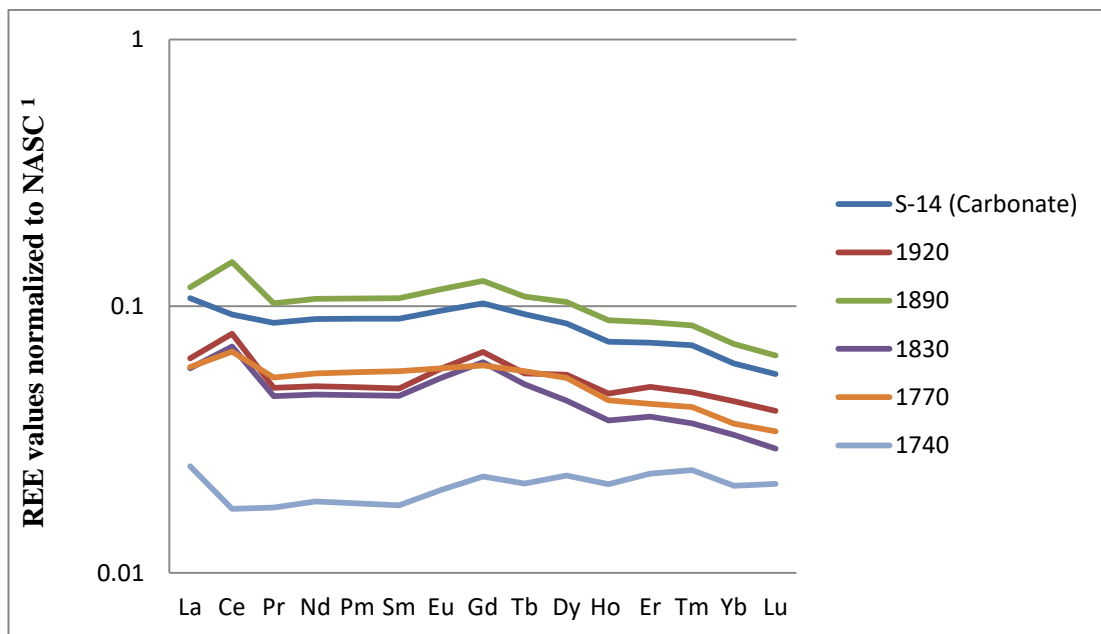


**Figure 106:** REE values patterns normalized to NASC<sup>1</sup>(Gromet et al. 1984) with the age, a positive Ce anomalies appear in all laminae of A-6 except the first lamina from 1740 A.D., meaning oxidizing conditions were present at the beginning.

### 5.3 Sustainability of watermills

This watermill was in operation for 200 years, which is a long period for an engineering structure. Brackish water was utilized for energy production. In general, watermills provided the community with stable jobs and economic stability, furthermore, they were part of the cultural and social life (Sabri et al. 2016). Unlike, the use of coal and diesel for energy production, watermills involve a clean production that has neither an influence on water quality nor carbonate. There is no trace of pollution in the sample A-6 in terms of As or REE. The decentralized system

used the water available locally that could not have been used for domestic purposes. Thus, there was no need to transport the water over long distances.

## **6. Conclusions and recommendation**

### **6.1 Conclusions**

Samples of carbonate deposits accumulating in water structure that were used from the Roman period into the Ottoman period were collected in order to date and analyze these samples and derive information about the paleoclimate, anthropogenic influence and water management during those times. Unfortunately, not all carbonate samples were suitable for dating. Yet, each sample was able to contribute to the story through different indicators. For this reason geoarchaeology is an appropriate tool to solve questions that have been prompted by earlier work, however, some sites need further sampling and analysis.

With every population increase, engineers try to find new solutions to deal with water shortages, such as building aqueduct, excavating tunnels in groundwater-bearing rocks or the underground qanat system (Frumkin 2002b).

From the work in the two study areas, one main conclusion can be made: in a country with limited water resources, large cities easily reach a critical point. In general, it would be better to implement clean energy and localized wastewater treatment plants in the rural areas. Such a decentralized system in rural areas showed less adverse effects on environments and on sustainable growth. As seen in this study, the water in tunnels is prone to contamination due to the transport of water and also wastewater. Despite the lack of a central wastewater infrastructure in rural areas, the influence in groundwater is less obvious.

The installation of the modern water network system in the region of interest was introduced by the British. It likely was considered to have been a successful way to civilize a country by implementing well-known techniques, but the consequences and other alternatives should have been considered. The installation of the water and wastewater network has influenced the water consumption behavior. While water consumption in households increased with the existence of water networks, the absence of wastewater networks had a negative impact on local groundwater bodies and in particular, on recharge areas and well head protection zones. Furthermore, with water available from the tap, water loses the spiritual value that it had in all

ancient societies. This is a socio-economic issue of great importance because of a new public awareness about water, the environment, and its vulnerability; awareness needs to be raised in people living in modern urban environments and mega cities.

## **6.2 Recommendations**

### **6.2.1 Recommendation for further research**

Additional research is recommended to analyze lead isotope ratio measurements in the samples in order to determine further anthropogenic influences. It would be also possible with laser ablation techniques (LA-ICP-MS) to measure Sr isotope ratio for samples such A-5 and thereby to determine the water source.

It would also be advisable to make a historical review in order to find supporting documents, not only about the transport of water from Ijnisinya spring to Sebestia, but also about the construction of the tunnel.

### **6.2.2 Recommendation for policy makers**

One obvious recommendation would be to detect the failures in the sewage system such as the part leaking into the tunnel and to fix it.

The amount of rainfall 1600 years ago was enough to live in a rather luxurious way and to transport the water over long distances. As previously mentioned, during the drier Islamic period, Palestinian communities switched back to water harvesting techniques. Accordingly, if in the future the amount of water leakage from the water and wastewater pipes is not reduced, it would not be recommendable to keep the same centralized system in developing new cities.

Recently, a newly developed city to the north of Ramallah, Rawabi, has a severe problem to connect with the water grid; new houses, paved streets are without water. At the same time, young architects from the Shamsard design studio developed a new concept based on an old tradition that involves building small-scale houses in remote areas with local materials. This concept is more suitable for the current water availability.

Finally, instead of connecting remote areas with both electricity and water transport systems with long cables and pipes, it would be recommendable to upgrade the abandoned watermills with modern and high efficient water turbines, where water is still available.

As mentioned in the literature review, the tunnel might have been used as a water run-off channel during the Mamluk period. It could be one solution to utilize the channel for surface runoff drainage during storm events as it is located under the main road.

## References

- Abdel-Raheem, M.B. (2011). Tulkarem and its vicinity 1281–1337 a.H / 1864–1918 A.D. Master Thesis, An-Najah National University, Nablus.
- Abualhaija I., A. Ghenma and S. I. A. Arawi (2013). Rainfall seasonal report (in Arabic). General directorate of soil and irrigation. Ramallah: Ministry of Agriculture
- Abusaada M., and M. Sauter (2013). Studying the flow dynamics of a karst aquifer system with an equivalent porous medium model. *Groundwater* 51: 641–650.
- Agatemor C., and D. Beauchemin (2011). Matrix effects in inductively coupled plasma mass spectrometry: A review. *Analytica Chimica Acta* 706(1): 66–83.
- Alawi, A., I. Al-Masry and C. Messerschmid (2015). Nablus spring source of life through history (in Arabic). Ramallah: House of Water and Environment.
- AlKhalili, F. (2000). Rainfall quantities from the season 1967/1968 until 1998/1999. Nablus: Water and wastewater department, Nablus Municipality.
- Allison, V.C. (1926). The antiquity of the deposits in Jacob's Cavern. *Anthropological Papers of the American Museum of Natural History*, 19(6):293–335.
- Al-Maqdisi, (1906). *Ahasan al-taqasim fi ma'rifat al-aqalim* (in Arabic). M. J. D. Goeje. Berlin: Brill.
- Amnesty International (2009). *Troubled waters – Palestinian denied fair access to water*. London: Amnesty International.
- Amsha, A. A. (2009). *Stories about water springs in Palestine* (in Arabic). The First Artistic Conference: Arts and Folklore in Palestine: Challenges and Current Situation. H. Nairat. Nablus: Najah University
- Anders, E. and N. Grevesse (1989). Abundances of the elements: Meteoritic and solar. *Geochimica et Cosmochimica Acta* 53(1): 197–214.
- Andersen, M. B., C. H. Stirling, E. K. Potter and A. Halliday (2009). *Understanding future sea level rise: Low-temperature isotopic fractionation of uranium*. Woods Hole: Woods Hole Oceanographic Institution.
- Anker, Y., H. Shulman, J. Guttman, A. Yellin-Dror and A. Flexer (2009). Specific regional hydrological aspects. In H. Hötzl, P. Möller and E. Rosenthal (eds.). *The water of the Jordan Valley: Scarcity and deterioration of groundwater and its impact on the regional development*, 181–198. Berlin, Heidelberg: Springer
- Bailey, T. R., J. M. McArthur, H. Prince and M. F. Thirlwall (2000). Dissolution methods for strontium isotope stratigraphy: Whole rock analysis. *Chemical Geology* 167(3–4): 313–319.
- Bakeer, M. A. (2005). *Palestinian cities during the Mamluk period* (in Arabic). Master Thesis, Birzeit University, Birzeit.
- Bar-Matthews, M., A. Ayalon and A. Kaufman (1998). Middle to late Holocene (6,500 yr. period) paleoclimate in the eastern Mediterranean region from stable isotopic composition of speleothems from Soreq cave, Israel. In A. S. Issar and N. Brown (eds.). *Water, environment and society in times of climatic change*, 203–214. Dordrecht: Kluwer Academic Publishers.
- Bar-Matthews, M., A. Ayalon, A. Kaufman and G. J. Wasserburg (1999). The eastern Mediterranean paleoclimate as a reflection of regional events: Soreq cave, Israel. *Earth and Planetary Science Letters* 166(1–2): 85–95.

- Bar-Yosef, O. (1998). The Natufian culture in the Levant, threshold to the origins of agriculture. *Evolutionary Anthropology: Issues, News, and Reviews* 6(5): 159–177.
- Beck, C., J. Grieser and B. Rudolf (2004). A new monthly precipitation climatology for the global land areas for the period 1951 to 2000. *Klimastatusbericht, DWD*: 181–190.
- Bender, F. (1974). *Geology of Jordan*. Berlin, Stuttgart: Gebrüder Borntraeger.
- Bobée, C., S. Huon, J. L. Guendon, J. Salomon, C. Gébara, J. M. Michel and M. Regert (2011). High resolution (PIXE) analyses of carbonate deposits in a roman aqueduct (Fréjus, Se, France): Implications for the study of palaeohydrological variability and water resources management in southern Gaul during the Roman period. *Archaeometry* 53(2): 241–260.
- Bögli, A. (1980). *Karst hydrology and physical speleology*. Berlin, Springer.
- Bruland, K. W., R. Middag and M. C. Lohan (2014). Controls of trace metals in seawater. In K. K. Turekian (ed.). *Treatise on geochemistry* (second edition), 19–51. Oxford: Elsevier.
- Campbell, E. F., L. C. Ellenberger and G. R. H. Wright (2002). *Shechem III: The stratigraphy and architecture of Shechem/tell balâtah*. Boston: American Schools of Oriental Research.
- Canaan, T. (1922). Studies in Palestinian customs and folklore: Haunted springs and water demons in Palestine. *The Journal of the Palestine Oriental Society* 1: 153–170.
- Carlut, J., G. Chazot, H. Dessales and É. Letellier (2009). Trace element variations in an archeological carbonate deposit from the antique city of Ostia: Environmental and archeological implications. *Comptes Rendus Geosciences* 341(1): 10–20.
- Chancey, M. A. and A. L. Porter (2001). The archaeology of Roman Palestine. *Near Eastern Archaeology* 64(4): 164–203.
- Clark, I. D. and P. Fritz (1997). *Environmental isotopes in hydrogeology*. Boca Raton: Lewis Publishers.
- Conder, C. R. and H. H. Kitchener (1880). *Map of western Palestine in 26 sheets [cartographic material]*. London: Committee of the Palestine Exploration Fund 2.
- Conder, C. R. and H. H. Kitchener (1882a). *The survey of western Palestine memories of the Topography, Orography, Hydrography and Archaeology*. In: Palmer, E. H. and Besant, W. (eds.). London: Committee of the Palestine Exploration Fund 2.
- Conder, C. R. and H. H. Kitchener (1882b). *The survey of western Palestine memories of the topography, orography, hydrographic and archaeology*. Palmer, E. H. and Besant, W. (eds.). London: Committee of the Palestine Exploration Fund 1.
- Conder, C. R. and H. H. Kitchener (1882c). *The survey of western Palestine memories of the topography, orography, hydrographic and archaeology*. E. H. Palmer and W. Besant (eds.). London: Committee of the Palestine Exploration Fund 3.
- Cook, P. (2011). *Shekhem sheet 5. Geological map of Israel*. Jerusalem: Geological Survey of Israel.
- Crowfoot, J. W., K. M. Kenyon and E. L. Sukenik (1966). *The buildings at Samaria*. London: Palestine Exploration Fund.
- Daraghma, A. (2010). *Wadi Al Malih and Bedouin tribes' (in Arabic)*. Al Malih: the community council for Al Malih and the Bedouin's area in northern Jordan Valley.

- De Feo, G., A. N. Angelakis, G. P. Antoniou, F. El-Gohary, B. Haut, C. W. Passchier and X. Y. Zheng (2013). Historical and technical notes on aqueducts from prehistoric to medieval times. *Water (Switzerland)* 5(4): 1996–2025.
- Dierx, W. and G. Garbrecht (2011). *Wasser im heiligen, Land biblische Zeugnisse und archäologische Forschungen*. Mainz: Phillip von Zabern.
- Dorale, J. A., R. L. Edwards, E. C. A. Jr., C.-C. Shen, D. A. Richards and H. Cheng (2004). Uranium-series dating of speleothems: Current techniques, limits applications. In I. D. Sasowsky and J. Mylroie (eds.). *Studies of cave sediments (physical and chemical records of paleoclimate)*, 177–197. Dordrechts: Springer.
- Drexler, J.Z., J.B. Paces, C.N. Alpers, L. Windham-Myers, L.A. Neymark, T.D. Bullen, H.E. Taylor (2014).  $^{234}\text{U}/^{238}\text{U}$  and  $\delta^{87}\text{Sr}$  in peat as tracers of paleosalinity in the Sacramento-San Joaquin Delta of California, USA. *Applied Geochemistry* 40: Pages 164–179.
- Edwards, R. L. (1988). High precision thorium-230 ages of corals and the timing of sea level fluctuations in the late quaternary. PhD Thesis, California Institute of Technology, Pasadena California.
- Environment Canterbury (2011). Earthquake impacts on groundwater Update # 3. Environment Canterbury Groundwater Resources Section Technical report. Viewed 06.07 2016, <http://ecan.govt.nz/publications/General/earthquake-impacts-groundwater-update-3-010911.pdf>
- Fairchild, I. J. and A. Baker (2012). *Speleothem science: From process to past environments*. Chichester: Wiley-Blackwell.
- Fanni, I. (1999). *Nablus fi al-hadaratayn al-yunaniyah wa-al-rumaniyah* (in Arabic). Nablus: Nablus Municipality.
- Flexer, A. and A. Yellin-Dror (2009). State of the art geology. In H. Hötzl, P. Möller and E. Rosenthal (eds.). *The water of the Jordan Valley: Scarcity and deterioration of groundwater and its impact on the regional development*, 15–54. Berlin, Heidelberg: Springer
- Flexer, A., J. Guttman, M. Haddad, H. Hötzl and E. Rosenthal (2009). Regional setting. In H. Hötzl, P. Möller and E. Rosenthal (eds.). *The water of the Jordan Valley: Scarcity and deterioration of groundwater and its impact on the regional development*, 3–14. Berlin, Heidelberg: Springer.
- Fontes, J. Ch., Matray J. M. (1993). Geochemistry and origin of formation brines from the Paris Basin, France. *Chemical Geology* 109 (1): 149–175
- Frisia, S. (2015). Microstratigraphic logging of calcite fabrics in speleothems as tool for paleoclimate studies. *International Journal of Speleology* 44(1): 1–16.
- Frisia, S. and A. Borsato (2010). Karst. In A. M. Alonso-Zarza and L. H. Tanner (eds.). *Developments in sedimentology: Elsevier*. 61: 269–318.
- Frisia, S., A. Borsato and J. Susini (2008). "Synchrotron radiation applications to past volcanism archived in speleothems: An overview." *Journal of Volcanology and Geothermal Research* 177(1): 96-100.
- Frontinus (1925). *The stratagems and the aqueduct of Rome* (translated: Charles e. Bennett). *Frontinus Stratagems De Aqueductu*. M. B. McELwain. London: Leob Classical Library.
- Frumkin, A. (2002a). The water-supply network of Samaria-Sebaste. In D. Amit, J. Patrich and Y. Hirschfeld (eds.). *The aqueducts of Israel*, 267–276. *Journal of Roman Archaeology Supplementary Series* 46.

- Frumkin, A. (2002b). The hydrogeology of Israel and the problem of water supply in antiquity. In D. Amit, J. Patrich and Y. Hirschfeld (eds.). The aqueducts of Israel, 21–24. *Journal of Roman Archaeology Supplementary Series* 46.
- Frumkin, A. and A. Shimron (2006). Tunnel engineering in the Iron Age: Geoarchaeology of the Siloam tunnel, Jerusalem. *Journal of Archaeological Science* 33(2): 227–237.
- Gat, J. R. (1983). Precipitation groundwater and surface water: Control of climate parameters on their isotopic composition and their utilization as paleoclimate tools. *Paleoclimates and paleowaters – A collection of environmental isotope studies*, IAEA Vienna, 3–12
- Gat, J. R. (2010). *Isotope hydrology. A study of the water cycle*. London: Imperial College Press.
- Gat, J. R. and I. Carmi (1970). Evolution of the isotopic composition of atmospheric waters in the Mediterranean Sea area. *Journal of Geophysical Research* 75(15): 3039–3048.
- Griffith, C. S. and S. M. Jack (2005). Monumental modified speleothem sculpture: New patterns in a class of ancient Maya cave art. In: J. K. Huang and E. V. Culley, (eds.) *American Rock Art Research Association*.
- Gromet, L. P., L. A. Haskin, R. L. Korotev and R. F. Dymek (1984). The "North American shale composite": Its compilation, major and trace element characteristics. *Geochimica et Cosmochimica Acta* 48(12): 2469–2482.
- Haensel, S. and K. Zurba (2015). Precipitation characteristics and trends in the Palestinian territories during the period 1951–2010. *Freiberg Online Geoscience (FOG)* 39: 103–130.
- Hareuveni, E. (2011). *Dispossession and exploitation: Israel's policy in the Jordan Valley and Northern Dead Sea*. Y. Stein: B'Tselem.
- Hill, C. A. and P. Forti (1997). *Cave minerals of the world*. Huntsville, Alabama: National Speleological Society.
- Hirschfeld, Y. (2004). A climatic change in the early Byzantine period? Some archaeological evidence. *Palestine Exploration Quarterly (PEQ)* 136(2): 13.
- Hoffmann, D. L., C. Spötl and A. Mangini (2009). Micromill and in situ laser ablation sampling techniques for high spatial resolution MC-ICPMS U–Th dating of carbonates. *Chemical Geology* 259(3–4): 253–261.
- Hu, Z., S. Haneklaus, G. Sparovek and E. Schnug (2006). Rare earth elements in soils. *Communications in Soil Science and Plant Analysis* 37(9–10): 1381–1420.
- Huntington, E. (1908). The climate of ancient Palestine. Part III (conclusion). *Bulletin of the American Geographical Society* 40(11): 641–652.
- Huntington, E. (1911). *Palestine and its transformation*. Bulletin of the American Geographical Society. Boston New York: Houghton Mifflin company.
- Ibn-Batuta (1964). *Tuhfat al-nuzzar fi gharaib al-amsar wa-`ajaib al-asfar* (in arabic). Bayrūt: Dār Şādir.
- Ibraheem, H. I. M. (2011). *The administrative, economic and social life in Jenien district between 1799–1831 AD/1214–1247*. Master Thesis, An-Najah National University, Nablus.
- Isaac, B. H. (1998). *The near east under Roman rule: Selected papers*. Leiden, New York: Brill.
- Isaac, P. C. (1958). *Roman public-works engineering*. University of Durham, King's College, Department of Civil Engineering and the Institution of Civil Engineers (Northern Counties Association).

- Issar, A. (1998). Climate change and history during the Holocene in the eastern Mediterranean region. In A. S. Issar and N. Brown (eds.). *Water, environment and society in times of climatic change*, 113–129. Dordrecht: Kluwer Academic Publishers.
- Issar, A. and M. Zohar (2004). *Climate change – environment and civilization in the Middle East*. Berlin: Springer.
- Iwais, M. K. Y. (2008). Road networks in Palestine during early Islamic period Negev case study (in Arabic). Master Thesis, Birzeit University, Birzeit.
- Jones, B. (2010). Microbes in caves: Agent of calcite corrosion and precipitation. In H. M. Pedley and R. M. (eds.). *Tufas and speleothems. Unravelling the microbial and physical controls*, 7–31. London: Geological Society.
- Josephus (1889). *The work of Flavius Josephus (translated: Whiston)*. London: George Bell and Sons 2.
- Kafle, H. and H. Bruins (2009). Climatic trends in Israel 1970–2002: Warmer and increasing aridity inland. *Climatic Change* 96(1–2): 63–77.
- Kawasaki, A., R. Kimura and S. Arai (1998). Rare earth elements and other trace elements in wastewater treatment sludges. *Soil Science and Plant Nutrition* 44(3): 433–441.
- Kessener, P. (2000). The Aspendos aqueduct and its inverted siphon. *Journal of Roman Archaeology* 13: 104–132.
- Kessener, P. (2016). The Aspendos siphon and Roman hydraulics. In G. Wiplinger (ed.). *De Aquaeductu Atque Aqua Urbium Lyciae Pamphylicae Psidiae. The legacy of Sextus Julius Frontinus, 261–274*. Leuven – Paris – Bristol: Peeters 27.
- Koutsoyiannis, D., N. Zarkadoulas, A. N. Angelakis and G. Tchobanoglous (2008). Urban water management in ancient Greece: Legacies and lessons. *Journal of Water Resources Planning and Management* 134(1): 45–54.
- Kresic, N. (2013). *Water in karst: Management, vulnerability, and restoration*. New York: McGraw-Hill.
- Le Strange, G. G. (1890). *Palestine under the Moslems; a description of Syria and the holy land from A.D. 650 to 1500*. Translated from the works of the mediaeval Arab geographers. Toronto, London: A.P. Watt.
- Li, D., G. A. Shields-Zhou, H. F. Ling and M. Thirlwall (2011). Dissolution methods for strontium isotope stratigraphy: Guidelines for the use of bulk carbonate and phosphorite rocks. *Chemical Geology* 290(3–4): 133–144.
- Long, P. O. (2008). Hydraulic engineering and the study of antiquity: Rome: 1557–1570. *Renaissance Quarterly* 61: 1098–1138.
- López-Ruiz, C. (2014). Greek and Canaanite mythologies: Zeus, Baal, and their rivals. *Religion Compass* 8(1): 1–10.
- Lowe, D. and T. Waltham (2002). *Dictionary of karst and caves*. Malvern, Worcs: British Cave Research Association.
- Marchandise, S., Robin, E., Ayrault, S., Roy-Barman, M. (2014). U-Th-REE-Hf bearing phases in Mediterranean Sea sediments: implications for isotope systematics in the ocean. *Geochim. Cosmochim* 131: 47–61.
- Masterman, E. W. G. (1902). The water supply of Jerusalem, ancient and modern. *The Biblical World* 19(2): 87–112.
- Mattey, D. P., I. J. Fairchild, T. C. Atkinson, J. P. Latin, M. Ainsworth and R. Durell (2010). Seasonal microclimate control of calcite fabrics, stable isotopes and trace elements in modern speleothem from St. Michaels cave, Gibraltar. *Geological Society Special Publication*. 336: 323–344.

- Milwright, M. (2009). An introduction to Islamic archaeology. Edinburgh: Edinburgh University Press.
- Ministry of National Economy (2012). The annual statistical report 2011. Ramallah: Ministry of National Economy, Palestinian Authority.
- Möller, P. (2000). Rare earth elements and yttrium as geochemical indicators of the source of mineral and thermal waters. In I. Stober and K. Bucher (eds.). *Hydrogeology of crystalline rocks*, 227–246. Dordrecht: Springer Netherlands.
- Möller, P., E. Rosenthal and S. Geyer (2009a). Regional hydrochemical and hydrogeological aspects of groundwater in the Jordan-Dead Sea rift system. In H. Hötzl, P. Möller and E. Rosenthal (eds.). *The water of the Jordan Valley: Scarcity and deterioration of groundwater and its impact on the regional development*, 149–180. Berlin, Heidelberg: Springer.
- Möller, P., E. Rosenthal and S. Geyer (2009b). Characterization of aquifer environments by major and minor elements and stable isotopes of sulfate. In H. Hötzl, P. Möller and E. Rosenthal (eds.). *The water of the Jordan Valley: Scarcity and deterioration of groundwater and its impact on the regional development*, 149–180. Berlin, Heidelberg: Springer.
- Möller, P., E. Rosenthal, P. Dulski and S. Geyer (2009c). Characterization of recharge areas by rare earth elements and stable isotopes of H<sub>2</sub>O. In H. Hötzl, P. Möller and E. Rosenthal (eds.). *The water of the Jordan Valley: Scarcity and deterioration of groundwater and its impact on the regional development*, 123–148. Berlin Heidelberg: Springer.
- Morf, L. S., R. Gloor, O. Haag, M. Haupt, S. Skutan, F. D. Lorenzo and D. Böni (2013). Precious metals and rare earth elements in municipal solid waste – sources and fate in a Swiss incineration plant. *Waste Management* 33(3): 634–644.
- Nablus Municipality (1925). Water claims file (in Arabic). Archive Department Nablus Municipality Public Library. Nablus: Nablus Municipality.
- Nablus Municipality (1945). File: Reports of water inspector (in Arabic). Archive Department Nablus Municipality Public Library. Nablus: Nablus Municipality.
- Nablus Municipality (no date). Nablus municipality during the Ottoman era: Building and belonging (in Arabic). Archive Department Nablus Municipality Public Library. Nablus: Nablus Municipality.
- Natsheh, Y., M. F. A. Khalef, O. Hamdam and M. Jaradat (2007). Exploring the shared heritage draft inventory of Palestinian sites of shared regional heritage. Koch, E. (ed.). *European Union Partnership for Peace Programme (PUSH)*.
- Needham, J. (1992). *Science and civilization in china*. Cambridge: Cambridge University Press.
- Nikolic, M. (2008). Cross-disciplinary investigation of ancient long-distance water pipelines. PhD Thesis, University of Victoria, Canada.
- Oleson, J. P. (1984). A Roman water mill on the Crocodilian river near Caesarea. *Zeitschrift des Deutschen Palästina-Vereins* (1953–) 100: 137–152.
- Olmez, I., E. R. Sholkovitz, D. Hermann and R. P. Eganhouse (1991). Rare earth elements in sediments off southern California: A new anthropogenic indicator. *Environmental Science & Technology* 25(2): 310–316.
- Olmstead, A. T. (1912). Climatic changes in the nearer East. *Bulletin of the American Geographical Society* 44(6): 432–440.
- O'Neil, J. R., R. N. Clayton and T. K. Mayeda (1969). Oxygen isotope fractionation in divalent metal carbonates. *The Journal of Chemical Physics* 51(12): 5547–5558.

- Orland, I. J., Y. Burstyn, M. Bar-Matthews, R. Kozdon, A. Ayalon, A. Matthews and J. W. Valley (2014). Seasonal climate signals (1990–2008) in a modern Soreq cave stalagmite as revealed by high-resolution geochemical analysis. *Chemical Geology* 363: 322–333.
- Ortloff, C. R. (2005). The water supply and distribution system of the Nabataean city of Petra (Jordan), 300 BC–AD 300. *Cambridge Archaeological Journal* 15(1): 93–109.
- Ortloff, C. R. and A. Kassinos (2003). Computational fluid dynamics investigation of the hydraulic behaviour of the Roman inverted siphon system at Aspendos, Turkey. *Journal of Archaeological Science* 30(4): 417–428.
- Ortloff, C. R. and D. P. Crouch (1998). Hydraulic analysis of a self-cleaning drainage outlet at the Hellenistic city of Priene. *Journal of Archaeological Science* 25(12): 1211–1220.
- Ortloff, C. R. and D. P. Crouch (2001). The urban water supply and distribution system of the Ionian city of Ephesos in the Roman imperial period. *Journal of Archaeological Science* 28(8): 843–860.
- Palestinian Water Authority (2008). Palestinian water authority database department: GIS database. Ramallah: Palestinian Water Authority Database department.
- Palestinian Water Authority (2011a). Palestinian Water Authority database department: Spring discharge data. Ramallah: Palestinian Water Authority.
- Palestinian Water Authority (2011b). Palestinian water authority database department: Spring water chemistry data. Ramallah, Palestinian Water Authority Database department.
- Palestinian Water Authority (2013). Status report of water resources in the occupied state of Palestine–2012. Ramallah: Palestinian Water Authority
- Panchuk, K.; Ridgwell, A.; Kump, L.R. (2008). Sedimentary response to Paleocene–Eocene Thermal Maximum carbon release: A model-data comparison. *Geology* 36 (4): 315–318
- Patrich, J. and D. Amit (2002). The aqueducts of Israel: An introduction. In D. Amit, J. Patrich and Y. Hirschfeld (eds.). *The aqueducts of Israel*, 9–20. *Journal of Roman Archaeology Supplementary Series* 46.
- PCBS (2002). Dumping sites survey in the Palestinian territory–2001. The Palestinian Central Bureau of Statistics. Ramallah.
- PCBS (2006). Comparison study on the industrial activities, 1999–2004. The Palestinian Central Bureau of Statistics. Ramallah.
- PCBS (2008). Population, housing and establishment census 2007, final results – buildings report. Ramallah: Palestinian Central Bureau of Statistics.
- PCBS (2009). Meteorological conditions in the Palestinian territory annual report 2008. Ramallah: Palestinian Central Bureau of Statistics.
- PCBS (2015a). Localities in Nablus governorate by type of locality and population estimates, 2007–2016. Ramallah: Palestinian Central Bureau of Statistics.
- PCBS (2015b). Needed, supply and consumed quantities and deficit in domestic supply in the West Bank by governorate, 2014. Ramallah: Palestinian Central Bureau of Statistics.
- PCBS (2015c). Water indicator. Ramallah: Palestinian Central Bureau of Statistics.
- PCBS (2015d). Building license statistics, second quarter 2015. Ramallah: Palestinian Central Bureau of Statistics.
- Pedley, H. M. and M. Rogerson (2010). Introduction to tufas and speleothems. In H. M. Pedley and M. Rogerson (eds.). *Tufas and speleothems. Unravelling the microbial and physical controls*, 1–6. London: Geological Society.

- Pentecost, A. (2005). *Travertine*. Berlin Heidelberg: Springer.
- Petersen, A. (2001). *A gazetteer of buildings in Muslim Palestine*. Part 1. Oxford: Oxford University Press.
- Pin, C. and C. Bassin (1992). Evaluation of a strontium-specific extraction chromatographic method for isotopic analysis in geological materials. *Analytica Chimica Acta* 269(2): 249–255.
- Pliny, E. (1885). *The natural history of Pliny* (translated: John Bostock and H. T. Rilly). London: Henry G. Bohn. 5.
- Pollio, M. V. (1860). *The architecture of Marcus Vitruvius Pollio: In ten books* (translated: G. Joseph) London: J. Weale.
- Pons-Branchu, E., E. Douville, M. Roy-Barman, E. Dumont, P. Branchu, F. Thil, N. Frank, L. Bordier and W. Borst (2014). A geochemical perspective on Parisian urban history based on U–Th dating, laminae counting and yttrium and REE concentrations of recent carbonates in underground aqueducts. *Quaternary Geochronology* 24(0): 44–53.
- Pons-Branchu, E., S. Ayrault, M. Roy-Barman, L. Bordier, W. Borst, P. Branchu, E. Douville and E. Dumont (2015). Three centuries of heavy metal pollution in Paris (France) recorded by urban speleothems. *Science of The Total Environment* 518–519(0): 86–96.
- Porath, Y. (2002). Hydraulic plaster in aqueducts as a chronological indicator. In D. Amit, J. Patrich and Y. Hirschfeld (eds.). *The aqueducts of Israel*, 25–35. *Journal of Roman Archaeology Supplementary Series* 46.
- QGIS (2015). QGIS geographic information system. QGIS development team, Open Source Geospatial Foundation.
- Raab, M., Friedman, G.M., Spiro, B., Starinsky, A. and Zak, I. (1997). The geological history of Messinian (Upper Miocene) evaporites in the Central Jordan Valley (Israel) and how strontium and Sulfur isotopes relate to their origin. *Carbonates Evaporites*, (12): 296–324.
- Rice, E. W. (1886). Rainfall in Palestine. *Journal of the Society of Biblical Literature and Exegesis* 6(1): 69–72.
- Rofe and Raferty Consulting Engineers (1965). *Nablus district water resources survey: Geological and hydrological report, February 1965*. R. C. V. Bellen (ed.). Westminster, London: Hashemite Kingdom of Jordan, Central Water Authority.
- Roy-Barman, M. and E. Pons-Branchu (2016). Improved U–Th dating of carbonates with high initial  $^{230}\text{Th}$  using stratigraphical and coevality constraints. *Quaternary Geochronology* 32: 29–39.
- Ruddiman, W. F. (2013). Bridging a disciplinary gap. In L. Giosan, D. Q. Fuller, K. Nicoll, R. K. Flad and P. D. Clift (eds.). *Climates, landscapes, and civilizations*, 1–10. Washington D. C.: American Geophysical Union.
- Ruppel, S. C., E. W. James, J. E. Barrick, G. Nowlan and T. T. Uyeno (1996). High-resolution  $^{87}\text{Sr}/^{86}\text{Sr}$  chemostratigraphy of the Silurian: Implications for event correlation and strontium flux. *Geology* 24(9): 831–834.
- Russell, Kenneth W. (1980). The Earthquake of May 19, A. D. 363. *Bulletin of the American Schools of Oriental Research*, no. 238: 47–64.
- Sabri, B. (1992). Urban aspects in the city of Nablus in the first half of the nineteenth century. *An-Najah University Journal for Research – Humanities* 6(1): 32.
- Sabri, N. R. (1998). *Housing as an internal leading sector in the Palestinian economy*. Geneva: The International Labor Organization

- Sabri, R., B. Merkel and M. Tichomirowa (2015). Has the water supply network of Sebestia been connected to that of Nablus? *Freiberg Online Geoscience (FOG)* 41.
- Sabri, R., B. Merkel and M. Tichomirowa (2016). Watermill as sustainable development. In G. Wiplinger (ed.). *De Aquaeductu Atque Aqua Urbium Lyciae Pamphyliae Psidiae*, 313–320. The legacy of Sextus Julius Frontinus. Leuven – Paris – Bristol: Series Babesch Supplements Peeters 27.
- Semhi, K., S. Al-Khirbash, O. Abdalla, T. Khan, J. Duplay, S. Chaudhuri and S. Al-Saidi (2010). Dry atmospheric contribution to the plant–soil system around a cement factory: Spatial variations and sources—a case study from Oman. *Water, Air, and Soil Pollution* 205(1–4): 343–357.
- Shaw, T. R. (1997). Historical introduction. In C. Hill and P. Forti (eds.). *Cave minerals of the world* (second edition). Huntsville, AL: National Speleological Society.
- Slovak, N. M. and A. Paytan (2012). Applications of Sr isotopes in archaeology. In M. Baskaran (ed.). *Handbook of environmental isotope geochemistry*. Berlin, Heidelberg: Springer 743–768.
- Spötl, C. and D. Matthey (2006). Stable isotope microsampling of speleothems for palaeoenvironmental studies: A comparison of microdrill, micromill and laser ablation techniques. *Chemical Geology* 235(1–2): 48–58.
- Spötl, C. and R. Boch (2012). Uranium series dating of speleothems. In B. W. Williams and C. C. David (eds.). *Encyclopedia of caves* (second edition), 838–844. Amsterdam: Academic Press.
- Stern, E. J. (1999). The sugar industry in Palestine during the crusader, Ayyubid and Mamluk periods in light of the archeological finds. Master Thesis, the Hebrew University, Jerusalem.
- Strabo (1854). *The geography of Strabo* (translated: C. Hamilton & W. Falconer). London: Henry G. Bohn 2.
- Sürmeli Hindi, G., C. W. Passchier, C. Spötl, P. Kessener, M. Bestmann, D. E. Jacob and O. N. Baykan (2013a). Laminated carbonate deposits in Roman aqueducts: Origin, processes and implications. *Sedimentology* 60(4): 961–982.
- Sürmeli Hindi, G., C. W. Passchier, O. N. Baykan, C. Spötl and P. Kessener (2013b). Environmental and depositional controls on laminated freshwater carbonates: An example from the Roman aqueduct of Patara, Turkey. *Palaeogeography, Palaeoclimatology, Palaeoecology* 386: 321–335.
- Tachikawa, K., M. Roy-Barman, A. Michard, D. Thouron, D. Yeghicheyan and C. Jeandel (2004). Neodymium isotopes in the Mediterranean Sea: Comparison between seawater and sediment signals. *Geochimica et Cosmochimica Acta* 68(14): 3095–3106.
- Taha, H. (2009). Some aspects of sugar production in Jericho, Jordan valley. In E. Kaptijn and L. Petit (eds.). *A timeless vale, archeological and related assays on the Jordan valley, in honor of Gerrit van der Kooij on the occasion of his sixty-fifth birthday*, 181–191. Leiden: Leiden University Press.
- Tai, C. Y., M.-C. Chang, C.-C. Liu and S. S.-S. Wang (2012). Calcite growth in a simulated cooling water environment. In J. Dobrev and P. Markovic (eds.). *Calcite: Formation, properties and applications*. New York: Nova Science Publishers.
- Temper, L. (2009). Creating facts on the ground: Agriculture in Israel and Palestine (1882–2000). *Historia Agraria* 48: 75–110.

- Temporelli, G. and F. De Novellis (2010). Hydraulic engineering of inverted siphons in Roman age: A review. *Water Science and Technology: Water Supply* 10(3): 445–452.
- Thackston, W. M. (1986). *Naaoser e Khosraw's book of travels: Safarnama*. Persian Heritage Series. (ed., translated: E. Yarshater). New York: Bibliotheca Persica 36.
- Tyler, G. (2004). Rare earth elements in soil and plant systems – a review. *Plant and Soil* 267(1–2): 191–206.
- Underhill, H. W. (1969). Carbonate scale in roman and modern canals in the Jordan Valley. *Journal of Hydrology* 7: 389–403.
- UNEP (1992). *World atlas of desertification*. London: Arnold.
- USGS (1973). Landsat satellite 1 data, recorded in January 1973, U.S. Geological Survey: <http://earthexplorer.usgs.gov> (accessed on 04.09.2015).
- USGS (1987). Landsat satellite 5 data, recorded in August 1987, U.S. Geological Survey: <http://earthexplorer.usgs.gov> (accessed on 04.09.2015).
- USGS (2009). Landsat satellite 7 data, recorded in October 1987, U.S. Geological Survey: <http://earthexplorer.usgs.gov> (accessed on 04.09.2015).
- USGS (2011). ASTER GDEM 2 data: 60x60 m, recorded in October 2011, U.S. Geological Survey: <http://earthexplorer.usgs.gov> (accessed on 20.07.2015).
- USGS (2015). Landsat satellite 8 data, recorded in August 2015, U.S. Geological Survey: <http://earthexplorer.usgs.gov> (accessed on 04.09.2015).
- Veizer, J. and P. Fritz (1976). Possible control of post-depositional alteration in oxygen paleotemperature determinations. *Earth and Planetary Science Letters* 33(2): 255–260.
- Veizer, J., D. Ala, K. Azmy, P. Bruckschen, D. Buhl, F. Bruhn, G. A. F. Carden, A. Diener, S. Ebner, Y. Godderis, T. Jasper, C. Korte, F. Pawellek, O. G. Podlaha and H. Strauss (1999).  $^{87}\text{Sr}/^{86}\text{Sr}$ ,  $\delta^{13}\text{C}$  and  $\delta^{18}\text{O}$  evolution of phanerozoic seawater. *Chemical Geology* 161(1–3): 59–88.
- Whitcomb, D. (1988). Khirbet Al-Mafjar reconsidered: The ceramic evidence. *Bulletin of the American Schools of Oriental Research* (271): 51–67.
- Wikander, Ö. (1985). Archaeological evidence for early water mills – an interim report. In N. Smith (ed.). *History of technology* London: Mansell Publishing Limited. 10: 151–180.
- Zhao, J., K. Yu, Y. Feng (2009). High-precision  $^{238}\text{U}$ – $^{234}\text{U}$ – $^{230}\text{Th}$  disequilibrium dating of the recent past: a review, *Quaternary Geochronology* 4(5): 423–433.